SUPERSONIC FILM COOLING INCLUDING THE EFFECT OF SHOCK WAVE INTERACTION

Thesis by

Khalid A. Juhany

In Partial Fulfillment of the Requirements

for the Degree of

Doctor of Philosophy

California Institute of Technology

Pasadena, California

1994

(Submitted Oct 8, 1993)

To my parents, Samiyah and Ahmed

Acknowledgements

First, I thank my parents for their love and support, and for providing me with all the necessary means to get the best education. My mother taught me kindness and patience. My father's vision and charisma had a profound impact on me. I am thankful for the support of my sisters and brothers, Hind, Ghadah, Bassim, and Rakan.

I thank my thesis advisor Melany Hunt, for her guidance and help throughout this work. I want to express my gratitude to the "man with a big heart" Professor Edward Zukoski for his constant encouragement and fruitful discussions, his sense of humor has made the tough times during this work more manageable. My appreciation goes to Professor Toshi Kubota for many helpful discussions, especially at the beginning of this program. I am particularly grateful to Professor Donald Coles whose door was always open for me; I've learned a great deal from him. I want to thank Professor Hans Hornung and Rolf Sabersky for being on my committee.

I am very thankful to Marty Gould for putting up with machining the model, his exceptional machining skills proved instrumental to the success of this program. I also want to thank Rodney Rojas for his support in machining, Joe Fontana for machining the pitot probes, and Earl Dahl for wiring and welding the temperature

probe. Special thanks go to Herb Gaebler for his suport in maintaining the wind tunnel, and Jean Anderson for her help in the library.

Most of the learning was a result of the interaction with my colleges at GALCIT, in particular, Joe Sivo, who accompanied me with the initial stages of the program and whose fingerprints are found everywhere in this thesis, Taso Lappas, for being my CFD teacher, and Jeff Seto, for providing help whenever I needed it. I appreciate the help provided by Ian Waitz, Larry Hill, and Kevin Moore.

I appreciate the last minute help of Sudipto Sur for being the LaTeXguru that he is, Rajesh Kedia for helping me with pasting the figures, Nick Glumac for reading Chapters 3 and 4, and Cecilia Lin for preparing some figures.

When I was at G.W.U. Professor Joseph Foa introduced me to propulsion engineering. He fired up my interest in engineering research and inspired me, had a major impact on me, and I am indebted to him for a lot of what I know. I aspire to be like him to this day.

Last, but not least, I want to thank *zoejati* Deborah R. Molho, for her love, tolerance, and sharing so much with me.

Abstract

The current work is an investigation of supersonic film cooling effectiveness including interactions with a two-dimensional shock wave. Air and helium, which are either heated or cooled, are injected at Mach numbers between 1.2 and 2.2 into a Mach 2.4 air freestream. The adiabatic wall temperature is measured directly. The injection velocity and mass flux are varied by changing the total temperature and Mach number while maintaining matched pressure conditions.

Heated injection, with the injectant to freestream velocity ratios greater than 1, exhibit a rise in wall temperature downstream of the slot yielding effectiveness values greater than one. The temperature rise, which also occurs for cooled injection, is attributed to the merging of the injectant boundary layer and the lip-wake. As a result comparisons between heated and cooled injection may not be valid. With the exception of heated helium runs, larger injection Mach numbers slightly increase the effective cooling length per mass injection rate. The results for helium injection indicate an increase in effectiveness as compared to that for air injection. The experimental results are compared with studies in the literature.

Flow profiles at several axial locations, up to 90 slot heights, indicate that for the same Mach number the helium injections induce a larger wake and a thicker

boundary layer than air injection.

The influence of the shock impingement on the recovery temperature is not large if the flow remains attached. Once separation occurs the temperature changes drastically with downstream distance. The shock strength for incipient separation is smaller when helium is injected than when no film coolant is present. However, the converse is true with air injection even though, for the same Mach number, the momentum flux for the air injection is less than that for the helium injection. The induced separation in the case of helium is attributed to the reduced fullness of its momentum flux profile prior to interaction. This research demonstrates how the performance of supersonic film cooling for thermal control is undermined by the susceptibility to shock induced separation, and raises concerns about hydrogen film cooling for N.A.S.P.

Table of Contents

List of Figures

List of Tables

Chapter 1

Introduction

1.1 Motivation

New designs of supersonic and hypersonic vehicles have brought renewed interest in the areas of aerodynamic heating and active cooling techniques. One of the limiting design parameters for these vehicles is the maximum temperature and heat flux that is sustainable by the vehicle exterior and engine interior. Aerodynamic heating is particularly serious in the interior of a vehicle's engine where a combination of viscous dissipation, shock wave interactions, and combustion induced heating are present. For example, the afterburner temperature in an engine flying at Mach 5 is expected to exceed 2000 K (DeMeis 1987). An estimate of heating in the propulsion system is 10 kW/cm^2 with peak values upward of 50 kW/cm^2 (Simoneau *et al.* 1988). Although new materials and designs that integrate the propulsion system with the airframe are being introduced to account for the high temperatures and heat fluxes,

the vehicles must also rely on active cooling techniques.

One proposed cooling method for supersonic or hypersonic flight is tangential slot film cooling. Film cooling is a widely used technique to protect aircraft structures, rocket nozzles (Lucas and Golladay 1967), plug nozzles (Nosek and Straight 1976) and turbine blades (Gladden and Simoneau 1988) from high-temperature environments. A thin layer or film of low temperature gas is injected through a discrete slot along the surface, in the direction parallel to the freestream. A thin layer or film is formed downstream of the slot, where it serves as a thermal buffer between the main stream environment and the wall. As the film-coolant fluid mixes with the higher temperature mainstream, the temperature of the gas film increases, reducing the film-coolant performance. In a hydrogen propelled scramjet engine, such as that proposed for the NASP, hydrogen fuel would also serve as a coolant (Kors and Kissinger 1990) in a combination of internal convective cooling and film cooling. In the film cooling scheme shown in Fig. 1.1 (NASA 1990), cold hydrogen would flow through channels in the engine's structure, and then be injected through a slot parallel to the main stream. Film cooling represents an attractive scheme for active cooling since it is simple to construct, adds thrust to the engine, energizes the boundary layer to prevent separation, and reduces heating.

To apply such a method to a scramjet engine, appropriate correlations are needed to calculate the required film coolant design parameters. To improve film-cooling predictions more experiments are required to better understand the physical nature of film-cooling flows in high-speed environments. Previous experimental studies on film cooling have been predominantly in the area of incompressible flow. In the

area of compressible flow, extensive work on film cooling has been done in cooling jet engine turbine blades. These studies involve flows with velocities below sonic conditions.

Few studies have examined supersonic film cooling, especially with variable Mach number injection. More data are needed with low molecular weight gas injection as would be used in actual applications such as the National Aerospace Plane. Few studies have examined the effect of shock waves on film cooling. Furthermore, results from existing supersonic film cooling studies vary considerably and little work has been done to resolve the discrepancies or to explain the physical phenomena that impact the mixing between the freestream and the injectant (Simoneau and Hendricks 1988). Results of previous studies provide limited and contradicting information, so that concrete conclusions are difficult to reach.

1.2 Film Cooling Effectiveness

The film cooling effectiveness in incompressible flow is defined as:

$$\eta = \frac{T_{aw}(x) - T_\infty}{T_i - T_\infty} \tag{1.1}$$

where T_{aw}, T_∞, and T_i are the temperature of the wall for adiabatic conditions, the freestream temperature, and the injectant temperature, respectively. The definition in Eqn. (1.1) is not an arbitrary one, but one that is deduced from applying the energy equation to the problem of film cooling. According to the definition in Eqn. (1.1), an effectiveness of one corresponds with a wall that remains at the injection temperature. The axial distance over which this occurs is referred to as the effective cooling length,

X_{cl}. The injected fluid is heated as a result of mixing with the main flow, and the effectiveness decreases with downstream distance.

Early work on film cooling (Eckert and Drake 1972) has shown that under certain conditions, the value of the heat transfer coefficient with film cooling quickly approaches that of the undisturbed boundary layer flow. The same conclusion can be obtained theoretically if the incompressible, constant property, energy equation is applied to the film cooling flow (See Appendix A). As a consequence, the value of the adiabatic wall temperature in Eq. (1.1) is often not obtained directly, but is instead determined from measurements of the wall heat flux and from calculations of the boundary layer heat transfer coefficient.

Film cooling in low-speed flows has been thoroughly investigated (as reviewed by Goldstein 1971). A common purpose of these investigations was to develop a correlation for effectiveness, as defined in Eq. (1.1). The effectiveness results are often plotted as a function of downstream distance, x, divided by slot height, s, and by the ratio of coolant mass flux to that of the freestream λ, $x/(s\lambda)$ where $\lambda = \rho_i u_i / \rho_\infty u_\infty$. The dependence of η on $x/(s\lambda)$ is developed from integral models (see appendix 2) for air injection into an air stream (Goldstein 1971). The effect of foreign gas injection is incorporated in the integral analysis by including the specific heat ratios, and is usually presented as $[x/(s\lambda)][(c_{p\infty}/c_{pi})]$.

The film-cooling effectiveness in high-speed flow (compressible flow) is often defined by replacing the freestream temperature T_∞ in Eqn. (1.1) with the freestream total temperature $T_{t\infty}$, and T_{aw}, by T_{rw},

$$\eta = \frac{T_{rw}(x) - T_{t\infty}}{T_i - T_{t\infty}} \tag{1.2a}$$

where, the r subscript indicates the recovery temperatures measured for adiabatic conditions. However, this definition does not take into account the recovery effect of either the freestream or the injectant. In addition, it is possible for the effectiveness value to be greater than unity, since the recovery temperature $T_{rw}(0)$ of the injectant is lower than the total injectant temperature T_i ($T_{t\infty} > T_i$).

An alternative definition of effectiveness can be:

$$\eta = \frac{T_{rw}(x) - T_{r\infty}}{T_{ri} - T_{r\infty}} \tag{1.2b}$$

where again the r subscript indicates the recovery temperatures measured for adiabatic conditions. Thus, T_{rw} and T_{ri} are the adiabatic wall temperatures measured along the surface and at the injection slot exit, respectively. This definition takes into account the influence of high-speed recovery of the freestream and the injectant.

To correlate the data in high-speed flow, previous studies attempted to use modified incompressible flow correlations (Goldstein 1971). However, these correlations were not successful in predicting experimental measurements. The extension of the incompressible results to supersonic flow is complicated by two issues that are characteristic of high-speed flows: 1) the strong coupling between the momentum and energy equation, and 2) the appearance of shock waves. As a consequence of the strong coupling between the momentum and energy equations, the thermal features of the flow are strongly influenced by the hydrodynamic aspects, through the viscous dissipation term. Unlike incompressible flow, the heat transfer coefficient with

injection is expected to be different than the value of the undisturbed boundary layer. Beckwith and Bushnell (1971), and Banken *et al.* (1985), showed that the heat transfer coefficient with injection can differ significantly from that without injection. Therefore, the adiabatic wall temperature in Eqs. (1.2a) and (1.2b) should be determined directly and not be inferred from the heat flux.

Studies of film cooling in which the adiabatic wall temperatures were measured directly, include the works of Goldstein *et al.* (1966), Cary and Hefner (1970, 1972), Rousar and Ewen (1973), and Baryshev *et al.* (1975). The work by Goldstein *et al.* (1966) considered sonic and subsonic injection of air and helium into a Mach 3 freestream. Both the injectant and the freestream flows were laminar, and the boundary layer thickness at the injection slot was smaller than the slot height of the injectant (δ/s from 0.18 to 0.4). Goldstein *et al.* defined their effectiveness by replacing $T_{r\infty}$ in Eq. (1.2b) with the recovery temperature measured with the injection of fluid at the same total temperature as the freestream $T_r'(x)$. Using their definition would require a separate experiment to determine the value of the adiabatic wall measurement with isoenergetic injection. By including the isoenergetic temperature $T_r'(x)$ the effect of injection on η would result from thermal effects. However, the correlation would not be applicable for high-velocity ratios and high temperature ratios. Goldstein *et al.* obtained two correlations for $P_i/P_\infty < 1$ and $P_i/P_\infty > 1$. A separate correlation parameter was recommended for helium injection.

The work of Goldstein *et al.* (1966) demonstrated that sonic injection of air significantly increased the film cooling effectiveness over that for subsonic injection. In addition, the helium results indicated that the higher heat capacity of the injected

fluid further increased the effectiveness. However, the helium studies were only performed for subsonic injection Mach numbers and low values of mass flux ratio $\lambda \leq 0.02$.

The work by Cary and Hefner (1970,1972) involved sonic air injection into the hypersonic flow at Mach 6, and the results showed further increases in effectiveness over the supersonic results by Goldstein *et al.* In these experiments the freestream flow was turbulent and the boundary layer thickness at the injection nozzle was considerably larger than the slot height (δ/s from 4.6 to 32). Cary and Hefner's definition of effectiveness followed that of Eqn. (1.2a). The results indicated that the effectiveness increased with injection temperature. In the same facility used by Cary and Hefner (1972), Hefner (1976) demonstrated that increasing the size of lip thickness to a value of $\delta/t = 5.6$ did not influence the effectiveness.

Rousar and Ewen (1973) injected both hydrogen and nitrogen at Mach 1.9 into an air flow at Mach 2.3. The boundary layer was turbulent, but its thickness was not given. The effective cooling lengths for air injection were less than those found in the studies by Goldstein *et al.* (1966) and by Cary and Hefner (1970,1972), which could be due to differences in the experimental conditions. For hydrogen injection, the effective cooling lengths were larger than for any of the air studies, and the decrease in effectiveness as a function of downstream distance was significantly less for hydrogen. The injection Mach number and temperature remained constant, while the mass flow rates were varied by changing the injection pressure, so that the injectant was either underexpanded, overexpanded or at matched conditions. The resulting mass flux ratios were $0.14 < \lambda < 0.56$ for hydrogen, and $0.5 < \lambda < 2.2$ for

air.

To compare the air and hydrogen results, Rousar and Ewen modified the effectiveness definition using the difference in enthalpies,

$$\eta = \frac{h_{t\infty} - h_{tv}}{h_{t\infty} - h_{ti}} \tag{1.3}$$

where $h_{t\infty}$ indicates the total enthalpy of the freestream, h_{ti} is the total enthalpy of the injectant, and h_{tv} is the total enthalpy for the edge of the viscous sublayer for adiabatic conditions. This definition is useful in presenting results for dissimilar gas injections; however, the definition relies on models for the entrainment rate to determine h_{tv}.

In addition to these studies, several film-cooling studies have measured the wall heat flux using transient techniques. The studies by Alzner and Zakkay (1971), Zakkay *et al.* (1970) and Parthasarathy *et al.* (1970) used a transient thin wall technique, where the heat transfer is determined from the rate of change of the surface temperatures. The heat transfer coefficient value was calculated using flat plate turbulent boundary-layer correlations for flow without injection. As indicated earlier, this indirect method of determining the adiabatic wall temperature and the film cooling effectiveness can lead to significant errors because the heat transfer coefficient with injection can differ significantly from values without fluid injection.

In recent hypersonic film-cooling effectiveness studies by Holden *et al.* (1990), Olsen *et al.* (1990) and Majeski and Weatherford (1988), the heat transfer was measured using thin film resistance thermometers in a shock tunnel. In an approach similar to the earlier study by Richards (1967), the surface heat flux was measured

with and without fluid injection. The no-injection boundary-layer results were used to determine the heat transfer coefficient. These boundary-layer heat transfer coefficients were then used with results of the injection experiments to calculate the film cooling effectiveness. Although the measurement of heat flux was direct, and therefore more accurate than the studies of Alzner and Zakkay (1971), Zakkay *et al.* (1970) and by Parthasarathy *et al.* (1970), obtaining the adiabatic wall temperature with injection by using the heat transfer coefficient without injection results in inaccuracies.

The literature survey indicates that in the majority of film cooling effectiveness studies, the adiabatic wall temperature has been obtained indirectly. This narrows the number of existing studies on reliable adiabatic wall temperature measurements, to only a few. In reviewing selected studies in which the the adiabatic wall temperature is measured directly, it has been found that there is a lack of data on foreign gas injection, and that the influence of the injectant temperature is not understood. In addition, all of the studies examine injection at a single Mach number. In the following study, the Mach number will be a variable, and both helium air will be injected at different temperatures. Previous studies lack consistency in the film cooling effectiveness definition. Equation (1.2b) is chosen for this study because it takes into account the recovery effect of both the freestream and the injectant. The success of film cooling correlation depends on understanding the underlying physics of the problem. The fact that previous studies have provided different correlations is indicative of a lack of knowledge concerning the mechanisms involved. While there remain unanswered questions that should be resolved before attempting to correlate

effectiveness, this study seeks to understand certain aspects of the problem of film cooling; they are 1) the influence of Mach number on on the adiabatic wall temperature, 2) the influence of injectant temperature on the adiabatic wall temperature, and 3) the influence of the findings on the usefulness of the effectiveness definition.

1.3 Film Cooling Flow-Field

The variation in the effectiveness with downstream position is accompanied by changes in flow field structure. Some subsonic film cooling experiments (Seban and Back 1962) and other subsonic experiments involving wall jets with moving freestream (Launder and Rodi 1983) have shown that the flow-field can be divided into three regions (shown in Fig. 1.2): a potential core region, a wall-jet region, and a boundary layer region. The potential core region, like a free-jet, contains a viscous layer that emanates from the lip and ends when this layer meets the slot-flow boundary layer. In this region the wall temperature remains at a constant value equal to that of the injected fluid (in the case of subsonic injection) or equal to the recovery value (in the case of supersonic injection). Thus the effectiveness in the potential core region is unity. The wall-jet region starts when the viscous layer emanating from the lip merges with the injectant boundary layer. In this region intense mixing takes place, and the wall temperature increases towards the freestream value. In the boundary layer region, the flow then relaxes to that of a boundary layer. Consequently, the effectiveness decreases from unity near the injector and approaches zero far downstream. Thus, film cooling flows combine different types of familiar flows: a free-jet

flow, a wake, a shear layer, and a boundary layer.

The different hydrodynamic features of the flow in each region suggest using different scaling laws to predict effectiveness. This approach was attempted with some success in low-speed flow (Spalding 1961), where empirical data from jet flows and boundary layer flows were applied for near and far regions respectively. These approximate flow fields were used in the energy equation to solve for the distribution in wall temperature and the film cooling effectiveness. In these incompressible analyses, the thermodynamic properties were considered invariant within the flow field (Goldstein 1971).

Some information on the film-cooling flow field can also be gleaned from related studies on tangential slot injection for fuel mixing. In the area of fuel injection, one possible method of injection into supersonic flow is injection parallel to the wall. The advantage of using parallel injection, as opposed to the more mixing-efficient angled injection, is to avoid large momentum losses associated with angled injection. Yates (1971) provided detailed flow-field information on supersonic hydrogen slot injection of Mach 1.2 flow in an air stream of Mach 2.1 ($\lambda = 0.088$ and 0.120). Yates' probing was limited to three locations, the farthest being at 30 slot-heights downstream of the injection slot. Other work by Walker *et al.* (1988) and Hyde *et al.* (1990), used the same wind-tunnel model with freestream Mach number of 2.9 and an injectant Mach number of 1.7. Walker *et al.* (1988) studied isoenergetic injection, while Hyde *et al.* (1990) also used heated injection. Both mean and turbulent profiles were measured at four locations, the farthest being 20 slot-heights downstream. Kwok *et al.* (1990) in the same wind tunnel tested helium injection and compared the results

with that for air injection. These results show that helium mixed more efficiently than air when injected at the same Mach number.

In summary, information on flow-field probing in supersonic film cooling is practically nonexistent, whereas only limited use of existing slot-injection probing studies can be made. In the latter, the primary focus has centered on examination of mixing between the slot flow and freestream, resulting in measurements that deal with the growth rate and the trajectory of the mixing layer. The experiments have not presented measurements such as adiabatic wall temperature or wall heat flux, which could be used to evaluate effectiveness. In addition, these studies have used large slot heights compared to the incoming boundary layer, which is not typical of film cooling application. During the course of this study, probing will be made for several injection conditions, which, in conjunction with measurements of the adiabatic temperature, shall provide an understanding of the behaviour of the temperature variation in each of the regions of the film cooling flow-field.

1.4 Shock-Wave/Film-Cooling Interaction

Since the appearance of shock waves is characteristic of supersonic flow, one area that low-speed film cooling studies can not offer any information is on shock wave interactions. The interaction of shock waves with the film-coolant may enhance mixing between the freestream and the film-coolant, and if the shock waves are of sufficient strength, the flow may separate. Therefore, it becomes crucial to investigate shock-wave/film cooling interaction.

Related studies concerning the interaction of shock waves with tangential slot injection are found in the area of boundary-layer control. In the area of boundary-layer control, tangential slot injection has been employed as a mechanism to prevent shock-induced separation (Delery 1985). The addition of momentum from the slot flow enables the boundary layer to withstand the adverse pressure gradient caused by the shock waves. In some of the early work by Peak (1966), an air-air experiment was used with a freestream Mach number of 1.8, an isothermal injection of Mach number 2.37, and a mass flux ratio from $\lambda = 0.6 - 1.5$, to investigate the effect of injection to prevent shock-wave/turbulent boundary-layer induced separation. By varying the shock strength and the distance from the slot to the location of the shock-wave impingement, Peak concluded that the optimum position of the injectant was a distance of about six times the thickness of the freestream boundary layer upstream of the shock-impingement location (Peak 1966). This distance corresponds to 16 slot-heights for his experiment. By probing the flow field, using a pitot probe, Peak arrived at two criteria for boundary layer control. The first is that the minimum total pressure in the wake of the slot lip must be greater than the local static pressure to prevent flow reversal; the second is that the decrease in the peak total pressure of the jet must be gradual so that the new wall boundary layer is not separated. Peak's profiles were obtained in the potential core region of the flow-field ($x/s \leq 33$). In obtaining the velocity profiles, Peak assumed that the total temperature profile is constant. In addition, wall temperatures were not obtained and the wall was not insulated.

Howell and Tatro (1966), in an air-air experiment, with freestream Mach number

of $M_\infty = 3.2$, and injection Mach number $M_i = 3.0$, positioned the slot just upstream of the reflected shock wave. The boundary layer to slot height was $\delta/s = 2.97$. They found that with injection the interaction length was decreased from 6.5δ to 2.5δ, while the peak pressure rise associated with the interaction region was increased. The rise in peak pressure with reduced interaction length is in agreement with other works of Peak (1966), Grin and Zakharov (1974), Alzner and Zakkay (1971), and White *et al.* (1989). Only Peak attempted to explain this phenomena. He attributed it to the induction of a Mach stem by the injection.

The effect of molecular weight of the injectant on shock-wave/boundary-layer control was investigated by Grin and Zakharov (1974). Helium and air were injected at sonic velocities into an air stream at Mach 6. The injection was situated near or within the separation zone of a curved surface. Their work indicated that when injecting helium at the same momentum flux as air, helium was inferior to air in preventing separation. However, when injecting helium at the same mass-flux ratio as air, the helium and air were equally effective. Grin and Zakharov (1974) attribute the inferiority of helium at matched momentum flux to the associated increase in the pressure mismatch between the injectant and the freestream in the case of helium injection.

In the study by Walker *et al.*, mentioned earlier, a shock wave of pressure ratio 1.8 was impinged 15 slot heights downstream of the injection location. The interaction between the shock-wave and the viscous layer emanating from the lip produced an increase in the viscous-layer thickness (10 %) and the turbulence intensity.

Fewer studies have examined shock-wave and film-coolant interactions to deter-

mine the effect on the film-cooling effectiveness. Some early work by Alzner and Zakkay (1970,1971), and Ledford and Stollery (1972), have shown that the film coolant can reduce the heat transfer rise in the shock-wave interaction region. However, Holden *et al.* (1990), and Olsen *et al.* (1990) in an air-helium experiment, with a freestream Mach number of 6.4, injectant Mach number of 3.0, and a maximum mass flux ratio of $\lambda = 0.25$, indicated that shock waves degrade film cooling to the point where the coolant is not effective after the interaction. Furthermore, it was found that injection can induce separation. They compared their results to that of Alzner and Zakkay (1970,1971) ($Ma_\infty = 6.0$ and $Ma_i = 1.0$) and indicated a discrepancy between their results and that of Alzner and Zakkay (1971). However, the disparity results from the difference in slot location relative to the shock-wave impingement location. The results of Alzner and Zakkay (1971), used for comparison by Holden *et al.* (1990), involved a slot located within the separation bubble just upstream of the recompression point. This location is where the peak heating occurs for a shock-wave boundary-layer interaction. The results of Holden *et al.* (1990) were for a slot located at approximately 60 or 90 slot-heights depending on the slot height used. By comparing the Holden *et al.* (1990), and Alzner and Zakkay (1970) results at the location in which the injection occurred just upstream of the interaction, the results indicate similar trends in both pressure and heat transfer.

The general conclusion obtained from previous shock-wave/slot-injectant interaction is that slot injection seems to prevent shock wave induced separation as long as the injection is at sufficient blowing rate and is near the shock-wave impingement location. The conflict between previous studies seems to be in the area where the

shock wave impingement location is away from the slot, in the wall-jet region or the boundary layer region. The knowledge of the type of the film cooling flow would provide better understanding of the shock-injectant interaction process. However, most previous studies did not include flow profiles at the location of shock wave impingement.

There remains several issues that are not resolved in the literature that this study will deal with. The issues include the influence of shock-wave impingement on the adiabatic wall temperature with film cooling (investigated here for the first time), the influence of the shape of the flow profile on shock interaction and the influence of injection on separation.

1.5 Scope of Current Research

The objective of this research is to investigate two-dimensional slot film cooling in supersonic flow with supersonic injection, and its interaction with a two-dimensional shock wave. In most of the previous studies on film cooling, the adiabatic wall temperatures is mistakingly inferred from the heat flux measurements, and the calculated values of the heat transfer coefficient for a turbulent boundary layer. However, in this study the adiabatic wall temperatures are measured directly. The influence of the injectant Mach number on adiabatic wall temperatures has not been investigated previously, and is investigated here. Previous investigations have varied the mass flow rate by varying the pressure and/or the temperature, while keeping the injection Mach number fixed. In this study, the injection velocity and mass flux

are varied by changing the total temperature and Mach number while maintaining matched pressure conditions between the injected flow and that of the freestream. The effect of dissimilar gas injection is also investigated by using air and helium as injectants. The wide range of injectant conditions include values of injectant to freestream velocity ratio that were not obtained previously.

The correlation of effectiveness is also of interest. Several correlations are attempted. The large number of variables that influence film cooling makes correlating the data a formidable task, even for low-speed film cooling. As a result, limited success is expected in obtaining a correlation that will collapse all data. The primary purpose of this study is to better understand the physical nature of the film cooling flow, rather than purely develop a correlation. The effectiveness data are compared to earlier studies of Goldstein *et al.* (1966), Cary and Hefner (1970,1972), and Rousar and Ewen (1973) in which the adiabatic wall temperatures were measured directly.

In addition to the influence of varying the slot parameters on film cooling, the influence of shock waves on the performance of the film coolant is of primary interest. Previous studies have been shown to give contradictory results and an attempt is made here to resolve this discrepancy. A two-dimensional sock wave is created using a sharp fin with a variable angle of attack. The shock wave is allowed to interact with the flow at a location in which the film-cooling effectiveness is close to unity. The strength of the shock that impinges on the flow is varied so that the adiabatic wall temperatures and pressures can be determined for conditions with and without flow separation. The effect of the injectant Mach number and the specific heat of the injectant on shock wave induced separation are explored.

Flow-field measurements in film cooling studies are scarce. The flow field is probed to provide some knowledge of the impact of mixing on effectiveness and the effects of shock wave impingement. The flow field measurements include pitot probe measurements and selected cases of total temperature profiles that are reduced to velocity profiles.

A computationally investigation is undertaken to complement the experimental findings in assessing the impact of the slot flow shock structure on performance of film cooling. The computational code used for this investigation, solves the Euler equations using a MUSCL-type scheme developed by Lappas (1990).

Chapter 2

Experimental Setup

2.1 Wind Tunnel and Model Description

The experiments were conducted in the Graduate Aeronautical Laboratory, California Institute of Technology (GALCIT) Continuous Supersonic Wind Tunnel. The tunnel can operate in closed or open loop mode. For this study, the tunnel was operated in an open loop mode. The test section was modified by replacing the upper wall opposite the nozzle block with the film cooling model.

Air was drawn into the wind tunnel's reservoir from the room through an inlet containing a filter, which prevented particulates from entering the wind tunnel. Runs were conducted with a total pressure equal to the ambient pressure ($\approx 738 \pm 6$ mm Hg) and total temperature of about $26 \pm 4°$C. At the beginning of the test rhombus where the injectant slot was located, the boundary layer was turbulent with a thickness of about 3.4 mm, a displacement thickness of 1.2 mm, a momentum thickness of

0.27 mm, and a Reynolds number per meter of approximately 9.0×10^6. The nominal freestream Mach number was 2.44 ± 0.02. During the experiments, a condensation shock was observed by the schlieren system just downstream of the throat. The impact of a condensation shock was to reduce the freestream total pressure and Mach number. However, the measurements from the Mach number obtained from the pitot pressure $P_t'/P_{t\infty}$ and static pressure $P/P_{t\infty}$ were consistent indicating that the shock was very weak.

The total test-section length and height were 400 mm and 26 mm, respectively. The spanwise to height ratio of our test section was 2.6. A three-view drawing of the injection model is described in Fig. 2.1. The model consists of three separate sections: the plate assembly, the injection box, and the sliding block section.

An effort was made to choose the ideal material for the instrumented plate. It was required that the material have a low thermal conductivity to reduce conduction, a high thermal diffusivity to reduce test time, and a high modulus of elasticity to eliminate bending of the plate due to aerodynamic loading. Hastelloy-X was the optimum choice. It is a nickel-cobol alloy, with thermal conductivity of 9.085 W/mK at room temperature, a thermal diffusivity of 2.2×10^{-6} m^2/sec, and a modulus of elasticity of $197 Gpa$.

The plate assembly consisted of 2-mm thick Hastelloy-X plate that was curved at one end to form part of the injection nozzle. The small thickness of the plate reduced conduction from the injection slot to the downstream section and from the sides of the plate. The plate was silver soldered to two thin rails also made of Hastelloy-X. The plate-rail combination was attached to the tunnel upper wall using a hollow

wooden block. To minimize convective heat transfer from the instrumented plate to the exterior, the region behind the plate was open to the low-pressure downstream environment of the wind tunnel.

The injection box, made of wood, was carved on the inside to form a divergent channel. A slotted plate with a semi-circular cross section was located above the inlet of the injectant reservoir. The circular plate serves as a flow management device that distributes the injectant flow out of the inlet uniformly in the injectant reservoir. The slots were arranged so that they increase in size farther away from the entrance of the injectant.

The sliding block section was made of an aluminum and a Hastelloy-X block. A dovetail translation mechanism was employed to enable the Hastelloy-X block to slide over the aluminum block, which was fixed to the tunnel wall. The length of the dovetail provided a strong contact between the aluminum and Hastelloy-X block, while the mismatched metal contact provided smooth translation. The sliding Hastelloy-X block provided the flat plate portion opposite to the wind tunnel nozzle block and expansion part of the injection nozzle. Figure 2.2 shows the sliding-block injection nozzle. The end of the sliding block was tapered to an angle of 10° which was used to form the injection nozzle. The slot height of 1.5 mm was chosen such that the plate length becomes 300 slot heights long, which allowed the measurement of effectiveness at distances beyond what was obtained by most of the previous experiments, and the ratio of boundary layer thickness to slot hight $\delta/s = 2.6$ was large enough to make this variable, as shown by previous investigators (Cary and Hefner 1970,1972; Hefner 1976), independent of film cooling effectiveness.

Originally, the nozzle was designed to include a section that would have turned the slot flow parallel to the freestream, i.e., a downward concavity portion of the nozzle. However, machining that portion of the nozzle (which is made from Hastelloy-X) would have produced an uneven nozzle surface and a structurally weak lip. By moving the sliding block, the Mach number was varied by changing the height of nozzle throat. The termination of the nozzle at 10° resulted in a radial flow, so that the flow out of the nozzle was not parallel to the freestream flow. The effect of the injectant radial flow on the flow just downstream of the nozzle is discussed in section 3.1.

On the wall opposite the instrumented plate was a movable wedge that was used to generate a two-dimensional oblique shock wave. The wedge design is described in Fig. 2.3. The wedge angle may be continuously varied to the desired shock strength, and the wedge can be placed in several axial positions. The wedge was made of machining steel (a steel saw) that was silver soldered on a sharp support with a delta cross section. The center of rotation of the wedge was located nearer to the tip, so that the wedge can turn at large angles without being submerged into the boundary layer. The wedge was rotated by a screw that pushes against the bottom of a spring-loaded wedge support. To ensure two-dimensional shock interaction, the span of the wedge was less than the wind tunnel's by half a boundary layer thickness on each side.

The small height of the wind tunnel test section presented several challenges. In some instances, the wind tunnel would unstart when the angle of attack of the wedge exceeded a certain value. The wedge provided enough blockage to unstart the

tunnel. The sizes of any probe had to be small in order to ensure wind tunnel start up. Because of the wind tunnel fixed walls, adverse pressure gradients were expected to increase with injection. In order to ensure constant pressure distribution along the walls of the test section, the wall opposite to the instrumented plate would have to be flexible and made to diverge with increasing injection. This modification to the wind tunnel would be costly and it was decided to continue with the investigation without any modifications to the wind tunnel.

2.2 Injection Setup

Figure 2.4 shows a schematic of the injection set up, including the half-nozzle configuration used in this experiment. The injected gas was supplied from compressed gas bottles that were connected to a manifold and a pressure regulator. The regulator was used to adjust the pressure of the injectant before entering the turbine flow meter. Depending on the gas used, the injectant has the option of being directed to one of two lines using a switch valve. One line was for air injection and the other was for helium injection. The *EG&G* Flow Technology FT4-8NESA-GEA-1 flow meter was used in the air line, while the FT-10NES-GEA-2 was used for helium injection. The turbine flow meter was calibrated at the standard conditions of 100 Psi and $60°F$. The temperature and pressure just upstream of the flow-meter were measured and corrections could be made for any deviation from the standard conditions. The uncertainty in the mass flow measurements was less than 5%, with the largest values occurring at the highest flow rates of air injection. When the supply of compressed

gas bottles were full at approximately 2500 psig and were regulated to 100 psig at high-flow rates, the temperature upstream of the flow-meter drops to its minimum value. This large temperature drop at high-flow rates results in a maximum deviation from the flow-meter calibration temperature. This was resolved by waiting for equilibrium temperature in the injectant reservoir to be reached and by measuring temperature and pressure just upstream of the flow-meter.

After metering the flow, the injectant entered a heat exchanger that was used to increase or decrease the injectant temperature. For heated runs, the total temperature was increased to temperatures ranging from 70°C to 120°C using resistance tape heaters that were controlled with a variable voltage regulator. Additional heating of the injectant would have resulted in an unfavorable heat conduction to the freestream boundary layer through the injectant-nozzle lip.

For cooled runs, a dry-ice/alcohol mixture was used to decrease the injectant temperature to approximately -60°C. After exiting the heat exchanger, the flow was throttled to the injection reservoir first, by opening a ball valve until the flow rate was near the desired value, and second, by adjusting a fine metering valve until the desired value was achieved. During the experiment, the flow rate was controlled by readjusting the fine metering valve. The total and static pressures, and the total temperature of the injectant were measured within the injection reservoir. The total pressure was measured using a tube that faced the direction of the flow while the static pressure was measured at the wall; the difference between the two measurements was small, indicating that the flow was stagnant. To reduce conduction upstream to the primary flow, the injection reservoir was made from a wooden block.

2.3 Experimental Instrumentation

2.3.1 Wall Temperature and Pressure Instrumentation

The layout of wall temperature and pressure measurements is shown in Fig. 2.5. Fifty-nine thermocouples and forty-eight pressure taps were arranged in a diagonal fashion in the central third of the plate to provide concentrated measurements of pressure and temperature without interference. The diagonal arrangement made it possible to assess any heat exchange through the sides of the plate to the environment. The thermocouples were mounted on the back side of the plate, and were epoxied into 1– mm holes drilled 0.3 mm below the surface. The thermocouples were copper-constantan 'T' type.

To make the pressure taps, a laser was used to burn a hole in the metal and then reamed to a finish size of 0.254 mm. The pressure taps were connected to piezoelectric transducers. The pressure transducers were an AutoTran 600D-5, with a range of 0-5 psi pressure differential, and have an accuracy of 1% of full range. The low pressure side of all the differential transducers used in the experiments, including the ones used for injectant reservoir and pitot probe, were connected to a vacuum pump, so that the signal from the transducer measures the absolute pressure directly.

2.3.2 Pitot Pressure Probe

The pitot probe was a boundary-layer cobra type probe, fabricated from 1.58 mm O.D. 316 stainless steel tubing with the tip flattened and then filed to 0.20 mm × 2 mm and an opening of 0.1 mm. Fig. 2.6 describes the the probe design. The pitot

probe was pitched upwards at an angle of about 10° to the freestream direction, allowing the probe to approach the wall with minimum disturbance to the flow. The probe holder can be located at five fixed axial positions downstream of the slot. The probe was traversed perpendicular to the wall by means of a high-precision microhead traversing mechanism located under the test section. A linear potentiometer was attached to the traversing mechanism, which in turn was connected to the data acquisition system to record the position of the probe.

The pitot probe could slide within the holders' tube, allowing it to vary the distance in the streamwise direction by a small amount. This made the measurement of the injectant profile at the slot exit possible for different Mach number conditions. The pitot probe was sealed to the holders' tube by fastening a screw against a teflon ferrule. The seal was regularly checked for leakage by replacing the pitot tube with another tube that was soldered at one end, and applying a vacuum to the other end of the probe holder. Another check was obtained by comparing the pressure values obtained by the pitot probe to the ones determined by a pitot probe of different design. In addition, two probes were bent in such a way to measure off center profiles to check the two-dimensionality of the injectant flow.

Similar to the static pressure ports, the pitot probe was connected to a piezoelectric transducer (AutoTran 600D-15), with a range of 0-15 psi pressure differential, and an accuracy of 1% of full range. The low pressure side was connected to a vacuum pump so that the transducer measures the absolute pressure.

2.3.3 Recovery Temperature Probe

The temperature probe was a bare fine-wire stagnation type, similar to previous designs of Yanta (1970) and Behrens (1971). The probe is detailed in Fig. 2.7. It consisted of a fine 0.051 mm chromel-alumel thermocouple wire that was supported by a 0.254 mm chromel and alumel wires. The ratio of length to the diameter of the wire was 50. Unlike hot wires, the temperature probe measures the center temperature where the thermocouple junction of the fine wire was located, so that much lower values of l/d than used for hot wires can be used. The chromel and alumel sides of the fine wire were connected to the chromel and alumel sides of the supports, respectively. In addition to the fine wire junction, another chromel-alumel junction was attached to the chromel support wire side to monitor the support temperature for assessment of conduction losses. The support wires were insulated by teflon and inserted in hypodermic tubing. The tubings were pitched at an angle of 5°, to reduce the probe influence on the flow when approaching the wall. The tubing was epoxied to a brass holder that was connected to the traversing mechanism. Attempts to make a copper constantan thermocouple junction failed since connecting the copper side of the fine wire to the support always resulted in a weak connection because of copper's high thermal conductivity.

The recovery temperatures measured by the probe are assumed to be the same as that of a circular cylinder. The average recovery factor of a cylinder in air has been well documented for a combination of different Reynolds numbers, Mach numbers and Knudsen numbers. However, the influence of composition on the recovery factor has not been documented. Unfortunately, in the present experiments only measurements

of air injection at Mach 2.2 could be made. The shock wave off the probe holder tended to separate the flow at low Mach number injections in the case of air, and for all injections of helium.

The total temperature was obtained from the recovery value using previous correlations. The correlations are curve fitted by the following equations (Yanta 1970):

$$T_r/T_t = \eta^*(\eta_f - \eta_c) + \eta_c$$

where T_r and T_t are the recovery temperature obtained from the probe and the actual total temperature, respectively. η^*,η_f, and η_c are defined by

$$\eta^* = \frac{Kn^{1.193}}{0.493 + Kn^{1.193}}$$

$$\eta_c = 1 - 0.05\frac{M^{3.5}}{1.175 + M^{3.5}}$$

$$\eta_f - \eta_c = 0.2167\frac{M^{2.8}}{0.8521 + M^{2.8}} .$$

The Knudsen number Kn was defined in terms of the Mach number and the local Reynolds number Re_D based on the static properties and wire diameter:

$$Kn = 1.255\gamma^{1/2}M/Re_D .$$

The determination of the Re_D requires the knowledge of the local temperature, so that an iterative process is needed to acquire its value. However, due to the flow conditions, the recovery factor obtained by the above equations was high, so that the Reynolds number based on the actual total temperature was near the value obtained using the recovery value. Therefore, the Reynolds number Re_D was obtained using the recovery temperature without jeopardizing the accuracy of the results.

2.4 Data Acquisition System

All thermocouples and pressure transducers were connected to a PC-based data acquisition system. The system was a Metrabyte DAS-20, 16 channel, 12 bit accuracy, analog-to-digital converter, with a sampling rate of up to 100 KHz. Each channel allowed a connection of 16 channel multiplexers (EXP-20). The multiplexing allowed a connection of up to 128 input channels. A temperature sensor on the EXP-20 board monitored the cold junction temperature. However, this sensor produced heat that affected the temperature on each channel. The channels that were nearer to the temperature sensor had higher temperatures than the ones farther away. The temperature variation along the channels resulted in erroneous temperature readings of up to $\pm 5°C$. The problem was resolved by modifying the software to compensate for the temperature variation along the channels. Before each run, the temperature along the plate was measured and compared to room temperature. The measurement of the channel farthest from the temperature sensor was consistently the most accurate. The other channels were then corrected so that they all measured the same temperature.

All measurements of temperatures and pressures were obtained using the DAS-20. Occasionally, independent measurements were obtained using mercury manometers for pressures and a thermometer for temperatures to check the accuracy of the DAS-20.

2.5 Schlieren Flow Visualization

The wind tunnel was equipped with a continuous source schlieren system for flow visualization. A 1:1 image was obtained on a "polaroid" photograph. In order to resolve the structure of the slot flow (1.5 mm high) a larger magnification was required. The detection of large-scale structures within the viscous layer was also of interest. In order to achieve these objectives, a spark schlieren system was incorporated within the original system.

The spark source chosen was the Xenon Corporation's, "Nanolamp." It had a duration of 10 nanoseconds. The short duration of the "Nanolamp" made it possible to take "frozen" flow pictures for most of the flow conditions to be investigated. The maximum distance that the flow moved during the spark duration was 6×10^{-4} mm for air injection runs, and 1.5×10^{-3} mm for helium injection runs. The system setup for the old continuous system and the spark system is shown in Figs. 2.8 and 2.9, respectively. Placing the "nanolamp" light source in the position of the original continuous light source resulted in unfavourable attenuation of the light intensity.

The light source was connected to a spherical lens that acted as a condenser. Two lens (L1 and L2) in series captured the light issuing from the light source and focused it onto a point source. A rectangular slit placed at the location of the point source allowed part of the light to pass through. Lens L3 located equidistant from its focal length (f/1.4) away from the slit, sent a 150-mm diameter light beam through the test section. The selection of the f/1.4 lens and the condensing lenses L1 and L2 was based on the magnification requirement to study the slot flow and light intensity.

The parallel beam was then reflected the mirror M2 (f/7) that focused the beam on the knife edge and on to the focusing lens. The focusing lenses L4 (f/2.5) and L5 (f/6.5) system placed the image with a magnification of 1:3/4 onto a 35-mm film.

The most sensitive adjustment was to ensure that the slit image was focused onto the knife edge. Due to diffraction, the slit image was of a different sharpness than the light source slit. The exact position of the slit image was difficult to determine. If the image was positioned at the knife edge, then the illumination on the photographic plate would be uniform. To find the position of the slit image, the knife edge was used to cut part of the image. If the shading started from the bottom then the position of the slit image had passed the knife edge (assuming that the knife edge approaches the image from the bottom), and vice versa. After several trials, an optimum position was found.

Several difficulties were encountered with the nanolamp setup; the major one was the dim illumination. The dim illumination was partly compensated for using a "fast" film. Both Kodak T-Max 400 and P-3200 were used. The sensitivity of the schlieren system increases by decreasing the slit size, as long as it remained larger than the diffraction limit. The sensitivity of the schlieren system also depends on the intensity and uniformity of light illumination across the slit. The wrinkled discharge of the spark displaced the exact position where the slit should have been located. As a result, the slit was not evenly illuminated.

In the original set up, the two mirrors M1 and M2 had equal focal lengths (which is the common procedure in a schlieren system design), and the size of the slit would be reproduced on the knife edge. However, in the new setup the image of the slit

was magnified by approximately a factor of five. This magnification resulted in an increase in aberration when compared to the case of no magnification. Furthermore, to reduce the image size on the knife edge the slit size was decreased further, this gave rise to diffraction. It is concluded that using one focusing mirror M1 (f/7) and a lens L3 (f/1.4) of different and short focal length has adversely effected the quality of the pictures presented here. However, this was inevitable due to the slot size, light intensity, and space limitation.

2.6 Determination of Injection Mach Number

As indicated earlier, to vary the Mach number of the injectant only a slight axial movement of our nozzle was required. In order for the Mach number to change from sonic value to 2.2, the nozzle needed to move only 4 mm. As a result, the variation of Mach number per axial movement of the nozzle was large. A pressure tap designed to measure the exit pressure of Mach 1.2 injection would be located within the nozzle when injecting at higher Mach numbers. To obtain a pressure measurement at the exit of the slot for each Mach number, a large concentration of pressure taps at the exit locations would be required. A pressure tap of 0.254 mm in diameter was considered to be a large cavity in a nozzle of 1.5 mm height. As a result, only a few pressure taps were located within the slot. Two were located off center at the exit of the slot when positioned for the Mach 1.6 injection. Another tap was located near the throat.

The injection Mach number reported in the study was determined from the area

of the nozzle exit (1.5 mm height) assuming zero displacement thickness, and by measuring the total temperature, total pressure, and mass flow rate of the injected gas. The method of calculating the Mach number was tested against the pitot probe reading. The pitot probe was positioned at the exit of the slot for several Mach numbers. The Mach number measured with the pitot probe at the center of the slot exit agreed with the calculated value to within ± 0.1 for Mach numbers 1.5 and higher. However, the accuracy for the transonic Mach number injections range (≤ 1.2) was within ± 0.2, with Mach numbers always greater than unity. The reduced accuracy with the lower Mach number injection was expected since the mass flow rate per unit area ρu as a function of Mach number is not sensitive near Mach 1. The Mach numbers using the two methods were close, indicating that the displacement thickness was small.

2.7 Model Validation

Before proceeding with the experiments, some preliminary runs were executed to examine the model. The first check was for leakage in the supply line (using "snoop" fluid). This was especially important in the region downstream of the flow rate measurement point. Smoke was also used to detect air from the room environment that leaked into the test section. Detection for leakage was done regularly and it was found that the O-rings in the tunnel slowly deteriorated, eventually resulting in leakage. Over the period of this investigation the O-rings were changed three times.

Preliminary experiments were also made to assess the effect of heat transfer be-

tween the instrumented plate and the environment, and to examine the impact of the backward facing step formed by the slot and plate. As indicated by the thermocouples located nearer to the side walls of the test section, there was some heat conduction along the edge of the plate. Figure 2.10 shows the recovery factor measured on the plate without fluid injection. The data shown are measured on different days and for different run times. The temperature of the plate approached the highest curve within 2 minutes. Then the temperature slowly decreases and therefore the recovery factor decreases. No difference between the lowest two curves (15 minutes and 40 minutes after the run started) was found, indicating that steady state was reached. The variation of the wall recovery factor from the expected value of 0.89 for the undisturbed adiabatic wall is a result of several factors: the upstream history effect on the boundary layer, impingement of the step shock wave on the plate and conduction. As observed in the schlieren system and through the pressure distribution shown in lower curve of Fig. 2.10, the step shock and expansion wave were reflected several times within the test section. In regions where the pressure was constant, thermocouples located nearer to the side walls of the test section indicated that there was some heat conduction along the edge of the plate. After running for more than 15 minutes, the variation was less than 1° C. The preliminary runs determined that the plate responded quickly to temperature variation, but the wind tunnel glass windows and the wooden injectant reservoir slowly reached thermal equilibrium. In all runs, sufficient time was given to the plate and the injectant reservoir to reach thermal equilibrium, usually 15 minutes. Correcting the effectiveness for conduction proved to be difficult because the heat transfer coefficient with injection is unknown.

Because of the small thickness of the slot lip, an O-ring could not be placed to ensure the prevention of leakage from the sides of slot to the freestream. A series of experiments were made to investigate whether there was leakage in the absence of the O-ring. With the slot positioned for a given Mach number injection, the mass flow rate was increased, and the Mach number was determined from the mass flow rate, the total temperature, and the total pressure of the injectant. The Mach number was observed to decrease with an increase in mass flow rate, indicating the possibility that the injectant flow was escaping through the sides of the slot to the freestream. After placing silicon gaskets on the sides of the slot, the same experiment was repeated. This time the Mach number was consistently the same.

The two-dimensionality of the injectant flow was examined by obtaining pitot pressure profiles, wall pressures and temperatures off center and comparing them to center value. As an example, Fig. 2.11 shows a pitot profile of Mach 1.6 helium injection at the center of the slot, at 1/3 the span in one direction, and 1/2 the span in the other direction. The profiles look identical, indicating that the flow was nominally two-dimensional. The wall pressure and temperatures also indicated the same values.

Chapter 3

Slot Film Cooling Effectiveness

This chapter discusses and presents results on the influence of temperature and Mach number on film cooling effectiveness. As mentioned in the introduction, most of the previous film cooling experiments have incorrectly obtained the adiabatic wall temperature indirectly. The approach in this study is to obtain the adiabatic wall temperature directly by insulating the instrumented plate. The data are compared to results of studies that have directly measured the adiabatic wall temperature. In addition, the influence of the injectant Mach number on adiabatic wall temperature is investigated here for the first time.

The influence of the slot flow shock structure on performance of film cooling is not well understood. Before proceeding with the effectiveness results, the effect of nozzle geometry and the slot-flow/freestream boundary layer interaction on the flow-field is experimentally and computationally investigated.

3.1 Slot Flow Description

Experimental and computational studies were undertaken to investigate the flow in the vicinity of the slot exit. The interaction between the slot flow and the freestream flow produces a complex shock wave structure. The shock structure is influenced by several factors including the slot geometry, the ratio of boundary layer thickness to slot height, and the pressure ratio of the slot exit to the freestream. The experimental techniques employed in slot injection studies are hampered by the inherent small size of the slot used in film cooling. Flow visualization studies do not fully explain the shock structure just downstream of the slot, and intrusive instruments can influence the flow field especially when probing near the wall. The problems associated with experimental techniques necessitate the use of computational methods. The computational analysis was initiated to complement the experimental investigation in: 1) examining the structure of the shock waves at the slot exit, 2) examining the degree of influence of these shock waves on the initial conditions of the injectant, and 3) determining the wall pressure gradient downstream of the slot, since this pressure gradient influences the development of the boundary layer.

In previous film cooling studies, strong shock waves within the slot flow have been observed principally as a result of injecting at mismatched pressures ($P_i/P_\infty < 1$). For example, in Zakkay *et al.* (1970) a pressure mismatch at the slot resulted in a shock wave region that increased the pressure to a value three times that of the initial freestream value; this pressure rise rapidly disappeared in a short distance downstream of the slot. Other studies by Olsen *et al.* (1990) and Holden *et al.*

(1990) contain runs with injections at mismatched pressures. One case was tested at a pressure ratio of $P_i/P_\infty = 0.75$; this pressure ratio resulted in a lip shock that penetrated in the injectant flow and impinged on the film cooled wall. According to the data of effectiveness in Holden *et al.* (1990), the condition of $P_i/P_\infty = 0.75$ gave similar values of effectiveness per mass flow rate $\eta(x/s\lambda)$ to those obtained with matched pressure conditions. Due to viscosity and finite lip thickness, shock waves would always appear, even in situations of matched pressure conditions. Therefore, the influence of shock waves is not limited to mismatched pressure conditions. These results appear to indicate that shock waves arising at the slot exit do not seriously degrade film cooling effectiveness. However, it is not clear to what extent these shock waves affect the injectant initial conditions.

Flow visualization studies using the schlieren optics were first undertaken to investigate the flow downstream of the slot. The nozzle was set to an injectant Mach number, and then the injection mass flow rate was increased until its value reached the matched pressure condition. As the injectant flow rate was increased at constant temperature to the matched pressure value, a shock structure similar to that reported in the studies of Goldstein *et al.* (1966) was observed. When the flow rate out of the slot was less than the matched pressure condition, the slot flow was over-expanded, and a shock wave originating at the tip propagated through the slot flow. The inclination of the shock wave towards the slot was reduced as the injection flow rate (or pressure) was increased. Figure 3.1 is a schlieren photograph of a Mach 2.2 slot-flow, which is a typical flow pattern of all the other injectant Mach numbers. Also shown in the figure is a schematic of the flow shown in the schlieren photo-

graph. The difference between the lower Mach number injections and the Mach 2.2 is in the inclination of shock wave generated in the slot flow. For lower Mach number injections, the shock wave in the injectant flow is closer to the slot.

The knife edge for the schlieren photograph is positioned parallel to the flow direction. The schlieren photograph shows the freestream boundary layer interacting with the injectant. The injectant is the bright region next to the wall, while the freestream boundary layer is the dark region just above the injectant. The injectant at the point of interaction is at an angle of 10° with respect to the parallel freestream. Although the injectant and the freestream are at matched pressure, a shock wave in both the freestream and injectant sides is produced to make the flow in the injectant and the freestream parallel to the dividing streamline. The slot flow radial velocity is reduced as the wall is approached on the injectant side. Interaction between the freestream and the injectant flow starts at the slot tip, where the resulting disturbance is propagated through the Mach lines. Streamlines closer to the wall feel the disturbance at a larger axial distance from the slot exit than streamlines farther from the wall. At this stage, speculation is that streamlines closer to the wall expand more than the ones farther away from the wall, increasing in Mach number and decreasing in pressure. Therefore, the shock wave, produced in the injectant flow, increases in strength as it approaches the wall. (Computational verification of these hypotheses is to follow.)

The injectant shock wave interacts with its laminar boundary layer resulting in separation, but reattachement soon follows because the boundary layer is thin and the strength of the shock wave appears to be close to the incipient value. The leading

separation shock, the expansion wave and the recompression shock (characteristic of shock wave boundary layer separation) are indicated by two sharp bright lines surrounding a dark region (expansion wave).

To supplement the experimental findings and answer the issues raised in the beginning of this section, a computational study was undertaken. The computational code used in the study was developed by Lappas (1993), it solves the inviscid Euler's equations using a MUSCL-type Scheme (Monotonic Upstream Schemes for Conservation Laws). In order to study the slot flow using the MUSCL scheme, the flow out of the slot is assumed to be a radial type with a point source located upstream of the throat. The assumption of radial flow is a common procedure in designing the expanding portion of supersonic nozzles for wind tunnels. As a first trial, the flow in the freestream is assumed to be irrotational with constant velocity and Mach number of 2.4. This assumption allows the effect of slot geometry to be isolated from the influence of the freestream boundary layer. Air injections of Mach 1.2 and 2.2 are tested. Because the Mach number out of the slot is a variable, the injection Mach number and pressure is that of the tip value. The second trial adds a boundary layer to the freestream flow. The freestream boundary layer is assumed to be quasi-inviscid, with a thickness equal to the value obtained experimentally. The velocity distribution of the boundary layer is assumed to follow a $1/7^{th}$ power law, i.e., $u/u_\infty = (y/\delta)^{1/7}$. The density profile of the boundary layer is given by the Crocco-Busemann approximation. The initial Mach number profiles of all cases are shown in Fig. 3.2.

The computational domain in slot heights s is $4s$ long $\times$ $2.67s$ high with $s = 0.75$.

Since the freestream boundary layer is $2.6s$, the computational domain in the second trial includes only a portion of the boundary layer. The resolution used for the computations is 60×100 cells. The case of Mach number 1.2 injection with freestream boundary layer is shown with a higher resolution of 100×150. However, it was found that there was no advantage in using a higher resolution than 60×100. The no through flow boundary condition at the wall $y = 0$ and the outflow boundary conditions on the other boundaries are imposed.

Results of air injection at Mach numbers 1.2 and 2.2, with a uniform freestream Mach number distribution, are shown in Fig. 3.3 through Fig. 3.9. The contours are broken into 30 equal levels ranging from the maximum to the minimum value. The pressure contour of the Mach 1.2 injection case, shown in Fig. 3.3, indicates that the shock originating from the lip impinges at a downstream location of about $2/3s$. The pressure distribution for different heights, shown in Fig. 3.4, demonstrates the influence of slot geometry on the flow. The curves of $y = 0$ and 0.5 are the pressure distribution in the slot flow, while the ones of $y = 1$ and 1.5 are the pressure distribution in the freestream flow. The slot flow continues to expand, as indicated by the initial favourable pressure distribution, until the slot flow reaches the lip-shock. The favourable pressure gradient extends for longer axial distances as the wall is approached and reaches a maximum at the wall. The pressure distribution at the wall ($y = 0$) is of interest since it is the one experienced by the boundary layer. The wall pressure gradient, which is a result of slot geometry, appears to be the reason behind the the thin height of the injectant boundary layer (just downstream of the slot) and the small extent of separation caused by the slot shock wave (shown in

Fig. 3.1). The pressure distribution at the wall also indicates that the pressure jump due to shock reflection is about 1.4, which is near incipient separation for a laminar boundary layer at a Mach number of 1.2. It is also important to note that a weak oblique shock wave that produces a pressure jump of 1.16 upon reflecting from the wall produces a pressure jump of 1.4. The wall pressure after reflection appears to stay relatively constant at the initial freestream value. A pressure distribution at $y = 0.5$ indicates that the pressure rise due to the lip shock-wave at that location is about 1.14. After the slot flow passes the lip shock-wave, the pressure drops until the flow meets the reflected shock, where the pressure rises again, this time with a smaller pressure rise. Figures 3.5 and 3.6 show the axial velocity and density contours, respectively. The shear layer divides the freestream flow and the injectant flow. The number of contours beyond the reflected shock in the injectant side is small, indicating that the velocity is relatively constant (within the contour step value). The velocity profiles at different axial locations are shown in Fig. 3.7 and demonstrate that the initial velocity conditions are practically unaffected by the shock waves in the flow.

The pressure contours in the case of the Mach 2.2 injection are shown in Fig. 3.8. The slot-lip shock has moved downstream while the freestream-lip shock wave has moved upstream. This result is expected since the slot flow at the tip has a higher transverse velocity and momentum than the Mach 1.2 case. The slot-lip shock wave has moved to a distance equal to twice the slot height. Hence, the flow closer to the wall travels a greater distance than in the case of the Mach 1.2 injection before reaching the slot-lip shock wave. The pressure distribution along several heights is

shown in Figure 3.9. The pressure distribution at the wall indicates the favourable conditions that the boundary layer experiences. The pressure gradient at the wall extends to a distance as far as $x = 1.6$. The pressure jump at the wall resulting from the shock interaction is about 1.67. The pressure distribution at $y = 0.5$ shows that the pressure jumps are 1.19 and 1.20 for the lip shock and the reflected shock, respectively. The pressure rise due to the slot-lip shock and its reflected shock decrease when moving away from the wall; therefore, the slot-lip shock wave strength increases as the wall is approached. To illustrate this point, consider the streamlines issuing out of the slot. The streamline nearest to the tip is the first to interact with the freestream flow. The disturbance of the interaction is propagated through the Mach lines according to the local conditions. The second streamline does not feel the effect of interaction until it intersects the Mach line of the disturbance above it. Hence, the flow represented by the second streamline continues to expand, increasing in Mach number and decreasing in pressure. This pattern continues for all streamlines as the wall is approached, and the strength of the shock wave is therefore increased.

The development mechanism of the shock wave structure is the same in both Mach number injections. The same discussion on the shock structure could have been presented earlier, when discussing the Mach 1.2 injection. However, in the case of Mach 2.2 injection, the distance from the slot exit to the slot lip-shock impingement location occupies most of the computational domain, so that shock wave structure is easier to see in the case of Mach 2.2 injection. Conversely, the computational domain of the Mach 1.2 injection provides information at a larger distance, downstream of the

slot lip-shock impingement location, than that of the Mach 2.2 injection. Information about the locations downstream of the Mach 2.2 injection domain can be gleaned from the results of the Mach 1.2 injection computation.

A similar trend in pressure distribution is also visible when comparing the pressure distribution of both Mach number injections. The pressure at the end of the shock interaction, where the computational domain ends, for both cases appears to return to the initial freestream value, indicating that the influence of the shock structure is small.

The influence of including the freestream boundary layer on the slot flow for Mach 1.2 and 2.2 injection is displayed in Figs. 3.10 through 3.21. Figures 3.10, 3.11, 3.12, and 3.13 show the Mach 1.2 injection pressure contours, pressure distribution, axial velocity contours, and density contours, respectively. Figures 3.14, 3.15, 3.16, and 3.17 show the Mach 2.2 injection pressure contours, pressure distribution, velocity contours, and density contours, respectively. The contours indicate that the shock wave in the freestream is curved due to the vorticity in the boundary layer and that the slot shock wave has moved slightly farther downstream than the previous trial without the boundary layer. When comparing the pressure distributions of the cases with and without a boundary layer, it is found that the addition of the boundary layer has a small influence on the slot flow shock strength, even though the shock has moved farther downstream. The velocity and density contours show that a shear layer develops within the injectant flow. A shear layer roll up is visible in the density and velocity contours of $M = 1.2$ injection at $x = 1.25$.

The axial velocity and density profiles at $x = 0, 1, 2$, and 3 are shown in Figs. 3.18

and 3.19. The conditions at $x = 0$ represent the initial conditions of the injectant and the freestream, while the profile at $x = 3$ shows the conditions of both streams after passing through the shock waves. Comparison between the profiles at $x = 0$ and $x = 3$ indicates that neither the freestream nor the injectant are affected by the slot shock interaction. The same finding was obtained in the case of Mach 2.2 injection; in this case the injection Mach number and mass flux ρu^2 are shown in Figs. 3.20 and 3.21, respectively.

The above computational examples indicate that the shock structure is primarily a result of slot nozzle geometry and that the injectant flow shock interaction slightly affects the initial conditions. The configuration of the nozzle used in this study minimizes boundary layer growth, reduces conduction through the slot lip, and provides a structurally sound slot lip. In addition, this type of nozzle is simple to machine. These characteristics of the nozzle, combined with its weak influence on the flow field, make it ideal for film cooling applications. The computational examples also indicate that the strength of the shock waves in the slot flow ranges from 1.1 to 1.3 for the lowest and highest Mach number injections, respectively. The reflected shock adds to the pressure rise felt by the wall, which is the pressure rise that the boundary layer experiences. The wall pressure rises of 1.4 and 1.67 are considered near incipient values. But since the wall pressure gradient at the wall is a strong favourable one, the influence of shock interaction will not be significant. Such shock strengths were experienced in previous studies and showed no significant influence on effectiveness. The slot shock structure is shown in section 3.2 to have a small effect on the value of the adiabatic wall temperature. Also, the effect of weak shock

waves on the adiabatic wall temperature is not significant; this is shown in chapter 5, where shock wave interaction is discussed.

3.2 Film Cooling Studies of Air and Helium Injections

During this stage of the experiments the Mach number, molecular weight, and temperature of the injectant were varied. The exit pressure of the injectant was maintained constant and matched that of the freestream.

To obtain effectiveness, which is defined as:

$$\eta = \frac{T_{rw}(x) - T_{r\infty}(x)}{T_{ri} - T_{r\infty}(x)} \qquad (1.2b)$$

the values of of T_{ri} the wall temperature measured just downstream of the injection nozzle and $T_{rw}(x)$ the adiabatic wall temperature downstream of the slot have to be determined. Effectiveness data are commonly represented on a log-log scale, which may sometimes obscure the results. Before presenting the results on effectiveness, both the temperature and pressure distribution for the different injection conditions are presented on a linear scale, and carefully analyzed to identify any factors that may impact the effectiveness (as defined by Eq. 1.2b).

3.2.1 Wall Temperature and Pressure Distribution

The pressure distributions for different injection conditions are shown in Figure 3.22. It indicates that the addition of mass by injection, in the fixed test section area, resulted in a pressure increase that was proportional to the injection rate. The wall

pressure distribution shows that the pressure for most runs is nearly constant for the first 60 slot heights, but then gradually the pressure begins to increase. The highest pressure increase is from 6.2kPa near the injection slot to 9.6kPa at $X/s = 300$ for the $\lambda = 0.74$ case. The spikes in the pressure profile are a result of the lip shocks propagating through the test section and impinging on the wall. Although the shock waves in the tunnel are weak, their signature on the wall indicates the added effect of the reflected shock. In previous low-speed film cooling experiments, it was found that pressure gradients of the magnitude experienced under the current experimental conditions did not influence the film cooling effectiveness (Goldstein 1970). Thus, the comparisons in this study are based on the assumption that the pressure gradients of the magnitude experienced in the current experiments have little effect on the film cooling effectiveness. The effect of pressure gradient on film cooling effectiveness in supersonic flow is not well documented. Zakkay *et al.* (1974), in a supersonic flow experiment of Mach 1 injection in a Mach 6 freestream, found that, for the same injection mass flow rate, film cooling effectiveness was improved when adverse pressure gradient was present. However, their local adiabatic wall temperatures were inferred from the heat transfer measurement using the boundary layer reference enthalpy method.

As discussed earlier in the introduction, a typical plot of temperature with cooled injection versus distance downstream of the slot shows the temperature near the slot to be constant for a short distance in the inviscid core region. Then the temperature rises as the freestream mixes with the injectant. The opposite trend occurs when a heated injectant is used. In general, for both cooled and heated injection the effec-

tiveness value follows the same temperature trend. The cold injection temperature distribution is demonstrated in Fig. 3.23 , in the case of air injection at $M_i = 1.5$ and 1.8, and in Fig. 3.24, in the case of helium injection at $M_i = 1.3$ and 1.9. The figures show the measured wall temperature normalized by the injectant total temperature T_{rw}/T_{ti} as a function of axial distance normalized by the slot height.

The initial value of the wall temperature is expected to be approximately equal to the adiabatic wall temperature obtained by a flow over a flat plate at the same Mach number and total temperature as the injectant. The correlation for the recovery factor R for a boundary layer flow is $R = Pr^{1/2}$ for a laminar boundary layer and $R = Pr^{1/3}$ for a turbulent boundary layer, where Pr is the Prandtl number (Eckert and Drake 1972). When transition occurs, the recovery factor increases to a value larger than the recovery factor for either the laminar and turbulent boundary layers. The state of the boundary layer in the slot flow of this study was not determined experimentally, but since the Reynolds number based on the slot height ranges from 1,500 to 11,000, it is expected that the flow downstream of the slot could be laminar, transitional, or turbulent. The difference between the initial temperature downstream of the slot and the one calculated using the boundary layer recovery factor can be a result of conduction to or from the surrounding environment, as well as deviation of the slot flow from a regular boundary layer flow. Once the injectant boundary layer and the viscous shear layer emanating from the lip meet (the beginning of the wall jet region), the expected wall temperature may no longer follow that of a regular boundary layer.

The recovery temperatures measured near the slot exit for the air injection in

Fig. 3.23 were higher than expected. The high values are a result of a very thin ice layer that developed near the exit of the slot. In the case of helium injection, the initial recovery temperature ratios are 0.97 and 0.93 for the cases of $M_i = 1.3$ and $M_i = 1.9$, respectively. The recovery temperature ratios based on the correlations in the case of Mach 1.3 are 0.94 and 0.96 for a laminar and a turbulent boundary layer, respectively. The recovery temperature ratios for a flat plate in the case of Mach 1.8 are 0.92 and 0.94 for a laminar and a turbulent boundary layer, respectively. Comparing the calculated values to the experimental values for the case of $M_i = 1.9$ with helium injection indicates that the boundary layer is most likely laminar.

The recovery temperature distribution in the case of isoenergetic injection for helium at Mach 1.5 and 2.1 and air at Mach 1.6 and 2.0 are shown in Fig. 3.25. The temperature distribution is expected to start at the initial recovery value, then gradually reach the freestream value. The helium injections produce lower temperatures than air, as a result of the difference in specific heat ratio. The initial temperature ratios of helium injection indicate that boundary layers are most likely laminar. As expected the initial temperature decreases as the Mach number is increased, and the recovery temperature eventually returns to the freestream value. Although in the case of air injection, the data does display an initial temperature rise higher than the freestream value and the initial value of the injectant.

When injecting heated flow, the wall recovery temperature is expected to be constant in the jet core region and drop in the wall jet region. However, the temperature distribution exhibits a behavior that has not been observed previously. It is found that for heated injection at high velocities ($r \geq 1$), there is a distance downstream of

the slot where the recovery temperature clearly increases, even beyond the temperature T_{ri}. The temperature rises both in value and axial extent as the M_i increases. This behavior is shown in Figs. 3.26 and 3.27 at different Mach numbers for the cases of air injection and helium injection, respectively. All temperature ratios at the slot exit were found to have approximately the same values as the ones obtained using the recovery factor correlation.

In the case of air injection, the temperature distribution of Mach 2.2 injection is shown for two different injectant temperatures. For a constant Mach number, the initial value T_{rw}/T_{ti} should be independent of M_i, as long as the status of the boundary layer is the same. The difference may be due to the Reynolds number, since the initial value $T_{rw}/T_{ti} = 0.94$ in the case of $T_{ti}/T_{t\infty} = 1.14$ is close to the calculated value for a turbulent boundary of 0.95, while in the case of $T_{ti}/T_{t\infty} = 1.32$ the value $T_{rw}/T_{ti} = 0.92$ is close to the laminar boundary layer value of 0.93.

Several possibilities were investigated to determine the sources of the temperature increase. One possibility is that the temperature rise resulted from conduction. A reference to the model can be made in Fig. 2.1, which indicates that conduction from the stagnation reservoir along the plate would have resulted in a temperature distribution that is the opposite of what has been observed experimentally. In the case of heated injection temperature, conduction from the injectant reservoir (which has the highest temperature) along the plate would have resulted in a temperature that is largest near the the slot exit and decreases farther away from the slot exit.

Conduction from the side walls was also eliminated as a possible source of the temperature rise. The thermocouples nearer to the side walls of the tunnel did not

indicate a large difference in temperature when compared to the temperature measured in the center of the plate (the positions of the thermocouples are indicated in Fig 2.5). Conduction through the lip can also be checked by referring to the isoenergetic temperature distribution data. The isoenergetic injection of air at Mach 2.0 displayed an increase in temperature, even though the injectant reservoir temperature was nearly that of the freestream. Conduction to the freestream boundary layer through the lip in this case is not nearly as significant as that displayed by the observed rise. Conduction losses in the case of cooled injection have the opposite sign to the cases of hot injection. Thus, if the temperature rise in the case of hot injection is a result of conduction, then the cooled injection should display a temperature drop, which it does not.

The Reynolds number effect was entertained as another possible explanation for the unexpected rise in temperature. Knowing the injectant stream Reynolds number gives an indication on the status of the boundary layer, it was surmised that the flow could be transitional, which would have resulted in an increase in temperature. Difficulty arises in determining the length scale that should be used in defining the Reynolds number. Figure 3.28 and Figure 3.29 are plots of the injectant recovery factor vs. the Reynolds number based on the distance from the slot for air and helium injections, respectively. These plots indicate no apparent trend and can not be conclusive.

The influence of the pressure gradient near the slot is demonstrated in Fig. 3.30, which shows results of T_{rw}/T_{ti}, and pressure normalized by the freestream pressure P/P_∞ for Mach 2.2 heated injection of air and helium. The pressure distribution in

the first 50 slot heights is constant, indicating that the temperature rise occurs at constant pressure. The pressure rise at 70-75 slot heights is a result of the lip shock reflecting back from the upper wall and impinging on the plate. The length in which this rise occurs is shown to extend to the first forty-five slot heights in the case of air, and seventy slot heights in the case of helium. These distances are shown in Chapter 4 to be well beyond the jet inviscid core region.

An increase in temperature occurs if the injectant boundary layer downstream of the slot undergoes transition. However, it is difficult to prove the status of the boundary layer of the injectant or to detect transition experimentally. It is found that for most of the injection conditions the initial temperature measured near the slot exit (downstream of the shock impingement location) are close to the expected turbulent boundary layer value. Thus, the temperature rise appears to be due to the merging of the injectant boundary layer and the wake emanating from the lip, at the start of the wall jet region. The velocity and temperature profiles in the wall jet are very different than a well-behaved boundary layer so that the mechanism of transfer between momentum and energy are different. The velocity profile of heated air at Mach 2.2 injection (shown in Fig. 4.9), indicates that the velocity profile at distances where the temperature rise occurs have stronger velocity gradients than a normal boundary layer, so that the viscous dissipation is also higher.

If the recovery temperature measured at $x/s = 55$ and the injectant total temperature are used, in the case of Mach 2.2 air injection of Fig. 3.30, the value of freestream Mach number of 1.8 is obtained, which is approximately the value measured by probing that location (shown in Fig. 4.5). A crude explanation of the

temperature rise is that it results from the flow near the wall, which is mostly composed of injectant fluid, slowing down due to merging of the freestream and the injectant.

Because a temperature rise is a direct result of the fluid mechanics, it should also occur with cold injection. However, the effect is not noticeable since the temperature also rises due to the mixing with the hotter freestream. Speculation is that the cooled injection shown previously in Figs. 3.22 and 3.23 exhibits an inflection point at x/s of 50-75, which might indicate the presence of the temperature rise mechanism.

The increase in temperature, in the case of heated injection, results in an increase in effectiveness, as defined by Eq. (1.2b), with downstream distance to values above one. However, in the case of the cooled injection, the existence of the temperature rise mechanism is not advantageous, ultimately causing a reduction in effectiveness. The definition of effectiveness does not take this mechanism into account, a point that must be kept in mind when comparing the performance of heated to cooled injection. In the introduction, it was stated that Cary and Hefner (1972) found that increasing the injectant temperature, which decreases λ for the same Mach number and pressure, results in an increase in effectiveness per unit mass flow rate. It can be surmised that the increase may be partly, if not significantly, due to the recovery mechanism.

Figures. 3.31 and 3.32 are schlieren pictures of the heated Mach 2.2 air and helium injection, respectively. The schlieren pictures only show approximately the first 75 slot heights. The shock waves due to the interaction of the freestream and the slot flow are visible, as they propagate through the test section. Note that the

shock waves become weaker as they propagate downstream. The shock waves in the freestream are at a larger angle in the case of helium injection than in the case of air injection due to dependence of the shock angle on the specific heat ratio γ. The major portion of the upper part of the boundary layer seems to be unaffected as it moves downstream.

3.2.2 Film Cooling Effectiveness

Table 3.1 summarizes the parameters for this study compared to other studies in which the adiabatic wall temperature were measured directly. The flow parameters for the 10 different experiments are listed in Table 3.2. The air experiments are for Mach numbers between 1.2 and 2.2, mass flux ratios λ between $0.38 \leq \lambda \leq 0.82$, and velocity ratios r between $0.57 \leq r \leq 1.1$. The helium experiments are for Mach numbers from 1.2 to 2.2, mass flux ratios between $0.2 \leq \lambda \leq 0.44$, and velocity ratios between $1.6 \leq r \leq 2.6$. The definition of effectiveness for the presentation of the experimental results corresponds to the definition in Eq. (1.2b)

$$\eta = \frac{T_{rw}(x) - T_{r\infty}(x)}{T_{ri} - T_{r\infty}(x)} \qquad (1.2b)$$

where $T_{r\infty}$ is the measured adiabatic wall temperature without fluid injection. The value of T_{ri} is the wall temperature measured just downstream of the injection nozzle.

Figures 3.33-38 show the film cooling effectiveness as a function of downstream distance divided by slot height, x/s. Data above $\eta > 1$ is not shown but it occurs for all heated injection whose velocity ratio r is greater than one. The highest effectiveness value obtained in the cases of data sets shown in Fig. 3.30 are 1.2 and

1.5 for air and helium injection respectively. As indicated in the figures, for each flow the cooling length, X_{cl}, ranges from approximately 30 to 300 slot heights depending on the fluid, the injection rate, and the Mach number. The decrease in effectiveness downstream of X_{cl} also appears to depend on these parameters.

In Fig. 3.33 the results are presented for heated air injection ($T_t \approx 70°C$). For a fixed injectant temperature, increasing the injectant Mach number raises both the velocity ratio and mass flux ratio which results in an increased cooling length. By comparing the results for $M_i = 1.3$ and $M_i = 1.8$, the increase in cooling length is approximately $30s$ but requires a 60% increase in mass flux. When increasing the injection Mach number to 2.2, corresponding to a velocity ratio of unity, the rate of decay of effectiveness beyond unity is reduced compared to other Mach number injections. Additional heating of the Mach 2.2 injection to a value of $T_{ti}/T_{t\infty}$ =1.32 results in a 10% increase in velocity and a 6% reduction in mass flow rate, but this change only results in a small change in effectiveness. Figure 3.34 shows results for cooled air injection ($T_t \approx -40°C$). For cooled injection, the results for $M_i = 1.8$ indicate only a slight increase in cooling length beyond the results for $M_i = 1.5$. When the Mach number is increased to 1.8 in both cases of heated and cooled injection, the improvement in effectiveness is less in the case of cooled injection, whose increase in λ is even higher than that for the heated injection.

Figure 3.35 shows the results of effectiveness with heated helium injection. The results show a large change in effectiveness when the injection Mach number is increased from 1.3 to 1.6. High effectiveness values (greater than 0.8) are achieved for the entire test length of 300 slot heights, when the injection Mach number is

more than 1.6. Figure 3.35 also shows that effectiveness does not improve beyond the Mach 1.9 value, corresponding to a velocity ratio of $r = 2.4$. The injectant of Mach 2.2 is at a higher temperature and produces similar effectiveness values to the Mach 1.9 case. Figure 3.36 presents the measurements for the cooled helium injection studies. The results show an increase in cooling length of approximately $20s$ for a 120% increase in the fluid injection rate. The cooled helium injection produces cooling lengths much smaller than that produced by the heated helium injection. In contrast to air injection, increasing the helium velocity ratio beyond 1, $r > 1$, increases the effectiveness until the value of $r = 2.4$ is reached.

Figure 3.37 presents the effectiveness results for all of the experimental runs as a function of $[x/(s\lambda)][(c_{p\infty}/c_{pi})]$ which is the parameter suggested by the integral analyses (Goldstein 1971) described in appendix A. As shown in the figure, the parameter $[x/(s\lambda)][(c_{p\infty}/c_{pi})]$ nearly collapses all the data, with the exception of the cooled helium injection. Figure 3.37 indicates that the cooling length per mass injection rate $X_{cl}/(s\lambda)$ are close for all the air runs, although the values are slightly larger for the heated air runs. The effectiveness for heated runs also decay at a higher rate than found in the cooled runs, especially for helium. It was shown earlier that the recovery effect was responsible for an initial temperature rise beyond the value at the exit of the slot (this is apparent in the case of heated injection with $r > 1$). The temperature rise results in higher effectiveness values for heated injection and lower ones for cooled injection. This temperature rise with downstream distance occurs more significantly for helium injection. Therefore, the difference between effectiveness values of the heated and cooled injection is expected to be more significant for

helium. In addition to the physical phenomena of increased effectiveness with injectant temperature, higher values of effectiveness for a given $[x/(s\lambda)][(c_{p\infty}/c_{pi})]$ also result from the assumptions made in the integral analysis. The integral analysis that produces the correlation parameter $[x/(s\lambda)][(c_{p\infty}/c_{pi}])$ assumes that the adiabatic wall, $T_{rw}(x)$ in Eqs. (1.2), is equal to the mass averaged temperature downstream of the slot (Goldstein 1971). The mass averaged temperature value is between the adiabatic wall temperature and that of the freestream. Using the adiabatic wall temperature instead of the mass averaged value results in an overestimate of η for heated injection and an underestimated of η for the cooled injection.

In Fig. 3.37 the experimental results are also compared with the experimental measurements by Goldstein *et al.* (1966), Cary and Hefner (1970,1972), and Rouser and Ewen (1973). To compare these studies, the experimental curves of Cary and Hefner, and of Rouser and Ewen are recalculated from their figures to correspond with the effectiveness definition used in the present work. Also, the curves corresponding to experimental results of Cary and Hefner in Fig. 3.37 represents bounds of their data. Except for the results of cooled helium injections and that of Rouser and Ewen, the experiments show similar values of the cooling length parameter $X_{cl}/(s\lambda)(c_{p\infty}/c_{pi})$. Beyond $X_{cl}/(s\lambda)(c_{p\infty}/c_{pi})$, the drop in effectiveness is smallest for the hydrogen injection studies by Rouser and Ewen (1973), followed by the results for sonic air injection into a hypersonic freestream by Cary and Hefner (1970,1972). The drop in effectiveness of the current experiment is more rapid than that of Cary and Hefner (1970,1972). The difference may be attributed to slower mixing in hypersonic flow boundary layers as compared to the mixing in the current supersonic flow

results. The Goldstein *et al.* results are for a similar Mach number as the present experiments. However, their results indicate a much steeper decrease in effectiveness which may be due to the relatively large thickness of the nozzle lip as compared to the thickness of the boundary layer. Their geometry may induce a large wake that would enhance mixing between the injectant and the mainstream. The boundary layer to lip thickness ratio of 0.4 in Goldstein's study is small when compared to 6 and 39 of the study by Hefner, (1976) and 22 and 2.14 of the study by Olsen, *et. al.* (1990), whose finding was that lip thickness did not affect film cooling. The relatively low effectiveness results with air injection of Rouser and Ewen (1973) are anomalous since the flow conditions are similar to that for the present experiments. Their hydrogen results, as compared with that for air or helium injection, do demonstrate the effect of the increasing the injectant heat capacity.

In several of the references (Goldstein 1971; Majeski and Weatherford 1988; and Holden *et al.* 1990), correlation parameters such as $x/(s\lambda^{0.8})$, $x/(s\lambda)Re_i^{-0.25}\nu_\infty/\nu_i$, and $x/(s\lambda)Re_i^{-0.25}(\nu_\infty/\nu_i)(\rho_i/\rho_\infty)^{0.4}(1+0.5(\gamma-1)M_i^2)$ have been used to present the data. These parameters were tried, but they did not produce a better representation of the results than $x/(s\lambda)(c_{p\infty}/c_{pi})$. Note that these parameters are based on the injection conditions as compared to those of the freestream; as a result these parameters merely shift the curves along the axes of the graph and do not change the slope of the curves. In addition, the present data did not correlate with the velocity mixing function introduced by Rouser and Ewen (1970). The velocity function is necessary to obtain h_{tv} in the effectiveness definition of Eq. (1.3).

As a further comparison of the experimental findings, Fig. 3.38 shows the cooling

lengths for each of the experiments as a function of the mass flux ratios. The values of X_{cl} are determined by performing a least squares fit to the data points corresponding to $\eta < 0.80$ and extrapolating the curve to find the $x/(s\lambda)$ value for which $\eta = 1.0$. However, for the helium injection cases of $M_\infty = 1.9$ and $T_{ti}/T_{t\infty} = 1.16$, only the last point tested is near the value of 0.8, and hence the corresponding value of x/s is used. For the case of $M_\infty = 2.2$ and $T_{ti}/T_{t\infty} = 1.24$, all values are larger than 0.8, so its value of X_{cl}/s is not indicated in the figure. For the same injection rate, the helium results show a higher effectiveness than the corresponding air measurements which is due to the relatively high specific heat of helium as compared to that for air. The figure indicates that the heated helium runs clearly have the highest cooling lengths for a given injection rate. The figure shows that the cooling length increases with Mach number for a constant injection rate. The figure also suggests that, except for the anomalous cooling run with $M_i = 1.2$, the heating experiments produced larger values of X_{cl}. The cooling lengths for cold helium injection are not significantly larger than the air results; however, as noted earlier, the decrease in effectiveness downstream of X_{cl} occurred more slowly. The figure again indicates the correspondence between the present cooling lengths and the results from Goldstein *et al.* (1966) and Cary and Hefner (1970,1972).

3.3 Conclusion

The experiments presented in this chapter, examine supersonic film cooling effectiveness for air and helium injection. In the experiments, the static pressure between

the freestream and the injectant were matched, and the total temperature and Mach number of the injectant were varied. The wall pressure and the wall temperature were measured. The adiabatic wall temperatures were measured directly by insulating the surface.

The interaction between the slot-flow and the freestream boundary layer in the vicinity of the slot was investigated both experimentally and computationally. The interaction resulted in a shock structure that is found to be mostly dependent on the slot geometry. The initial injectant conditions were unaffected by the slot-flow shock wave. The presence of the the freestream boundary layer had a negligible effect on the shock structure or the initial injectant conditions. The computations have revealed the presence of a favorable pressure gradient at the wall (which is a result of the radial flow out of the slot-nozzle) that aids in thinning and energizing the boundary layer of the injectant. The reduced interacting effect between the slot-flow and the shock has been attributed to this favorable pressure gradient.

A thorough investigation of the temperature distribution revealed the existence of a temperature rise downstream of the slot, visible in cases of heated injection of velocity ratio greater than one, that is higher than both the injectant and freestream recovery temperatures. The observance of this temperature rise has not been documented before. To ensure that the temperature rise was a result of the fluid dynamics, the influence of conduction and pressure gradient were eliminated as possible causes for the temperature rise. The influence of the Reynolds number effect has also been discussed. As Chapter 4 will indicate, the temperature rise occurs in the wall jet region where the flow deviates from that of a regular boundary layer, resulting in

the differences in the recovery factor. The rise may be attributed to higher viscous dissipation in the initial region of the wall jet region (where the temperature rise occurs) than that experienced by the boundary layer.

Since this temperature rise is not visible in the cooled injection, it is hypothesized that the inflection point present in some of the cooled injections is a result of the heating mechanism. This mechanism may be responsible for earlier findings of increased effectiveness per mass flux ratio with increased temperature.

The consequence of the heating mechanism on the effectiveness definition is that it produced values greater than unity in the case of heated injection and reduces it in the case of cooled injection. Care has to be taken when comparison are made between heated and cooled injection or injections at different temperatures. The heating mechanism demonstrates that using the definition of effectiveness without knowing the underlying physics can lead to erroneous results.

Generally, effectiveness improves by increasing the injectant Mach number. However, for the cold runs of helium and air, the change in Mach number produces a small change in effectiveness. For a fixed mass flux ratio λ or velocity ratio r, varying the Mach number of air injection produces a small change in the cooling length per unit mass flux $X_{cl}/(s\lambda)$. In the case of helium injection, keeping λ constant and increasing the Mach number produces a higher cooling length. To vary the injectant Mach number while maintaining the same mass flux ratio λ or velocity ratio r involves changing the temperature. To attribute the increase in cooling length to Mach number alone is not conclusive, since the heating mechanism, results in an improvement for heated injection and the opposite for cooled injection. Comparison

between helium and air experiments indicates that the effectiveness increases with the heat capacity of the gas. However, the specific heat had a small effect on the value of cooling length per unit mass flux X_{cl}/s in the case of cooled injection, so that the improvement due to specific heat in the case of heated injected was also a result of the heating mechanism.

High effectiveness values far downstream are found with the heated injections for velocity ratios greater than one. Heated helium injection of velocity ratio greater than 2 produce effectiveness values greater than 0.8 for 300 slot heights downstream of injection point. The increase in temperature downstream of the slot could partly explain the high effectiveness values obtained in the cases of heated injections with velocity ratios r greater than one.

Previous studies that directly obtained the adiabatic wall temperature are compared with the current experiment. The simple correlation parameter $x/(s\lambda)(c_{p\infty}/c_{pi})$ is demonstrated to be the best choice for correlating the data. However, the cooled helium injection does not conform to this correlation.

Chapter 4

Flow-Field Measurements and Shock Wave Interaction

The focus in this chapter is directed towards the impact of shock interaction on film cooling effectiveness. It has been shown that film cooling can produce impressive results, as far as maintaining the wall temperature close to the coolant temperature. The question is raised to whether or not a shock wave impinging on the film coolant flow would hinder such achievement. Results from the previous chapter indicate that helium performs better than air as a film coolant, but it is not clear if that is still the case with shock interaction. It has also been mentioned in the introduction that recent studies (e.g., Holden *et. al.* 1990) indicate that there are discrepancies in the literature. These issues are tackled in this chapter by first probing the flow to identify the flow-field before interaction and then by impinging a two-dimensional shock wave on the flow. The temperature and pressure distribution are recorded for

different shock wave strengths and injection conditions.

4.1 Air and Helium Injection Pitot Probe Profiles

Preliminary runs were made to investigate the two-dimensionality of the injectant flow. The pitot pressure profiles of the injectant obtained at three spanwise locations were identical. An example of this was shown in section 2.7. In addition, values of wall pressures and temperatures located off center were the same as the center values.

The impact-probe profiles were measured for the injection of helium and air at the total temperature equal to that of the freestream, $T_{ti} = T_{t\infty} \approx 300$ K. The injection Mach numbers were $M_i = 1.3$ and $M_i = 2.2$ for helium and $M_i = 1.2$ and $M_i = 2.2$ for air, and the static pressure in the injected flow matched that in the freestream. For the film-heating experiments, the injected gas was heated to temperatures ranging from $T_{ti} = 335$ K to $T_{ti} = 425$ K. Table 4.1 presents the range of injection parameters for the heated and unheated conditions. The table also includes the momentum flux ratio $\rho_i u_i^2 / \rho_\infty u_\infty^2$ and the slot Reynolds number, Re_s, based on the injection Mach number, injection temperature, and slot height.

Impact-probe profiles are presented in Figs. 4.1 and 4.2 for air injection and in Figs. 4.3 and 4.4 for helium injection. The flow was probed at several axial locations during different experimental runs. While probing at a single location, the stagnation pressure of the injectant varied with time by no more than $\pm 3.8\%$ of the mean value. For profiles at a single injectant Mach number, the difference between the mean value of the injectant stagnation pressure for each profile was less than $\pm 5\%$. In both the

air and helium studies at low-injection Mach numbers, the first station measured is not at the exit of the slot ($x/s = 0$) but downstream of the slot shock structure at $x/s = 3$.

In the case of the Mach 1.2 air injection shown in Fig. 4.1 for $x/s = 3$, 41, 58, and 96, the total pressure of the injectant is small compared to the freestream, $P_{ti}/P_{t\infty} = 0.18$. At $x/s = 3$, the profile clearly shows the slot flow and the freestream boundary layer as they start to mix. The sudden change in the profile at $y \approx 3.8$ mm is due to the probe passing the lip shock. By $x/s = 41$, the flat section of the injection profile has disappeared, indicating that the shear layer emanating from the lip has merged with the injectant boundary layer. For the profiles corresponding to $x/s = 58$ and $x/s = 96$, the pressure profiles for $y < 2$ mm appear to match the profiles at $x/s = 41$. At these downstream axial locations, the pressure profiles for $y > 4$ mm resemble the pressure variation for $y > 3$ mm at the axial location $x/s = 41$. In addition, these pressure profiles resemble the original freestream boundary-layer profile that is shown more clearly at $x/s = 0$ in Fig. 4.2. This comparison suggests that this region of the flow has not participated in the mixing process, but has been transversely displaced by the injectant. This behavior seems to be apparent for all cases tested.

The profiles for the air injection at $M_i = 2.2$ are shown in Fig. 4.2 for three axial locations, $x/s = 0$, 55, and 93. The ratio of the injectant total pressure to the freestream value measured at the end of the test rhombus is $P_{ti}/P_{t\infty} = 0.63$, which is closer to that of the freestream than for the Mach 1.2 injection test. The profile at the exit of the slot near the wall is indented. This indentation also appears in Peak's pitot pressure profiles. The experiment executed by Peak (1966) is an air-air

injection experiment with injection Mach number of 2.37 in a Mach 1.8 freestream. In addition, the slot height to probe diameter is comparable to this study. The indentation is a result of the probe interaction with the injectant boundary layer. As the probe approaches the wall, the probe's detached shock interacts with the injectant boundary layer. This interaction increases as the probe approaches the wall causing the boundary layer to separate and the pressure to rise. The indentation was first suspected of being a result of the slot geometry. However, a closer look indicated that any adverse effect due to the geometry would have induced a profile that had the opposite trend than that found by probing. In the cases of the Mach 2.2 and 1.2 injection, the radius of curvature to throat height is 13 and 7, respectively, exceeding values recommended for supersonic nozzles. The indentation is smaller in the Mach 1.6 case shown earlier in Fig. 2.11 and it does not appear in the Mach 1.2 case. Therefore, the indentation is reduced as the Mach number is lowered. Although the exit plane of the Mach 1.2 injection case is located closer to the curved surface than that of the Mach 2.2 injection case, the distortion due to geometry should have been more severe than the Mach 2.2 injection case.

The wake from the lip and the freestream boundary layer are more visible than in the previous case since, in this case, the first station is measured at the slot exit. By fifty slot heights the shear layer has merged with the injectant boundary layer, and the flow continues to form a boundary-layer type flow. As with the lower Mach number case, downstream of $x/s = 58$ the flow profile near the wall seems to be unchanged. The profile for Mach 2.2 at $x/s = 90$ resembles the profile for Mach 1.2 at $x/s = 58$. For a given axial location downstream of the slot, the width of the

viscous layer is slightly larger for $M_i = 2.2$ injection than for $M_i = 1.2$ injection.

In the case of Mach 1.3 helium injection in Fig. 4.3, behavior similar to the air injection of Mach 1.2 is observed for the flow development near the wall. The total pressure in the jet is $P_{ti}/P_{t\infty} = 0.2$. The boundary layer of the injectant leaving the slot is larger in this case than for the Mach 1.2 air injection. The shear layer in the case of helium injection is also larger than for air, which is possibly due to the higher velocity difference between the injectant and the freestream.

In Fig. 4.4, the injection of helium at $M_i = 2.2$ shows a profile at the exit of the slot similar to that for air at $M_i = 2.2$. The injectant impact pressure is near that of the freestream with a total pressure ratio of $P_{ti}/P_{t\infty} = 0.7$. By fifty-five slot heights, the shear layer merges with the injectant boundary layer. The flatness of the impact-probe profile at the lower part of the lower layer is due to the high-injectant total pressure and is not due to the helium stream persistence at that location. The viscous layer in this case is larger than that of both air injection cases and slightly larger than the Mach 1.3 helium injection case.

For all the studies, the freestream profile shows that the value of the pitot pressure is nearly the same at all stations, indicating that the shock waves propagating through the flow are weak.

By reviewing the pitot pressure profiles presented for different injection Mach numbers, it can be generalized that the newly formed boundary layer can be divided into three layers: 1) the upper layer, which resembles the highest part of the initial freestream boundary layer, 2) the middle layer, which owes its development to the wake originating at the lip, and 3) the lower layer, whose shape is influenced by the

initial injectant boundary layer.

Before proceeding to the next section, a few points about the pitot pressure profiles can be made that are relevant to shock wave interaction. The behaviour of shock interaction depends on the local properties of each layer, which also depends on the location of interaction. In general, those profiles that are fuller are the ones that provide more resistance to shock wave induced separation.

In the cases of low Mach number injection the mixing occurs quickly, and the three layers are established by approximately $x/s = 41$, so that shock interaction with this case would qualitatively resemble that of the high Mach number injection at distances farther away from the slot (possibly $x/s > 90$).

By comparing the profiles of the Mach 1.2 injection for $x/s > 40$, the profiles for the helium injection are less full than that of air. The higher velocity of helium injection, which is approximately three times that of air, resulted in a larger slip velocity, therefore inducing a larger wake. The wake growth rate also shows a dependence on the density ratio but to a lesser degree than the velocity ratio. The same can be found when comparing the helium and air injections at Mach 2.2. Also of concern is the fullness of the injectant boundary layer (or the lower layer) located beneath the wake. In the cases tested, the flow conditions are such that the boundary layers next to the wall are less full for the cases where the flow middle layer is less full.

4.2 Temperature and Velocity Profiles of Mach 2.2 Air Injection

The temperature profiles are obtained for both isoenergetic and heated injection ($113 \pm 3°C$) for Mach 2.2 air injection. The recovery temperatures are measured at x/s =17, 34, 72 and 110. To reduce the recovery temperature to the actual total temperature, the Mach number profile at each station had to be known. The total temperature profiles are estimated from the Mach number profiles at $x/s = 0, 55, 93$. The Mach number profile nearest to the recovery temperature profile is used to reduce the recovery temperature to the total temperature. The Mach number profiles were obtained using the static pressure and the pitot pressure, and they are shown in Fig. 4.5. At $x/s = 55$, the Mach number profile exhibits a nearly flat region in Mach number (≈ 1.8) at $1.5\ mm < y < 2.5\ mm$. If the boundary layer next to the wall at $x/s = 55$ can be thought of as one that behaves like a regular turbulent boundary layer with a uniform free Mach number of 1.8, a wall recovery temperature of 0.95 is obtained which corresponds to the value measured experimentally at that location (shown in Fig 3.30). This was pointed out earlier in section 3.2.1 in association with the temperature rise observation.

The temperature profiles of isoenergetic injection and heated injection are shown in Fig. 4.6 and Fig. 4.7, respectively. In the case of isoenergetic injection, the injectant temperature was not the same as the freestream; injection temperatures ranged from $10°C$ to $16°C$. The potential core of the injectant and the wake are clearly visible at the first probing station $x/s = 17$. In the case of the heated injection, the

temperature distribution at $x/s = 17$ indicates a larger thermal layer and smaller thermal core than that of isoenergetic injection. The strong temperature gradients near the wall at the first station of the heated injection represent the injectant thermal boundary layer, which disappears later, resulting in a flat profile by $x/s = 100$. The temperature gradients for the last two stations are near zero, indicating that the wall is nearly adiabatic.

The temperature profile of the heated Mach 2.2 injection, shown in Fig. 4.7, indicates that the heating between $x/s = 17$ to $x/s = 110$ from $y > 1.5$ mm to $y < 3$ mm is much more than the insignificant change next to the wall. It is speculated that the shear layer emanating from the lip contains a small amount of boundary layer fluid and that mixing occurs between the shear layer and the injectant boundary layer at a slow rate; therefore, the change in wall temperature is gradual.

The Mach number profile and total temperature profiles are used to evaluate the velocity profiles. The velocity profiles are shown in Figs. 4.8 in the case of isoenergetic injection and Fig. 4.9 in the case of heated injection. The velocity profile indicates the absence of the potential core by the second station at $x/s = 34$. The velocity profile at $x/s = 34$ displays strong velocity gradients which in turn increases the viscous dissipation. The increase in viscous dissipation results in an increase in the recovery temperature, which has been displayed earlier in Chapter 3.

4.3 Wall Pressures and Temperatures Without Shock Interaction

Before discussing the experimental results obtained with an impinging oblique shock, the measurements of wall static pressure and the adiabatic wall temperature with injection of air and helium at the two different Mach numbers of $M = 1.2$ and $M = 2.2$ are reexamined. Figures 4.10 and 4.11 show the distribution in wall static pressure normalized by the freestream static pressure, P/P_∞, and the recovery temperature normalized by the total temperature of the injected gas, T_{rw}/T_{ti}.

For air injection as shown in Fig. 4.10, the wall static pressure is fairly constant over the first sixty slot-heights. There is an increase near $x/s \approx 70$, which is due to the reflected lip shock impinging on the wall. The pressure distribution also indicates an adverse pressure gradient, associated with injection, which increases with the injection Mach number. The wall temperatures were measured for approximately the same total injection temperature ($T_{t\infty} = 342$ K). The temperature distribution for $M_i = 1.3$ decreases with downstream distance as the injected fluid begins to mix with the freestream at $T_{t\infty} \approx 300$ K. However, the recovery temperatures corresponding to $M_i = 2.2$ show an increase over the first forty slot-heights. In this region of the flow, the total pressure profiles, as shown in Figs. 4.1 and 4.2, are considerably different due to the difference in injection velocity and Mach number. For flows at different Mach numbers and at the same total temperature, the recovery temperature is lower for the higher Mach number flow. Hence, the recovery temperature for $M_i = 2.2$ is lower than for $M_i = 1.3$ in the region of the flow just downstream of the nozzle.

The helium results, as shown Fig. 4.11, are similar to those for air injection. The wall static pressure with fluid injection increases at $x/s = 60$ due to the impingement of the reflected lip shock at that location. The overall pressure increase is larger for the injection at $M_i = 2.2$ than for that at $M_i = 1.3$ and is slightly larger than the pressure gradient associated with air injection. For $x/s < 80$, the recovery temperature is higher for $M_i = 1.3$ than for $M_i = 2.2$. This difference can again be attributable to the difference in injection Mach number. As compared with the air results, the downstream distance is considerably longer over which the $M_i = 2.2$ temperatures are lower than the $M_i = 1.3$ results. For axial locations corresponding to $x/s \geq 80$, the wall temperatures are approximately the same; however, this similarity may be a result of the slight difference in total temperature of the injectants. Further downstream the $M_i = 1.3$ temperatures decrease more rapidly than for $M_i = 2.2$. In addition, the recovery temperature appears to increase in the region where the lip shock impinges on the flow; the increase is expected since the shock wave decelerates the flow, and the drop in the flow velocity results in an increase in the recovery temperature. However, this effect was not observed with the air experiments.

The pitot pressure profiles indicate that for all injection cases the jet core of the injectant disappears when reaching distances of less than 50 slot heights. The end of the inviscid core region is considered to be the point where the value of temperature changes from the initial value and effectiveness drops from unity. In the case of air at Mach 2.2 injection the velocity profiles indicates that the core jet region ends at a distances less than 34 slot heights; however, the wall temperature distribution

indicates no drop, but the value of the initial wall temperature is sustained for as long as 100 slot heights. Contrary to what has been previously believed, high value of effectiveness can occur in the wall jet region.

4.4 Wall Pressures and Temperatures with Shock Interaction

Figures 4.13-4.17 demonstrate the effects of an oblique shock wave on the film-heated flows. The results in Figs. 4.13, 4.15 and 4.16 were obtained by measuring the wall static pressure and the equilibrium wall temperatures for a flow with injection and with an impinging shock. Separation due to shock wave impingement was determined by: 1) inspection of the wall pressure distribution for the presence of an inflection point and 2) using the schlieren system. The type of separation discussed in this study is what has been termed "effective" separation, which refers to the onset of the most dramatic change in the flow field (Delery 1986). In several instances the tunnel unstarted just downstream of the interaction region. Since the separation process does not depend on the downstream conditions, only the recompression region is distorted by the tunnel unstart and not the strength of the leading reflected shock wave. In these cases, the data in the distorted region of the interaction are not shown in the plots. For one of the data sets in each figure, the shock strength was less than that required to produce separation in the flow. For this shock strength, the distribution in the wall static pressure and temperature were recorded, and then the injected flow was stopped. After the flow equilibrated and without changing the angle of attack of the wedge, the wall static pressure distribution was measured without

injection. A subsequent experiment was also run for the same injection conditions but with a slightly larger angle of attack so that the shock strength was large enough to separate the flow. The strength of the weaker shock is then seen as the strength at incipient separation. To compare incipient separation with and without injection, an experiment without injection showed that the boundary layer could withstand an increase in the pressure ratio up to a factor of 2.4 before separating.

For flow without injection, the shock wave caused by the nozzle step is weak and results in a change in freestream Mach number from 2.40 to 2.38. The boundary layer profile just upstream of the interaction location, shown in Fig. 4.12, is nearly identical to the profile just upstream of the slot. In the figure, the boundary layer profile of the freestream has been moved in the vertical direction to take into account the displacement of the step. The step shock returns after impacting the wall opposite to the instrumented plate and intersects the expansion side of the wedge's surface, and it does not interfere with the shock wave emanating from the wedge. However, for the isobaric injections presented in this section, the lip shock is stronger than the lip shock without injection. Moreover, on reflection from the opposite wall, the lip shock intersects with the shock wave caused by the wedge and increases its strength. This increase should be accounted for when comparing the shock interaction with and without injection.

Figure 4.13 shows the effect of shock-wave interaction with heated air injection at Mach 2.2. With injection, the flow did not separate for a pressure jump of 2.5, which is slightly higher than that required to separate the flow without injection. For a slightly larger wedge angle of attack, the flow separated as indicated in the figure

by the pressure plateau. Also shown in the figure is the pressure distribution for the same angle of attack but without injection. In comparing the two pressure profiles with separation, the separation point with injection is about twenty-slot heights further downstream, and the separation shock is stronger for the same angle of attack. A contribution to the increase in the peak pressure may result from the reflected lip shock intersecting with the shock generated by the wedge and increasing the intensity of the shock wave. The drop in the pressure distribution after 90 slot heights results from the expansion wave impinging on the wall from the trailing edge of the wedge. Also shown in the figure are the corresponding temperature distributions as well as the distribution without shock impingement. For the flow with the weaker shock, the difference in the temperature measurements does not start until approximately $x/s = 80$, near the end of the interaction region. The difference in the temperatures in this region may also be a result of the expansion wave from the trailing edge of the wedge that is not present for the no-shock experiment. For the separated flow, the temperature difference begins when the pressure starts to increase; then the temperature decreases sharply with downstream distance. The temperature distribution for this case indicates that as long as the flow is attached, the temperature distribution maintains its value and that effectiveness will not significantly change. However, since the expansion wave intersects with the flow at about 15 slot heights downstream from the beginning of the interaction (in the case of attached flow), this conclusion is limited to the 15 slot heights downstream of the interaction. Farther downstream of the interaction region, the shock wave may enhance the mixing between the injectant and the freestream boundary layer, so that effectiveness would

be decreased.

Figure 4.14 is a series of schlieren pictures of shock waves of increasing strength interacting with the Mach 2.2 air injection. The flow with shock interaction in the first two cases resembles that of a regular shock wave boundary layer interaction. The last picture, corresponding to incipient separation, shows a change in the flow near the wall. The reflected shock wave (bright region) is smeared over a larger distance as it propagates through the boundary layer to the freestream. The dark shading next to the reflected shock is an expansion wave. Unfortunately, due to the schlieren pictures quality, the distinction between incipient interaction as a result of shock wave interaction with and without injection cannot be resolved.

Figure 4.15 presents similar results for heated helium injection at $M_i = 1.3$. Without injection, the shock wave impinging on the boundary layer results in an increase in the wall static pressure by a factor of 1.6. For the same angle of attack but with injection, the static pressure rise appears more gradual than that produced by the shock-wave/boundary-layer interaction obtained without injection. The upstream influence is larger than without injection, and the pressure jump with injection is higher. A slight increase in the wedge angle of attack separated the injectant, indicating that the incipient pressure ratio is approximately 1.7, which is smaller than that obtained without injection of 2.4. This indicates that injection induces separation, which agrees with the finding of Holden *et al* (1990). With the stronger shock, the wall temperature shows an increase in the region further upstream and in approximately the same location as the beginning of the pressure increase. By the separation point, the temperature ratio begins to drop more quickly as compared to

that resulting from the weaker shock. The weaker shock had actually an insignificant influence on temperature, and it seems that, as long as the flow is attached, the temperature is slightly affected.

Figure 4.16 shows the shock interaction with injection of heated helium at Mach 2.2. With injection and at incipient separation, the shock strength corresponds to a pressure rise of 2.0, which is higher than the incipient shock strength at the lower helium-injection Mach number. By comparing the pressure profiles in Figs. 4.3 and 4.4, the Mach 2.2 injection profile upstream of the interaction is fuller than that obtained by Mach 1.3 injection at $x/s = 60$. The figure shows that the rise in the pressure occurs more rapidly than for the $M_i = 1.3$ results, and there is a more significant temperature increase in this region. When the injection is stopped and without change in the wedge angle, the ratio of the pressure rise to the upstream pressure is 1.9. The ratio of 1.9 is higher than separation value obtained in the case of $M_i = 1.3$ injection which was found to be 1.6. For the higher shock strength, the temperature distribution seems to follow the same pressure ratio distribution pattern and peaks where the pressure reaches its maximum. Even with injection at Mach 2.2, the flow separates at still a lower value than that without injection.

The influence of the shock wave on the film coolant flow is two-fold: one is to slow down the flow and the other is to enhance mixing between the injectant and the freestream boundary layer. If the injectant was cold, as in an actual application, the recovery temperature increases and effectiveness decreases due to the influence of deceleration and mixing, respectively. However, in the case of heated injection the deceleration causes the recovery temperature to rise and mixing causes it to drop.

In both cases of helium injection separation is induced; whereas in the case of air injection, it is not. As shown in table 4.1, the momentum flux for the Mach 2.2 helium injection condition is higher than the Mach 2.2 air injection condition, indicating that the prevention of separation is not solely a function of the initial momentum of the injected flow. An explanation can be deduced from the flow profiles of Figs. 4.2, 4.3, and 4.4. Separation depends on the fullness of the Mach number profiles and the size of the subsonic portion of the incoming boundary layer. The air injection profile in Fig. 4.2 at the location nearest to the shock impingement location ($\approx x/s = 60$) is fuller than that of both helium injections. Figure 4.17 compares the profiles of air and helium injection at $M_i = 2.2$ just upstream of the shock impingement location. For the case of air injection at $M_i = 2.2$, using the Rayleigh formula and the profile at $x/s = 55$, the sonic line is estimated as being within 0.1 mm from the wall. In the case of helium injection at $M_i = 2.2$, the composition of the flow must be known to estimate the location of the sonic point and the momentum flux. However, if the flow is assumed to be entirely helium or entirely air, the sonic point for either case would be greater than 0.2 mm from the wall, and the momentum flux of helium injection would be inferior to air injection. These comparisons (the fullness of the incoming profile and the size of the subsonic region) suggest that the flow with air injection could withstand a stronger adverse pressure gradient.

If the interaction was next to the slot, as in Alzner and Zakkay (1970, 1971), the helium would be expected to perform better than air in preventing separation due to the greater momentum flux for the helium injection. However, if the interaction takes place farther downstream, the situation is different. Mixing between the freestream

boundary layer and the injectant reduces the momentum of the injectant, and a new boundary layer or a layer made of a boundary layer and a wake is formed composed of the injectant and the freestream. Injecting a gas with a higher speed of sound increases the speed of sound and the size of the subsonic region within the new formed layer, reducing the fullness of the Mach number profile, making it more prone to shock wave separation. Similarly, in using hydrogen as a film coolant (as proposed for N.A.S.P.), a problem is likely to develop farther downstream of the injectant slot since hydrogen has a much higher speed of sound than air.

To illustrate the influence of injection on the fullness of the Mach number profile, consider a flow that behaves like a boundary layer, with a velocity profile of $u/u_\infty = f(y/\delta)$, where $f(y/\delta)$ is a monotonically increasing function. The Mach number distribution can be written as:

$$[M(y/\delta)/M_\infty]^2 = [(\gamma\Re)_\infty/(\gamma\Re)][(u/u_\infty)^2][T_\infty/T]$$

where γ is the specific heat ratio, $\Re$ is the gas constant. The temperature ratio can be approximated to be a function of the velocity ratio

$$T_\infty/T = g(u/u_\infty) = g(f)$$

where g is a monotonically increasing function. then

$$[M(y/\delta)/M_\infty]^2 = [(\gamma\Re)_\infty/(\gamma\Re)][f^2(y/\delta)][g(f)] \,.$$

For a homogeneous boundary layer, the ratio $[(\gamma\Re)_\infty/(\gamma\Re)]$ can be approximated to be unity, but for a mixture this ratio becomes important. For an identical velocity

profile (a prescribed value of f)

$$[M(y/\delta)/M_\infty]^2 \propto [(\gamma\Re)_\infty/(\gamma\Re)] \, .$$

For a boundary layer with helium injection the lower portion may be composed mostly of an injectant, the ratio of $[M(y/\delta)/M_\infty]^2$ can be reduced by a factor of 8 in some conditions of the experiments, and a factor of 14 if hydrogen is injected. The presentation of the Mach number ratio as the ratio squared is indicative of the relevance of the above discussion to the local momentum flux ratio, which is $\rho u^2 = \gamma p M^2$.

Because the profile of the flow with a film coolant exhibits several layers, two possibilities of flow reversal can exist: a boundary layer reversal in the lower layer and a wake reversal in the middle layer (first pointed out by Peak 1966). As a result, each region has to be treated separately. The preference would be to inject in a way that reduces the growth of the injectant boundary layer and the wake (the wake growth can be reduced if the velocity of the injectant is not too high). Perhaps, a high Reynolds number, low Mach number, and intermediate velocity injection. More experiments are required to determine the growth rate of the wake as a function of initial conditions injection, which will aid in determining the appropriate conditions that will minimize the loss of the axial momentum of the injectant flow.

Figure 4.18 presents results for a shock wave of strength that can separate the helium injectant. The plot shows a number of isoenergetic helium injection rates starting with no injection up to a mass flux ratio of $\lambda = 0.58$. The nozzle is positioned at the Mach 2.2 injection case. When the injection is increased to $\lambda = 0.063$ subsonic

injection the pressure rise is slightly reduced, but the upstream influence length is increased approximately twice. The first indication of separation occurs when the injection is increased to $\lambda = 0.16$. The influence length is large, nearly sixty slot heights. Since the upstream influence is a strong function of the size of the subsonic region of the incoming flow, it is conceivable that the injection of $\lambda = 0.16$ produces a large subsonic layer near the wall. Increasing the injection beyond $\lambda = 0.16$ results in a decrease of influence length which is due to the decrease in the subsonic region near the wall. However, after injecting 25% over the isobaric injection ($\lambda = 0.46$) no reduction is observed.

4.5 Conclusions

The current experiments investigate the effects of shock-wave impingement on both air and helium injection. Two injection Mach numbers are examined for each fluid injection. The impact-pressure profiles are obtained for distances up to ninety slot-heights. The total-temperature profiles for the Mach 2.2 air injection are also obtained and used to determine the velocity profiles.

The injection of the flow appears to lift the freestream boundary layer from the wall and transversely displace it. The upper part of the freestream boundary layer does not appear to participate in the mixing process. For the most part, the film cooling flow can be divided into three layers: 1) the upper layer which resembles the highest part of the initial freestream boundary layer, 2) the middle layer, a wake composed of freestream flow and injectant flow, and 3) the lower layer, a boundary

layer that is strongly influenced by the initial development of the injectant flow. The higher velocity of the helium injection induces a larger wake than that of air; this has been shown to have an influence on the fullness of the profile at downstream distances. Helium injection also results in a larger boundary layer next to the wall than in the case of air. The profiles and wall temperature distributions indicate that effectiveness values near unity are found in the wall jet region.

At approximately sixty slot-heights, a two-dimensional oblique shock is generated to impinge on the flow; the temperature measurements in this location of the flow indicate that the slot injection is beneficial for maintaining the surface at a desired temperature. However, with the shock impingement, the effectiveness of the film coolant is affected. In the experiments, the strength of the shock is varied to study flow with and without separation. Because the shock impingement is located well downstream of the injection nozzle, the experimental results cannot be directly compared with other experiments in which the shock impingement occurs much closer to the nozzle. It has been noted that discrepancies between previous studies are due to differences in the shape of the injectant profile at the shock impingement location, which is a function of downstream distance from the slot.

In the case of shock interaction, the helium injection is observed to induce separation. However, increasing the injection Mach number appears to delay separation. Air injection of Mach 2.2 is superior to both helium injection Mach numbers in preventing separation, even though its momentum flux is smaller than the Mach 2.2 helium injection. The induced separation in the case of helium injection has been attributed to the reduced fullness of its Mach number profile $M^2(y)$ just prior to the

interaction, when compared to air or the original freestream boundary layer. The sonic line location is estimated to be nearer to the wall for the air injection. Injecting a higher speed of sound fluid increases the speed of sound of the boundary layer, increasing its subsonic region and reducing the fullness of its Mach number profile, and, therefore, increasing its susceptibility to shock wave separation.

The effect of the shock induced separation on the recovery temperature is more pronounced for the high-Mach-number helium case. When the injectant is separated, the recovery temperatures decrease more rapidly with downstream distance than the flows in which separation did not occur. However, as long as the flow remains attached, the influence of shock impingement on the recovery temperature is not large.

Chapter 5

Summary and Concluding Remarks

The present work has been motivated by a rekindled interest in active cooling of hypersonic transport. Film cooling has been recognized as a potential method for protecting the surfaces of structures in the scramjet engine against the effects of aerodynamic and combustion induced heating .

A literature survey indicated a limited knowledge of the physical mechanisms that have an impact on film cooling performance. The goal of this study has been to investigate aspects of the underlying physics of the problem, in order to resolve some of the discrepancies that have surfaced during examination of the literature. The influence of several factors has been investigated, including the effects of injectant molecular weight, Mach number and temperature. The relationship of the injectant Mach number to the adiabatic wall temperature is investigated here for the first

time. The influence on the effectiveness of the impingement of a two-dimensional shock wave has also been studied. A combination of injection conditions and shock strengths have been investigated.

Computational and experimental investigations on the interaction between the freestream boundary layer and slot flow indicate that the injectant shock structure is mostly dependent on slot geometry. Shock waves in both streams have a small influence on the initial conditions prior to the streams' interaction. It is also demonstrated that the simple nozzle geometry used in this study provided a favorable pressure gradient for the injectant boundary layer. The short nozzle, which has a sharp trailing edge, can support both structural and thermal stresses at levels above those handled by a nozzle designed for parallel flow.

Careful investigation of the recovery wall temperature distribution revealed the existence of an initial temperature rise that has not been documented before. This temperature rise is visible when the injectant is heated and has velocities higher than that of the freestream. A temperature increase should also occur with cold injection. However, the effect is not as noticeable as in heated injections, since in the case of cooled injection, the temperature also rises due to the mixing with the hotter freestream. It is hypothesized that the existence of an inflection point in various cooled injection temperature distributions is due to the heating mechanism. If the injectant boundary layer is initially laminar, the rise in temperature can be due to transition. However, the recovery temperature near the exit of the slot indicates that most of the injectant boundary layers produce values that are typical of a turbulent boundary layer. Therefore, the increase in temperature is attributed to the merging

of the injectant boundary layer and the wake emanating from the lip. The merging process produces a layer with larger velocity gradients than that of a well-behaved boundary layer, resulting in higher viscous dissipation. Therefore, exchange of heat and momentum in the wall jet region, where the merging process occurs, is expected to be different than that of a well-behaved boundary layer. It is important to note that the occurrence of transition is unfavorable to film cooling effectiveness.

Behavior of the heating mechanism demonstrates that guidelines must be followed in order to accurately interpret effectiveness values or correlations. According to existing definitions of effectiveness, the heating mechanism in the case of heated injection improves the effectiveness, while in the case of cooled injection it reduces the effectiveness. Direct comparisons between effectiveness values for different injection temperatures without consideration of the heating mechanism can lead to misleading conclusions.

The influence of increasing the injection Mach number on effectiveness is found to be small for cooled injection and more pronounced for heated injection. This appears to be a direct result of the heating mechanism which augments the initial temperature rise as the Mach number is increased. An increase in the specific heat of the injectant, in the cases of cooled injection, slightly improves the cooling length per unit mass flux X_{cl}/λ. However, increasing the specific heat reduces the decay in effectiveness after the cooling length has been reached, thus, increasing the specific heat has a greater effect after some mixing has occurred. During the case of heated injection, an improvement in the cooling length when using helium instead of air may be a result of the heating mechanism. Matching the injectant and freestream

velocities is not optimum as suggested by previous studies, since effectiveness has been found to increase with velocity ratios greater than one.

In general, results from film cooling experimentation point to a promising technique for thermal control of walls under extreme thermal conditions. Cooling lengths greater than 100 slot heights were obtained, 300 in some cases of heated injection. Nevertheless, the capability of thermal control during film cooling has been undermined by an apparent susceptibility to shock wave induced separation. Although slot injection, when properly applied, can be used to prevent separation, the fullness of the Mach number profile prior to the shock interaction is the determining factor for resistance to separation, since M^2 is proportional to the momentum flux ratio ρu^2. Flow-field probing has shown that high velocity injections induce a large wake. This, in turn, influences the growth of the injectant boundary layer which results in reduced fullness of the Mach number profile. Helium injection, which has a higher velocity and a lower Reynolds number than air, causes a larger wake and thicker boundary layer near the wall. More importantly, the injection of the higher sound speed gas reduces the fullness of the Mach number profile.

For attached flow, the shock influences the wall temperature by slowing down the flow and enhancing mixing between the freestream boundary layer and the injectant. If greater mixing between the injectant and the freestream boundary layer occurs, the influence of the shock wave on the temperature is less. Once separation occurs, the film coolant is lifted from the wall and consequently the recovery temperature drops sharply.

In applying the findings of this research to the practical use of N.A.S.P.'s scramjet

engine in which hydrogen is the only available fluid for cooling, there is a compromise between injection conditions that are favorable for film cooling and ones that are unfavourable for shock wave induced separation. For example, it is preferable for heat protection that the injectant boundary layer to be laminar, but a turbulent injectant boundary layer would provide a stronger resistance to separation. Hydrogens has a high specific heat ($\approx$ 14.5 times that of air) which is advantageous for the purpose of film cooling beyond the cooling length. However, its high speed of sound increases its susceptibility to shock induced separation. For conditions that are favourable to preventing separation, the fullness of the Mach number profile can be reduced by decreasing the deficit in the wake and lowering the growth rate of the injectant boundary layer. However, injecting at a higher velocity than the freestream has been shown to increase film cooling effectiveness. Assuming that boundary layer of the injectant grows at approximately the same rate as a flat plate boundary layer, it is suggested that the injection be made at a high Reynolds number, low Mach number, and moderate velocities. Since hydrogen has a lower viscosity than both helium and air, it is expected that the lower viscosity of hydrogen influences the development of the injectant boundary layer differently. For matched pressure injection at the same Mach number and temperature, the Reynolds number of hydrogen injection is at least half that of air. Unfortunately, more studies are required to investigate the conditions that would result in favourable profiles that could withstand adverse shock interaction effects; this suggests a fruitful area of research.

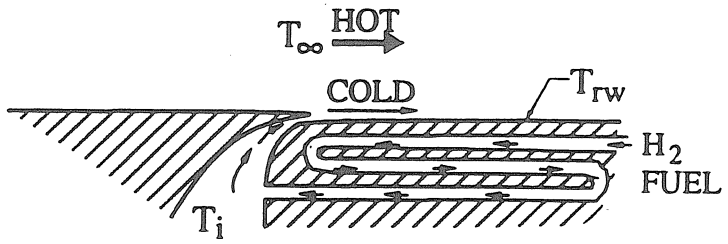

Figure 1.1: Proposed cooling of a scramjet engine

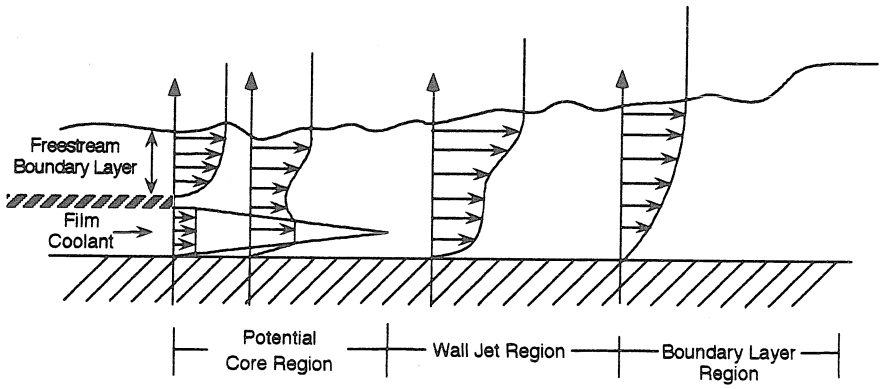

Figure 1.2: Film cooling flow-field description

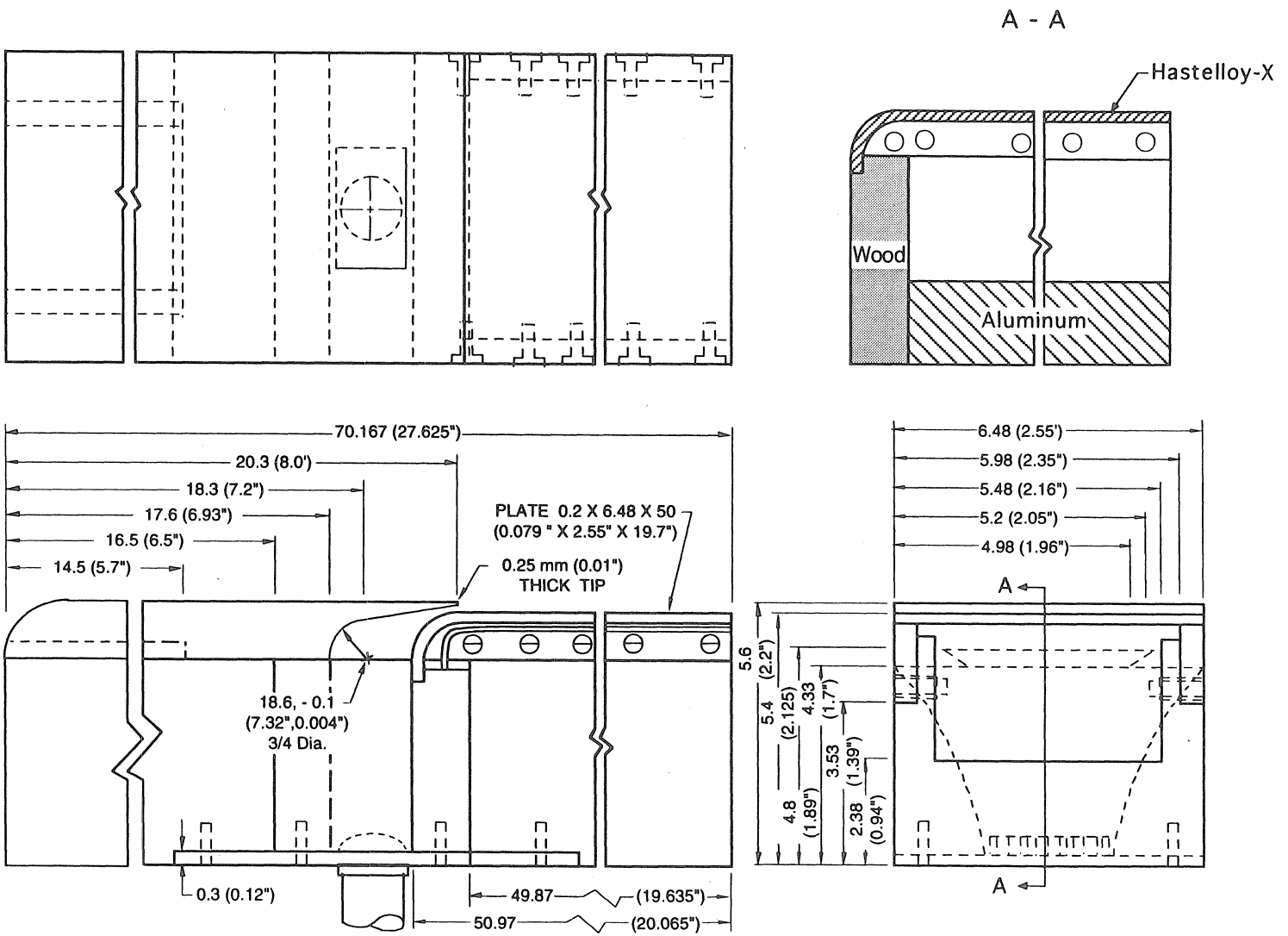

Figure 2.1: The injection model used in the experiment

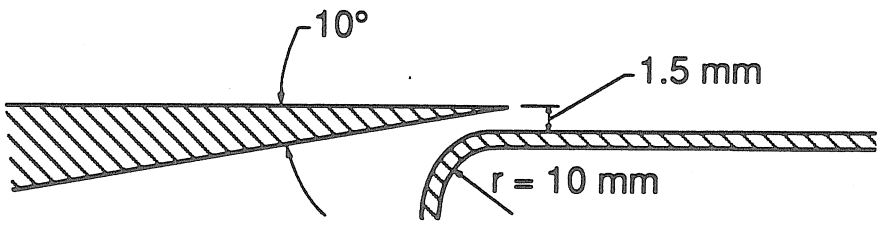

Figure 2.2: The injection nozzle

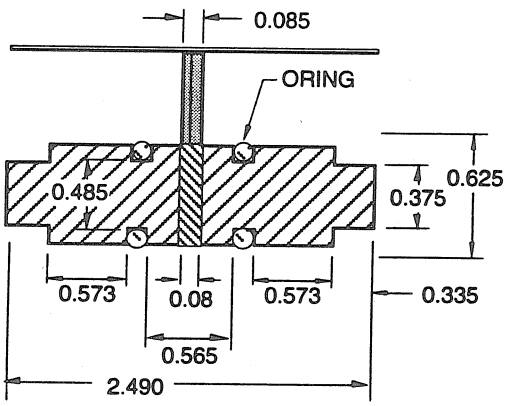

WEDGE FRONT VIEW

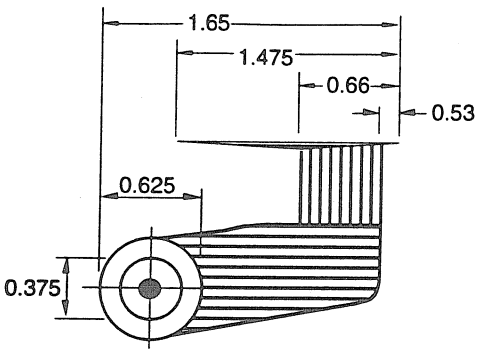

WEDGE SIDE VIEW

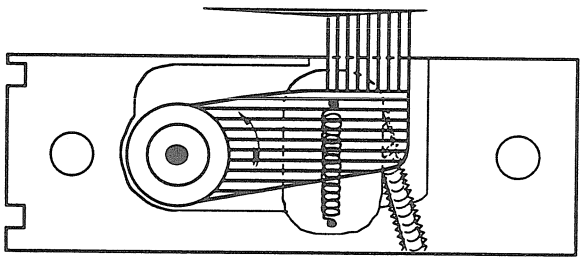

Wedge Assemblly

Figure 2.3: The wedge design

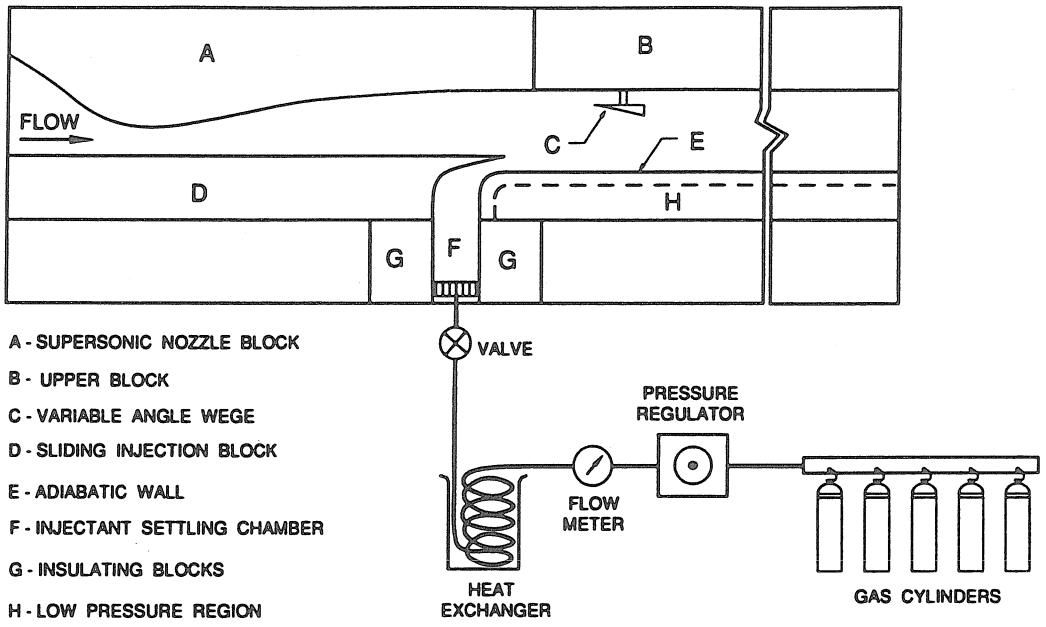

Figure 2.4: The injection setup

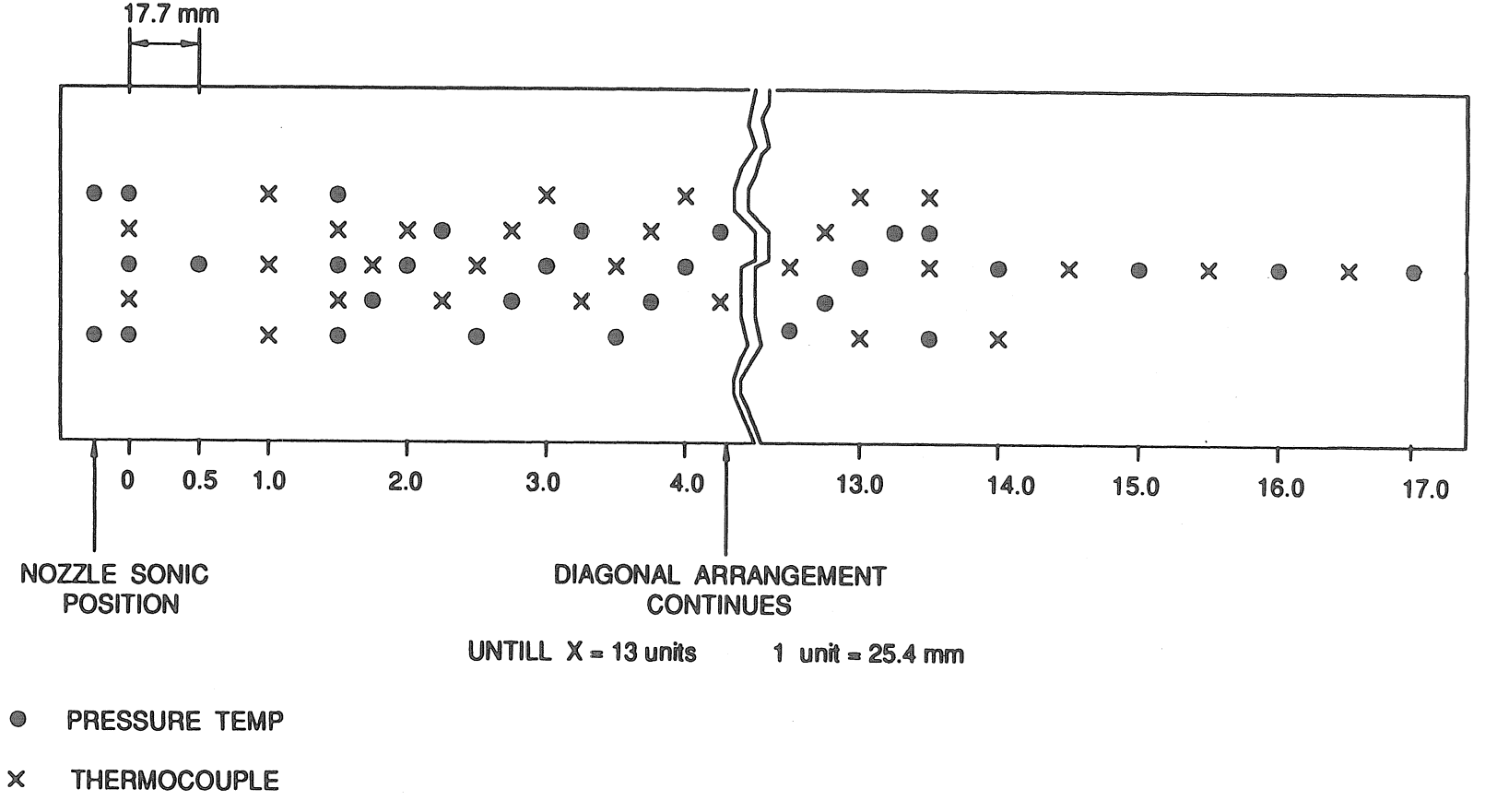

Figure 2.5: Layout of plate instrumentation

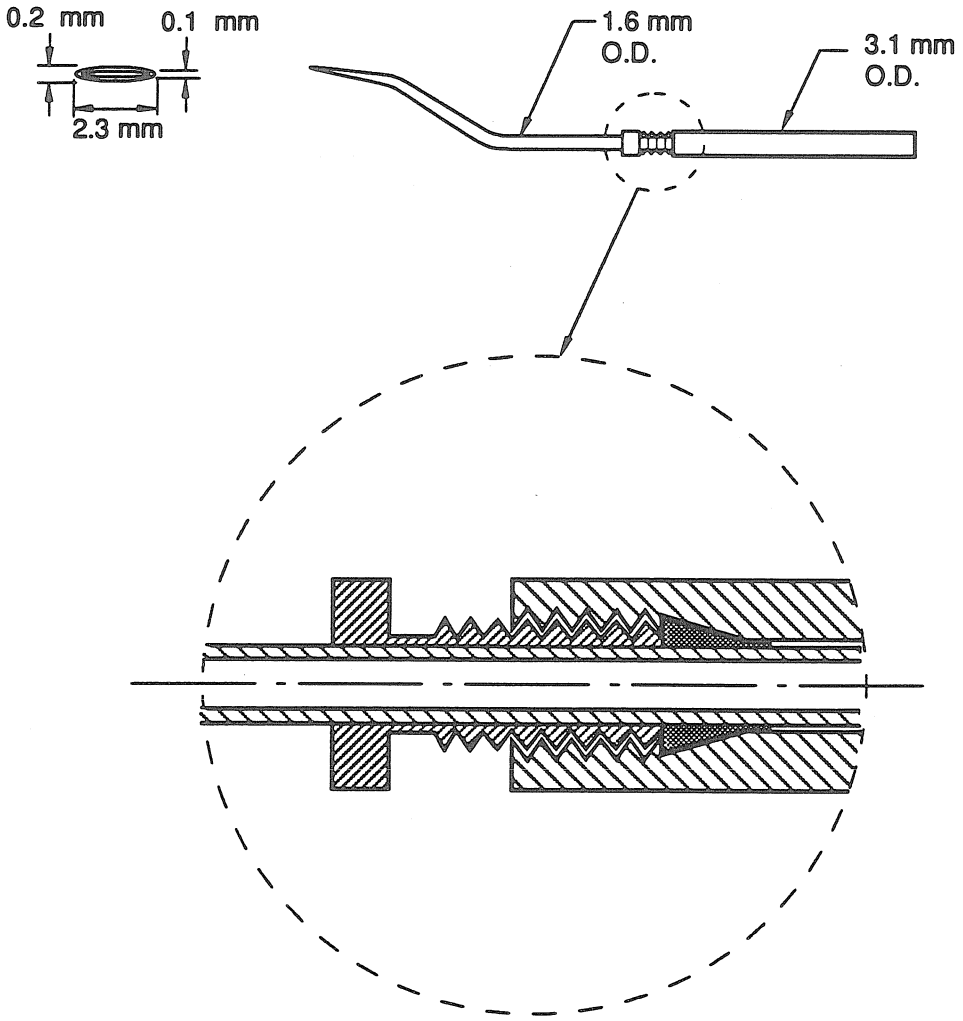

Figure 2.6: Description of the pitot pressure probe

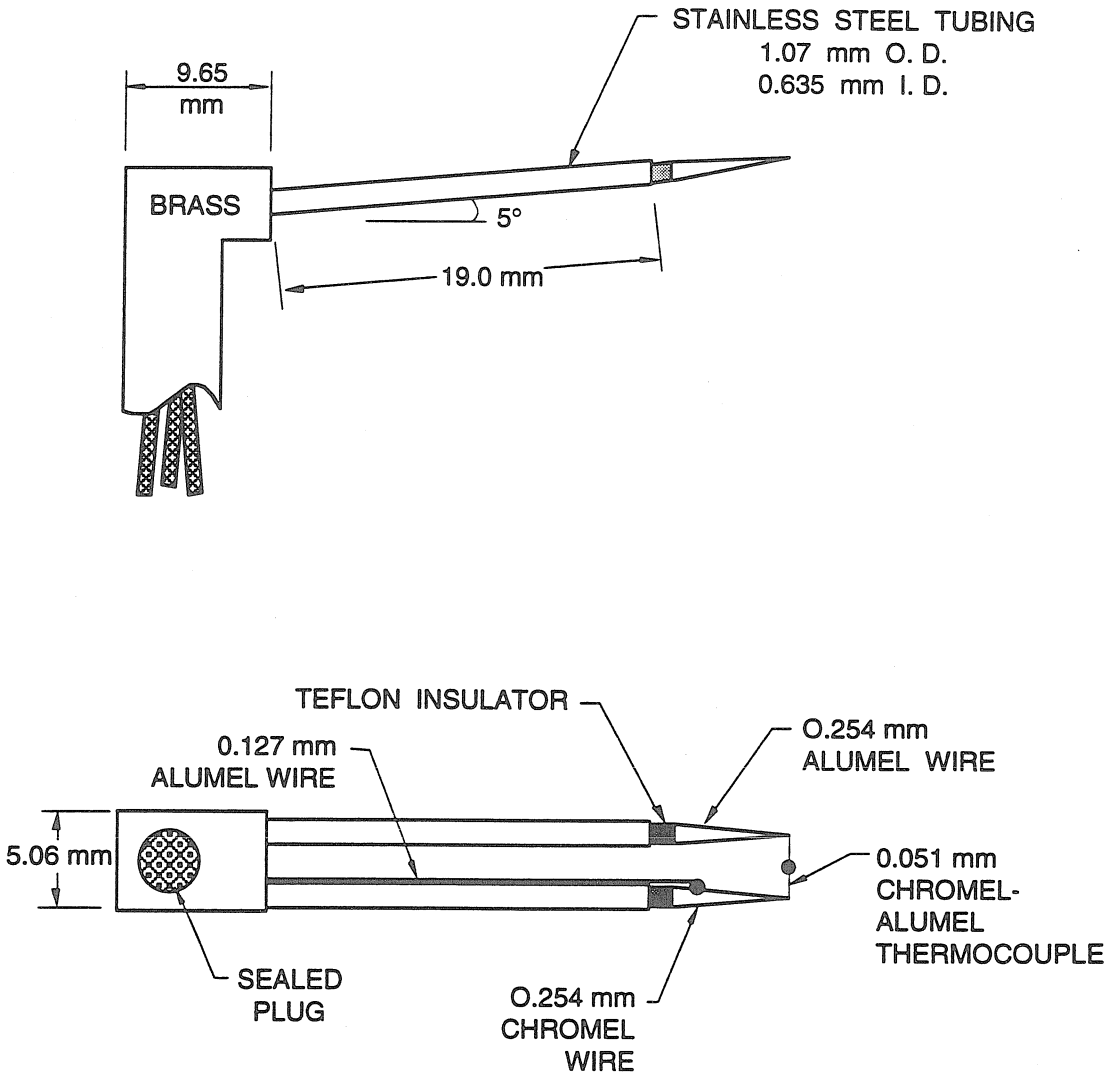

Figure 2.7: Description of the recovery temperature probe

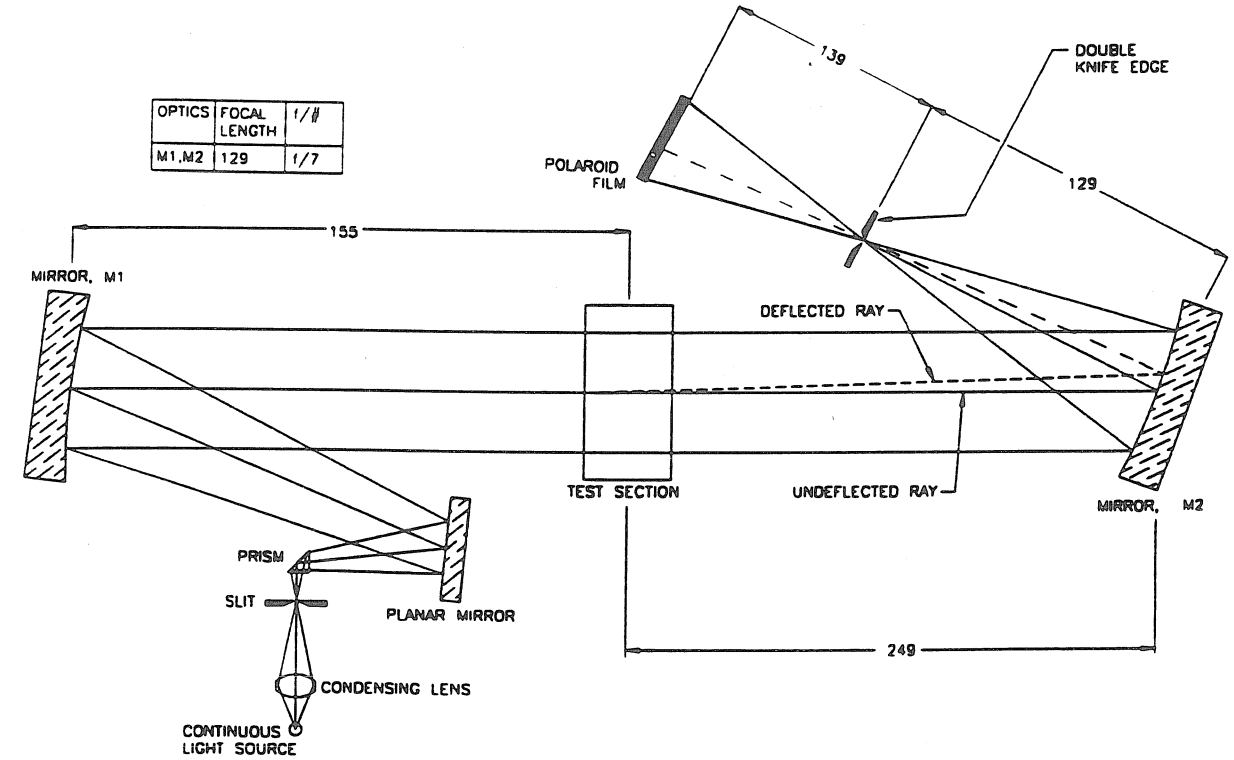

Figure 2.8: The continuous schlieren system

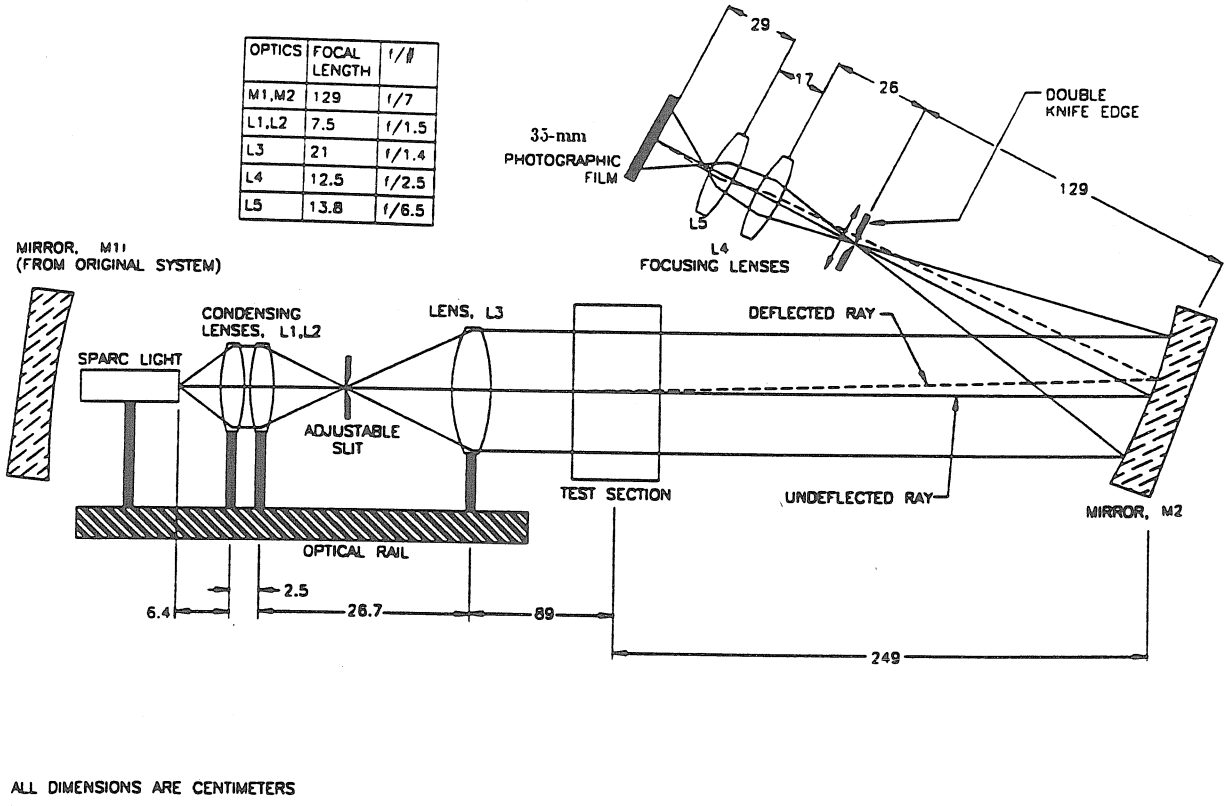

Figure 2.9: The spark source schlieren system

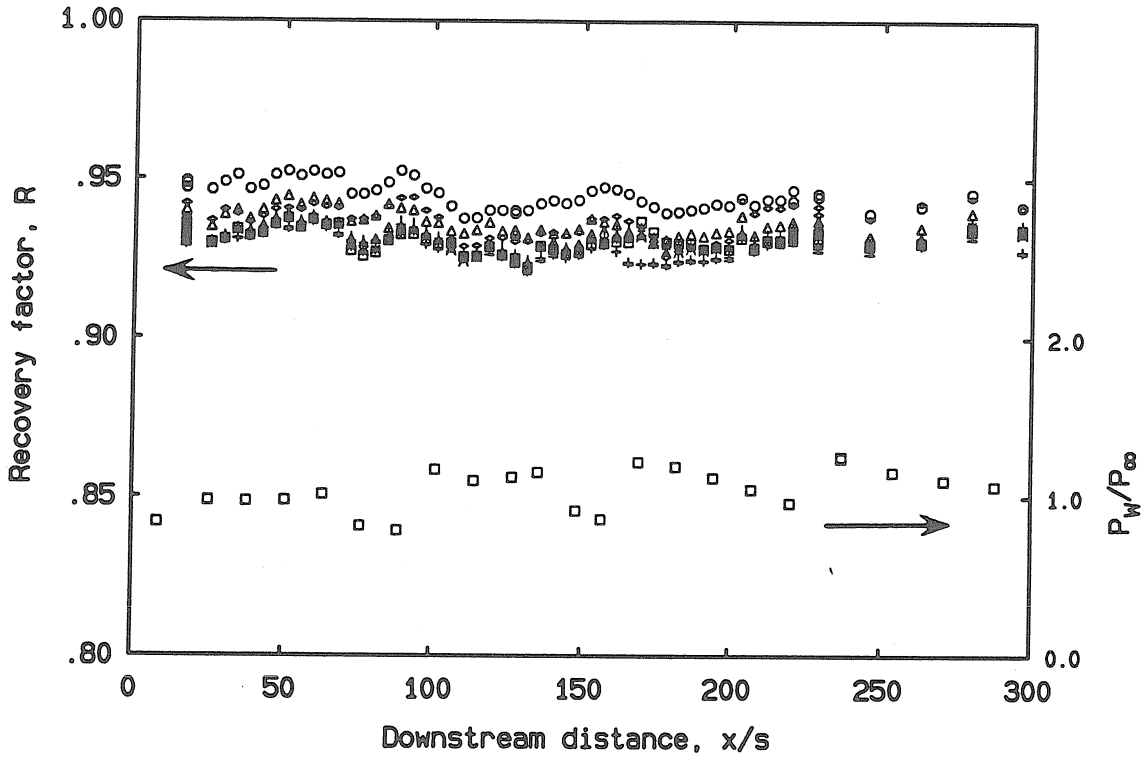

Figure 2.10: Wall recovery factor without injection at taken at different times

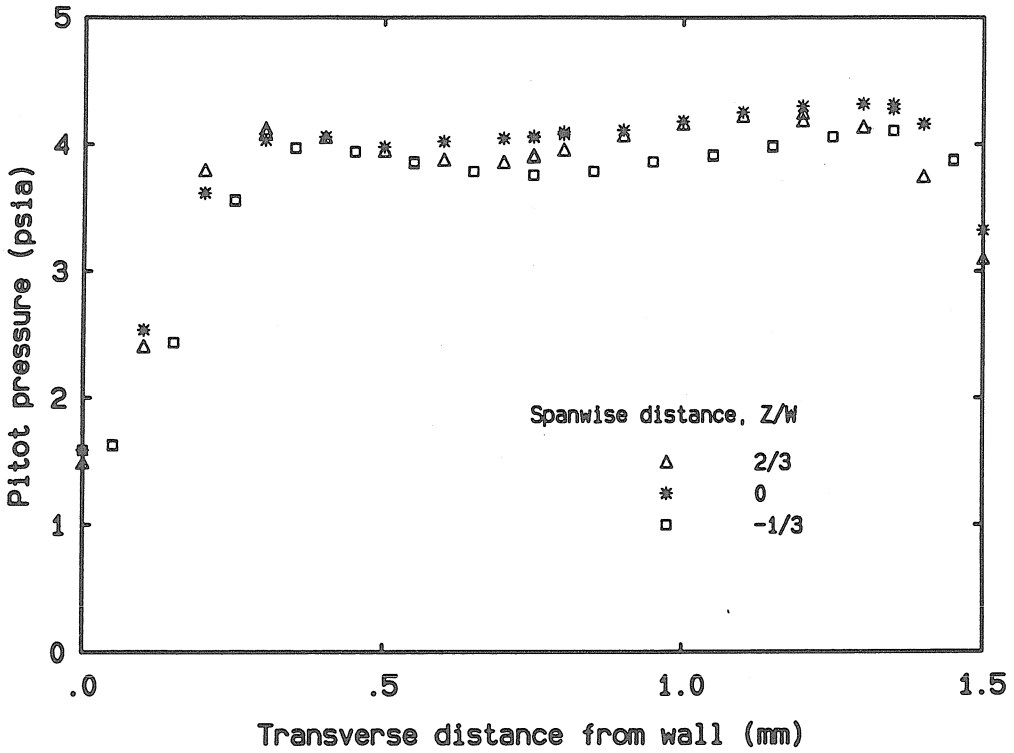

Figure 2.11: Exit pitot pressure profile of helium injection at Mach 1.6, indicating the two dimensionality of the injection.

Author	Fluid	M_∞	M_i	r	λ	P_i/P_∞
Goldstein, et al. [4]	air	3	≤ 1	≤ 0.5	0.1-0.41	≤ 1& ≥ 1
	He	3	< 1		0.01-0.02	< 1
Cary & Hefner [5,6]	air	6	1	0.29-0.35	0.03-1.6	≤ 1& ≥ 1
Rouser & Ewen [7]	H_2	2.3	1.9	1.95	0.15-0.58	0.5 -2.0
	N_2	2.3	1.9	0.54	0.47-2.2	0.5 -2.0
Current	air	2.44	1.2-1.9	0.57-1.1	0.38-0.77	1
	He	2.44	1.3-2.2	1.6-2.6	0.18-0.44	1

Table 3.1: Supersonic film cooling studies

Injectant	$T_{ti}/T_{t\infty}$	M_i	U_i/U_∞	$\rho_i U_i/\rho_\infty U_\infty$
air	1.13	1.3	0.72	0.38
	1.13	1.5	0.82	0.50
	1.13	1.8	0.91	0.61
	1.14	2.2	1.0	0.82
	1.32	2.2	1.1	0.77
	0.80	1.2	0.57	0.40
	0.76	1.5	0.66	0.59
	0.76	1.8	0.73	0.74
helium	1.16	1.3	2.0	0.18
	1.16	1.6	2.2	0.23
	1.16	1.9	2.4	0.30
	1.24	2.2	2.6	0.34
	0.75	1.3	1.6	0.20
	0.71	1.9	1.9	0.44

Table 3.2: Experimental Parameters

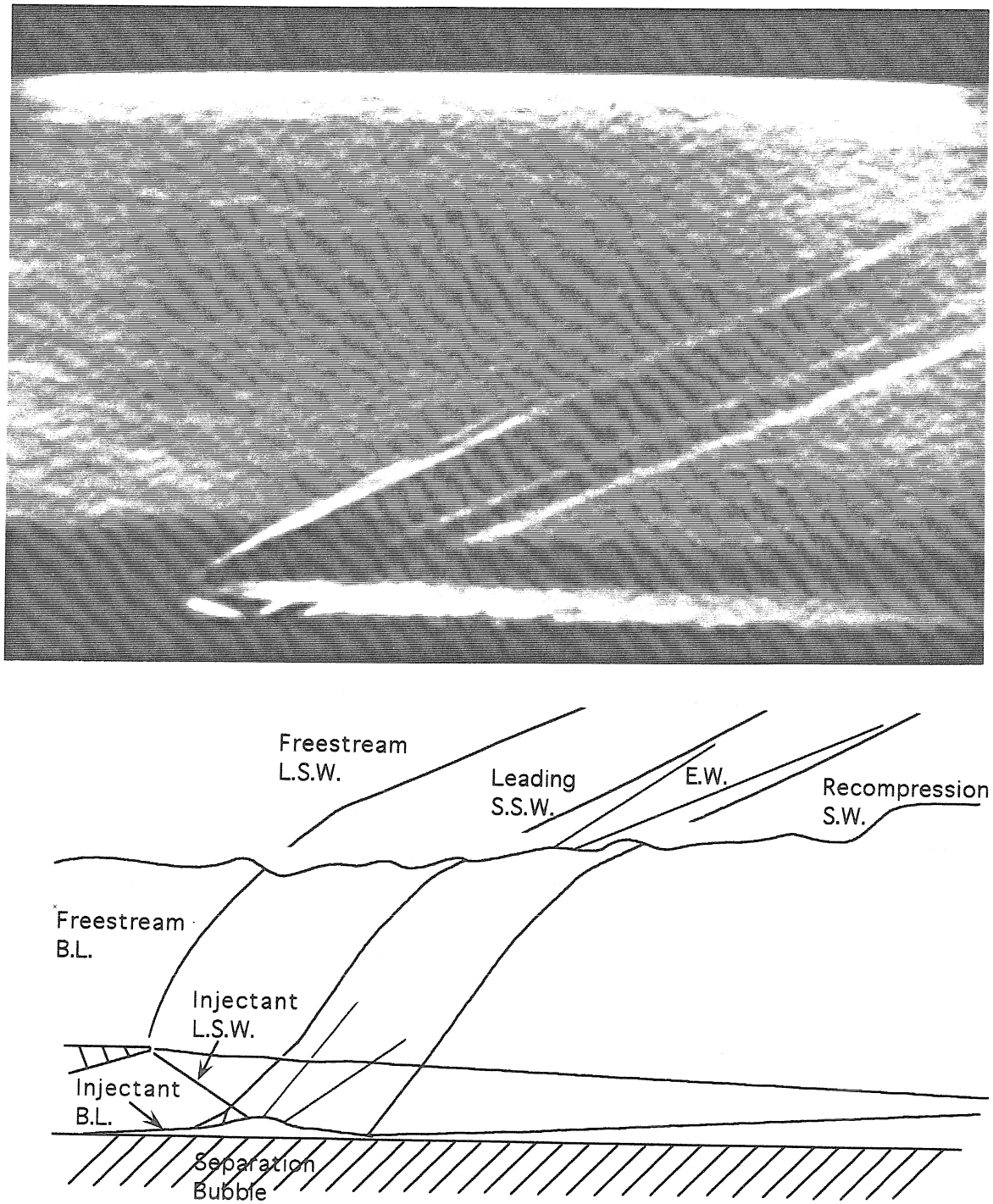

Figure 3.1: Schlieren picture and a schematic of Mach 2.2 air injection. The schematic symbols are: B.L. is boundary layer, L.S.W. is lip shock wave, S.S.W. is separation shock wave, E.W. is expansion wave, and S.W. is shock wave

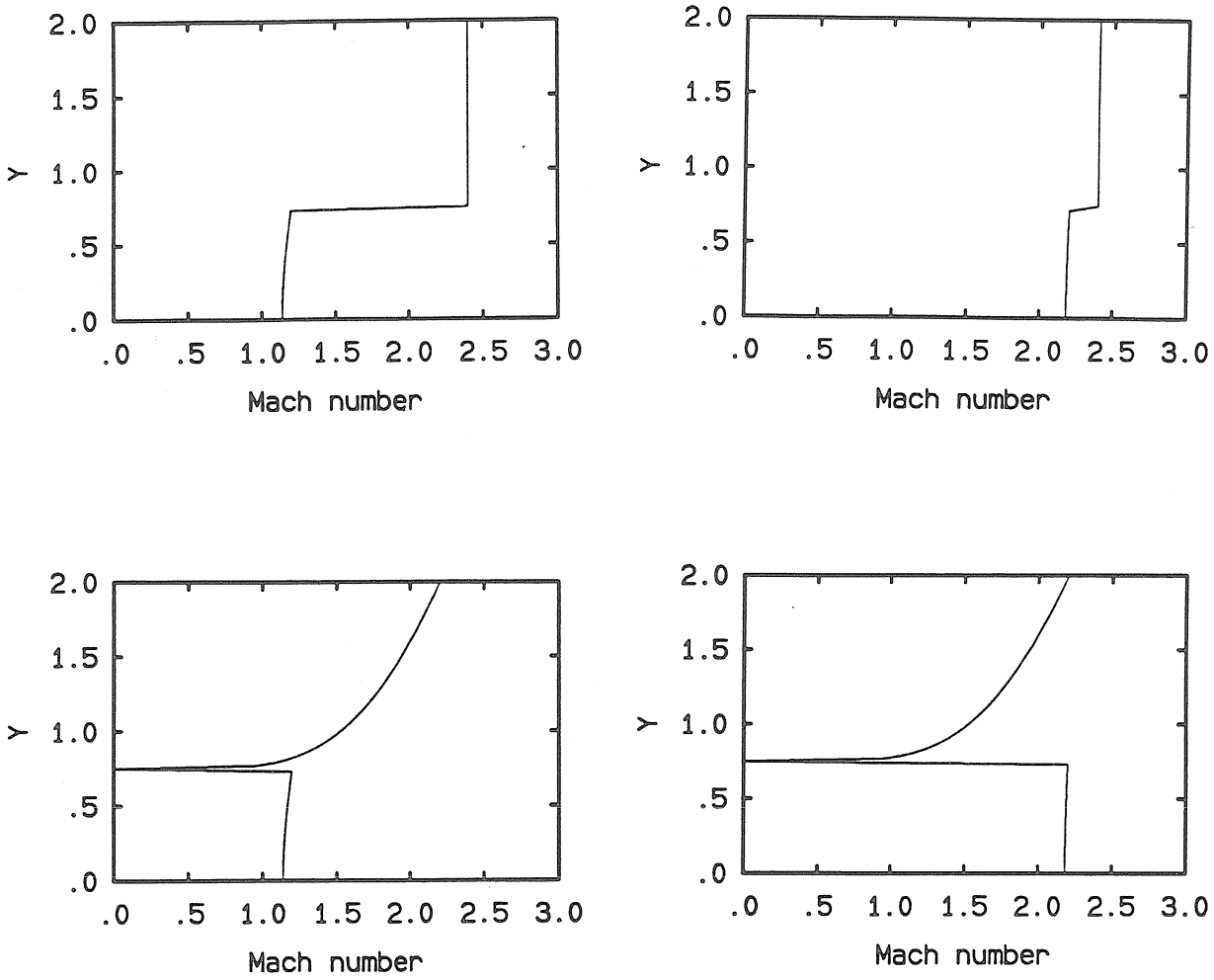

Figure 3.2: Initial Mach number profiles used in computational studies

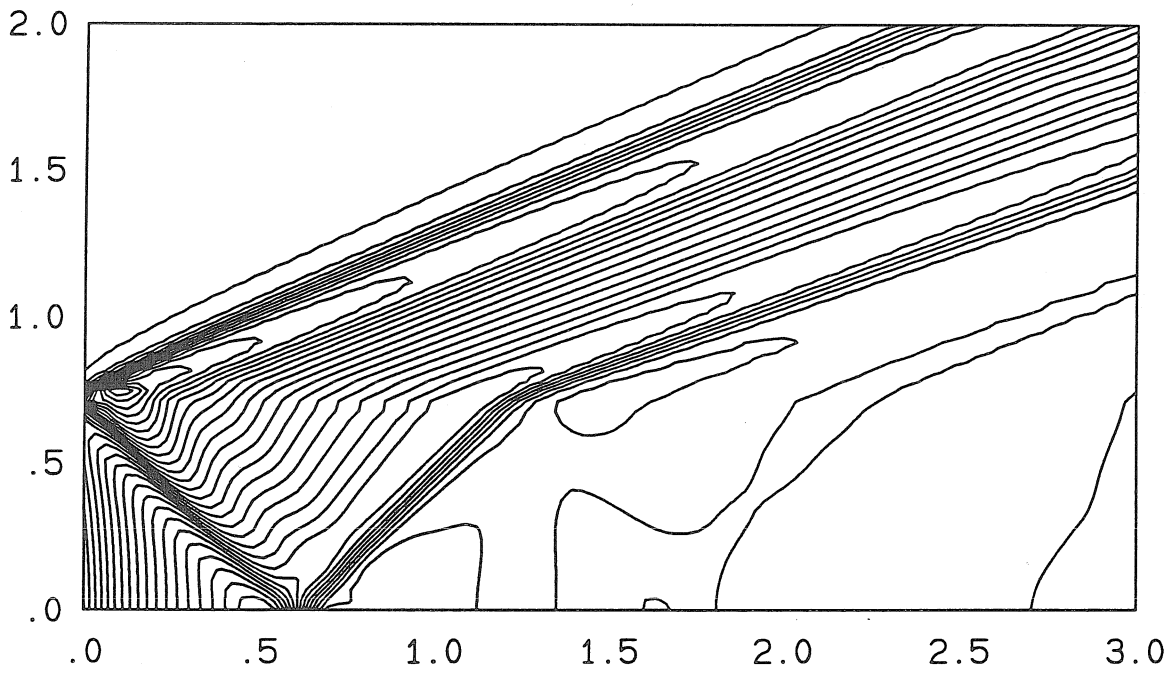

Figure 3.3: Pressure contour for Mach 1.2 injection, maximum $p/p_\infty = 1.26$ is at (0.12,0.77) and minimum $p/p_\infty = 0.72$ is at (0.51,0.0)

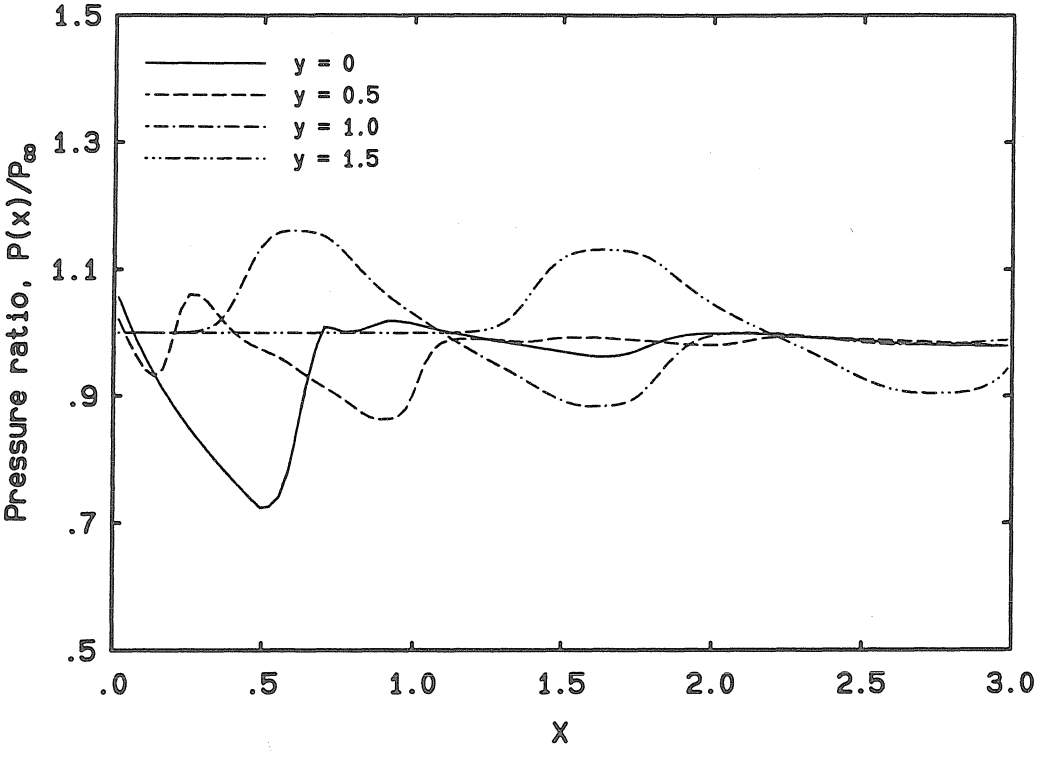

Figure 3.4: The pressure distribution for Mach 1.2 injection at different heights

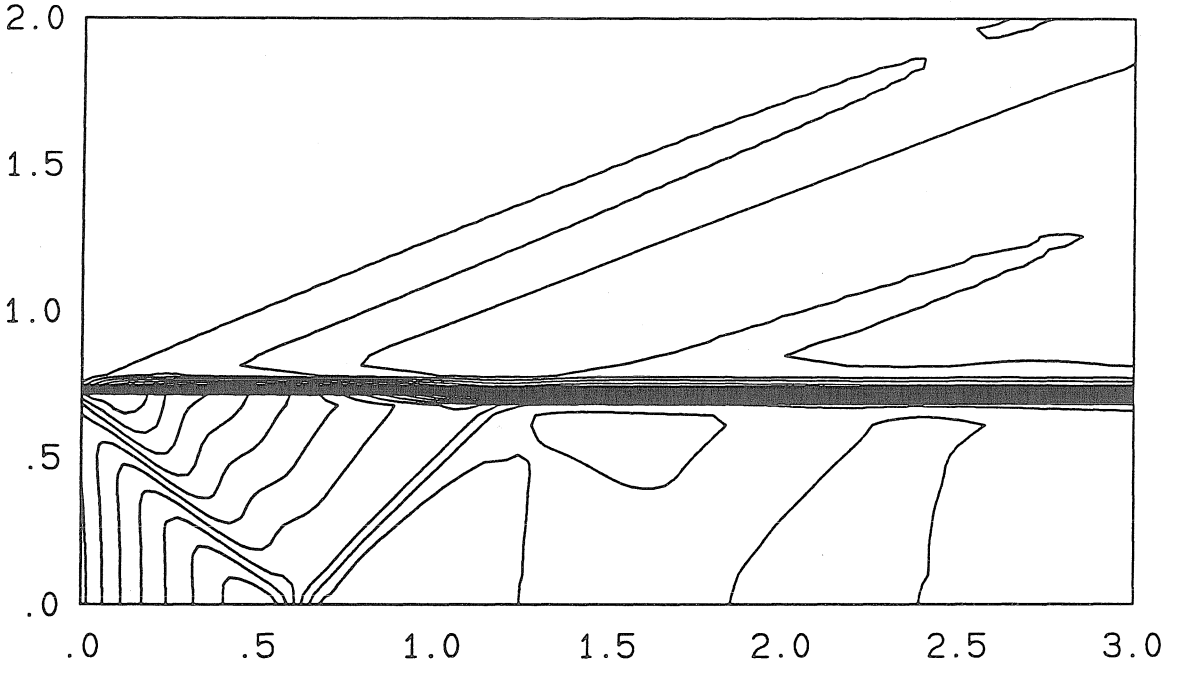

Figure 3.5: Axial velocity contours for Mach 1.2 injection, maximum $u/u_\infty = 1.01$ is at (1.32,0.87) and minimum $u/u_\infty = 0.57$ is at (0.12,0.73)

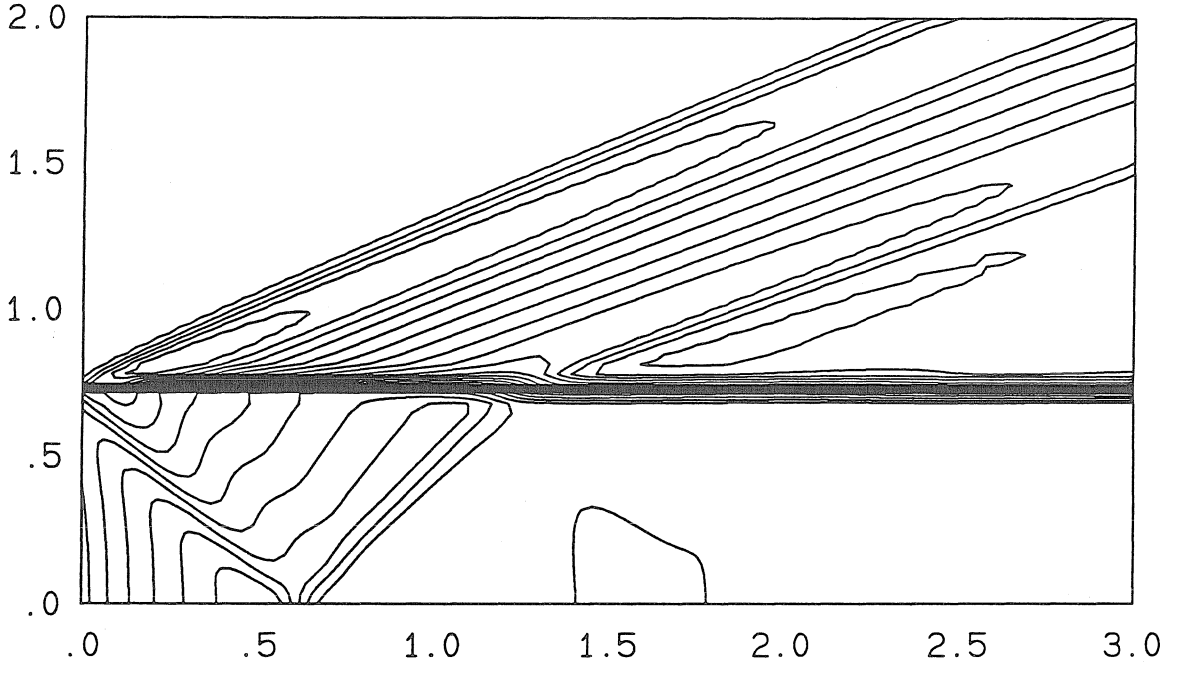

Figure 3.6: Density contour in the case of Mach 1.2 injection, maximum $\rho/\rho_\infty = 1.13$ is at (0.27,0.83) and minimum $\rho/\rho_\infty = 0.48$ is at (0.51,0.0)

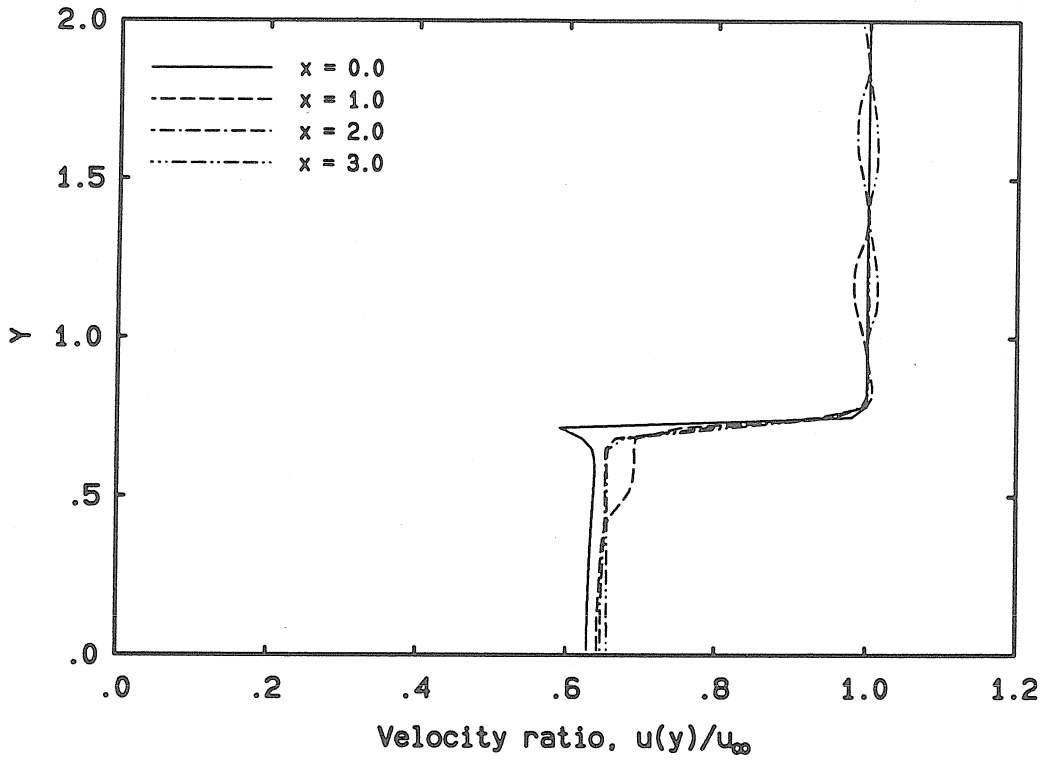

Figure 3.7: The velocity profile for Mach 1.2 injection at different axial locations

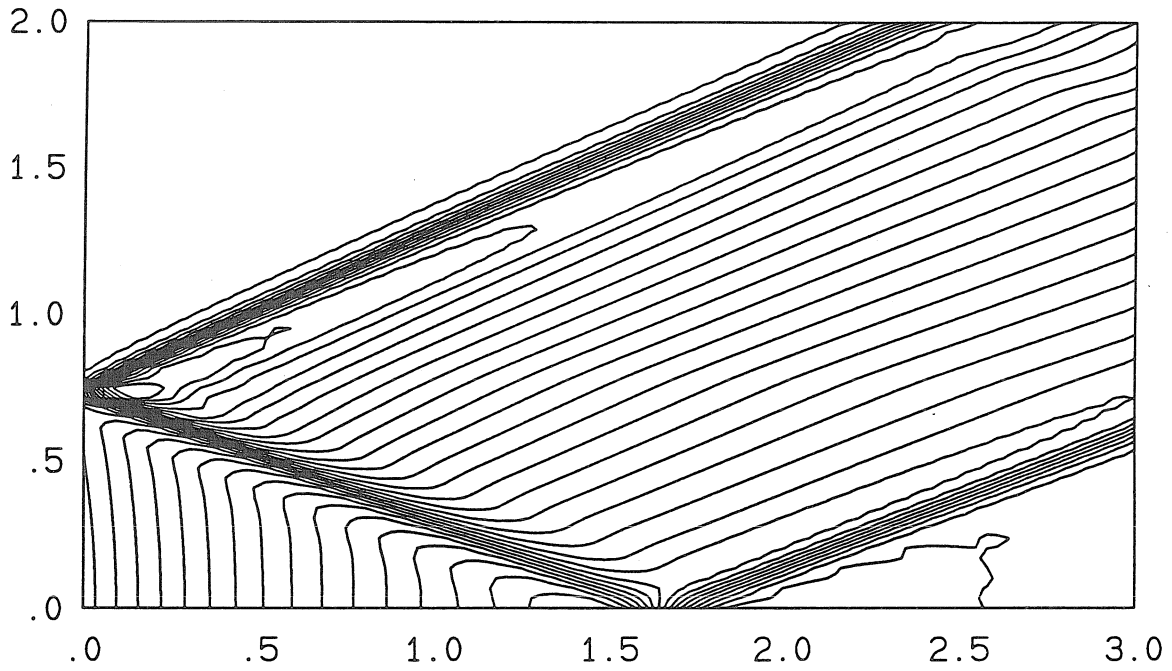

Figure 3.8: Pressure contour in the case of Mach 2.2 injection, maximum $p/p_\infty = 1.32$ is at (0.17,1.15) and minimum $p/p_\infty = 0.63$ is at (1.41,0.0)

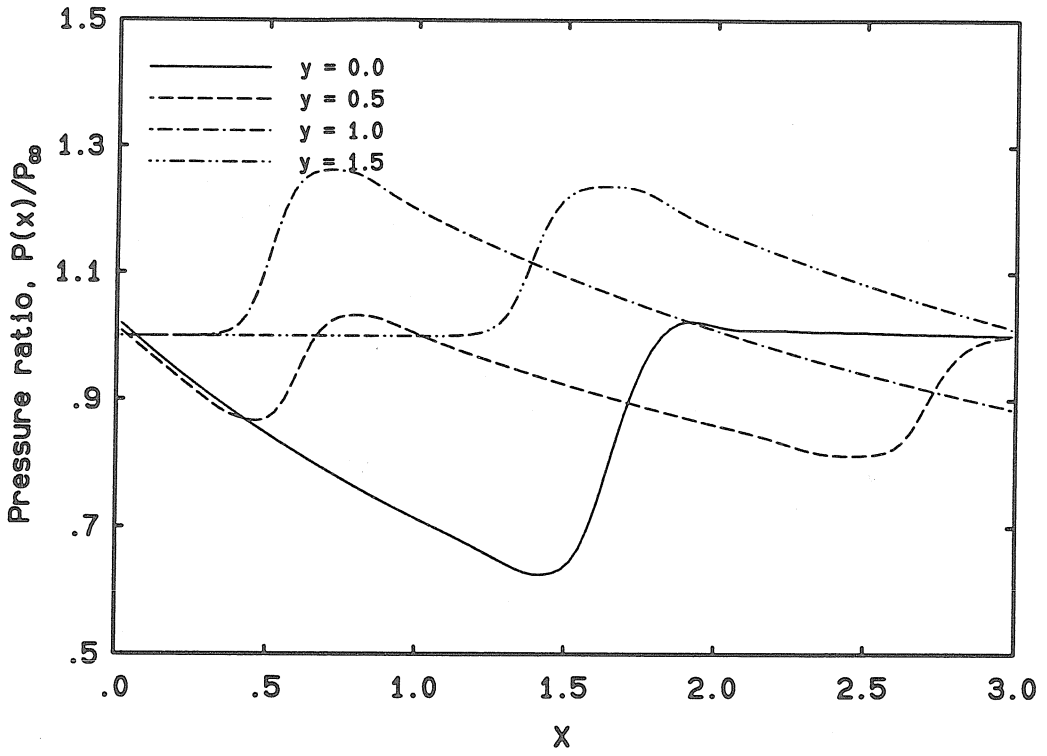

Figure 3.9: Pressure distribution in the case of Mach 2.2 injection at different heights

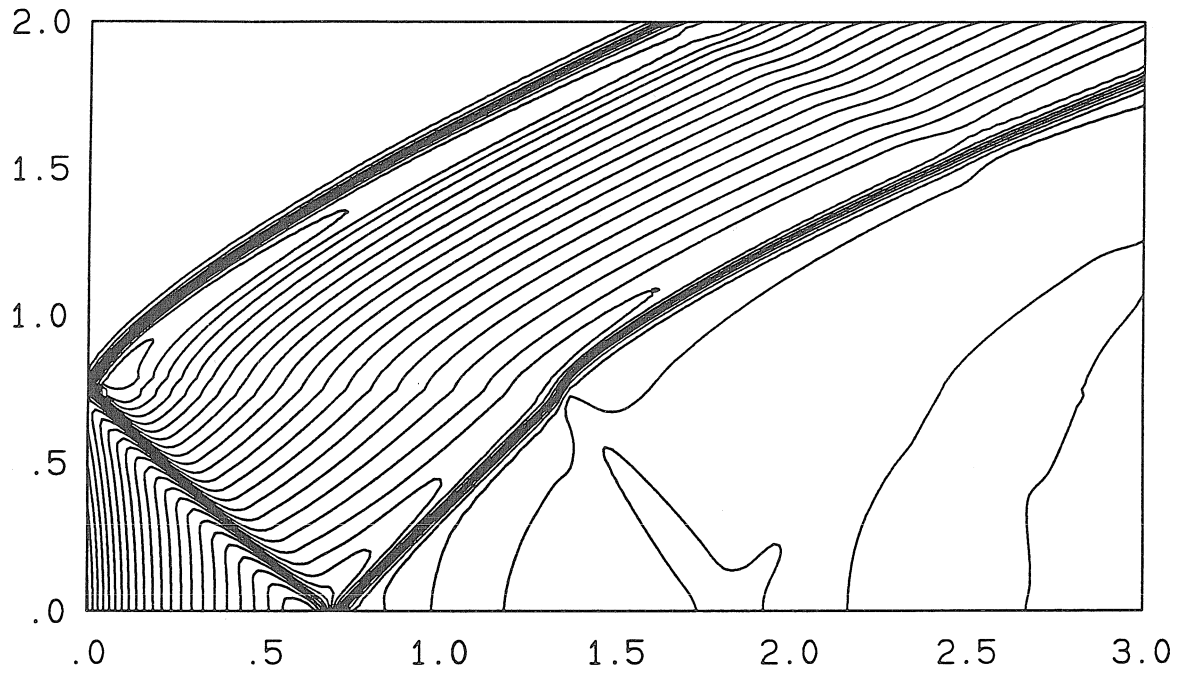

Figure 3.10: Pressure contours for the Mach 1.2 injection, indicating the influence of the boundary layer, maximum $p/p_\infty = 1.20$ is at (0.08,0.78) and minimum $p/p_\infty = 0.68$ is at (0.62,0.0)

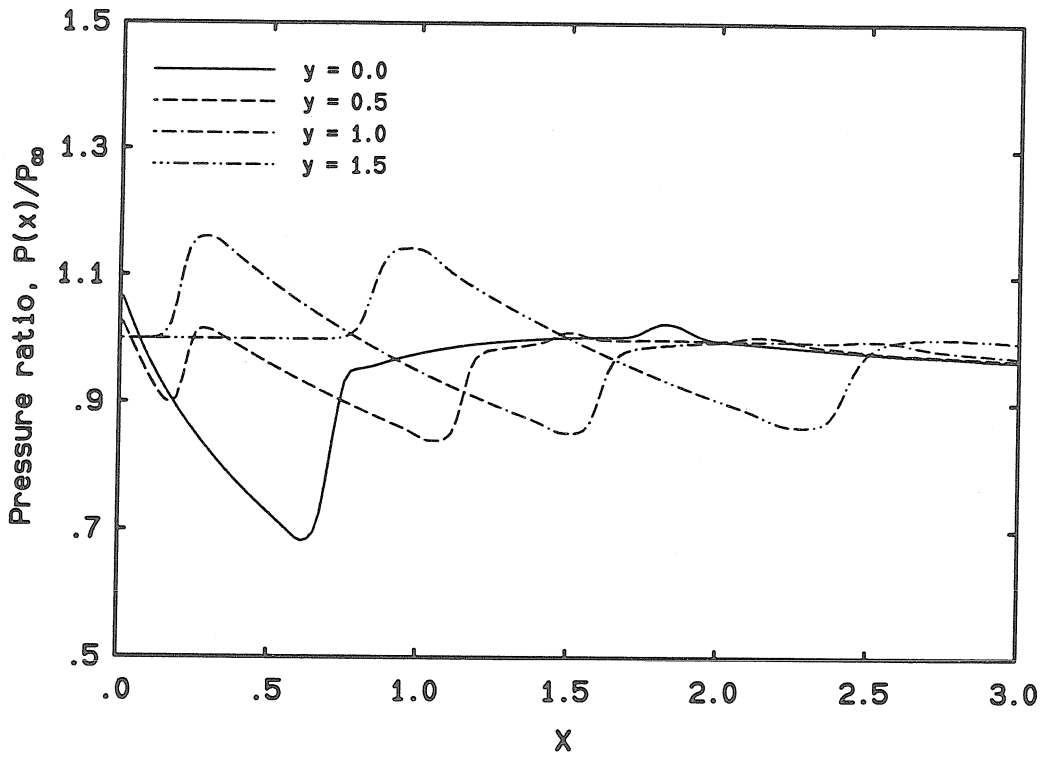

Figure 3.11: Pressure distribution for the Mach 1.2 injection, indicating the influence of the boundary layer.

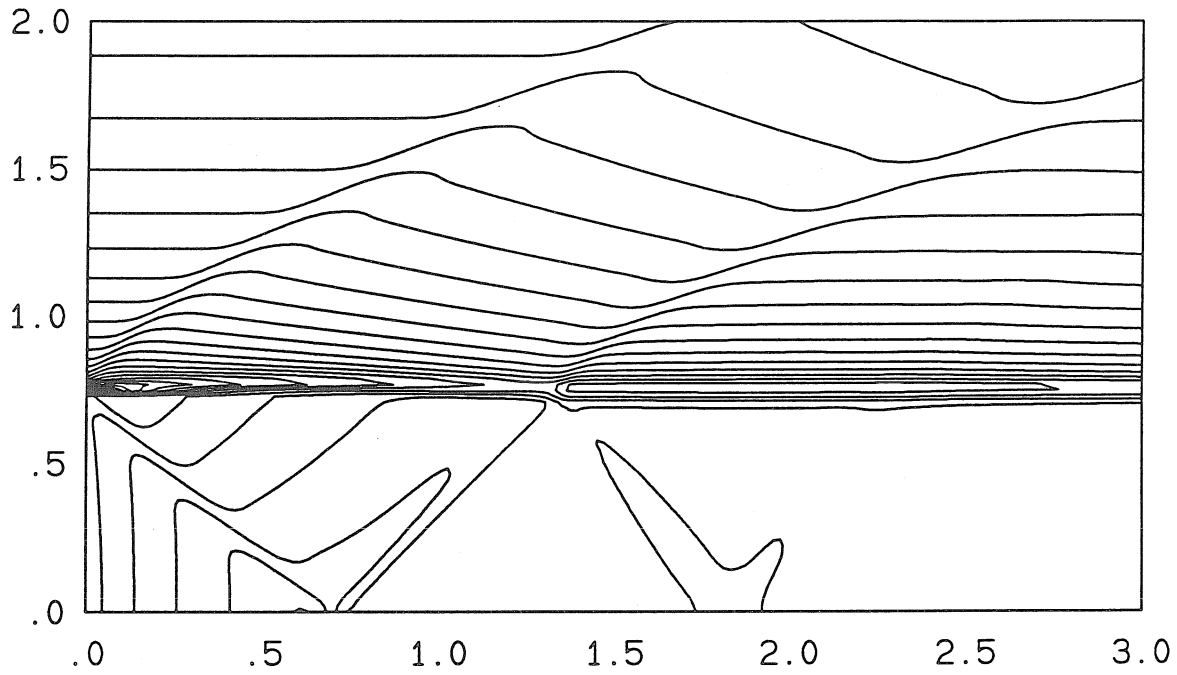

Figure 3.12: Axial velocity contours for the Mach 1.2 injection, in the presence of the boundary layer, maximum $u/u_\infty = 0.97$ is at (3.0,2.0) and minimum $u/u_\infty = 0.18$ is at (0.0,0.76)

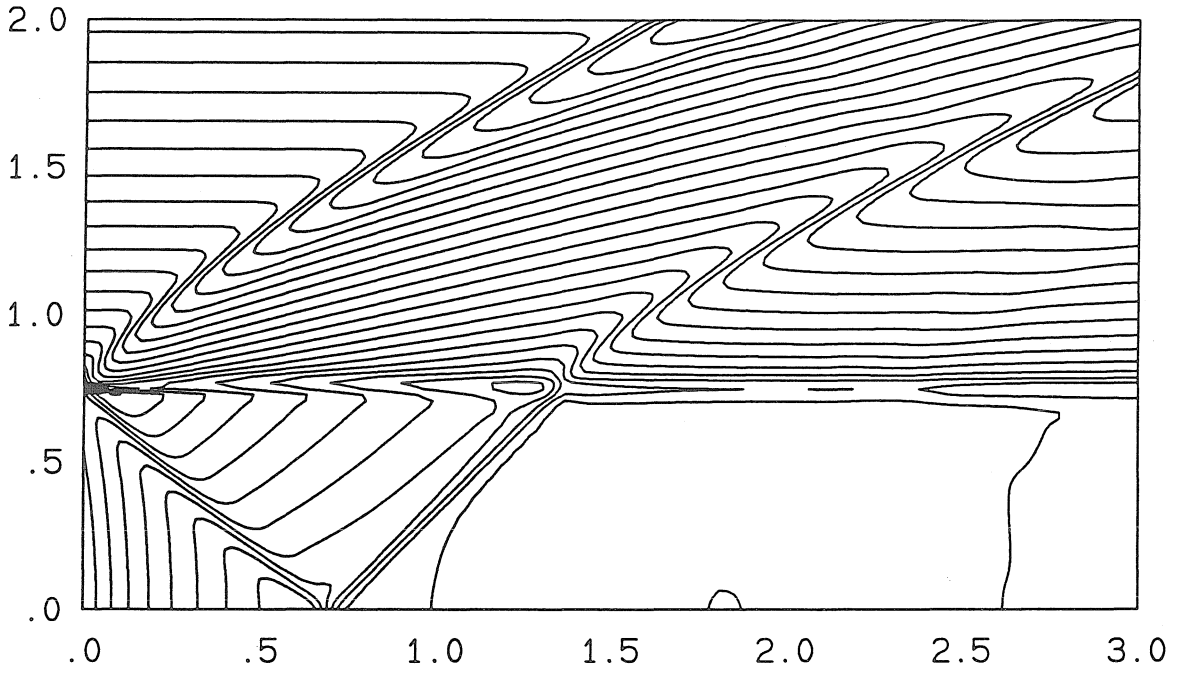

Figure 3.13: Density contours for the Mach 1.2 injection, in the presence of the boundary layer, maximum $\rho/\rho_\infty = 1.00$ is at (1.8,2.0) and minimum $\rho/\rho_\infty = 0.45$ is at (0.62,0.0)

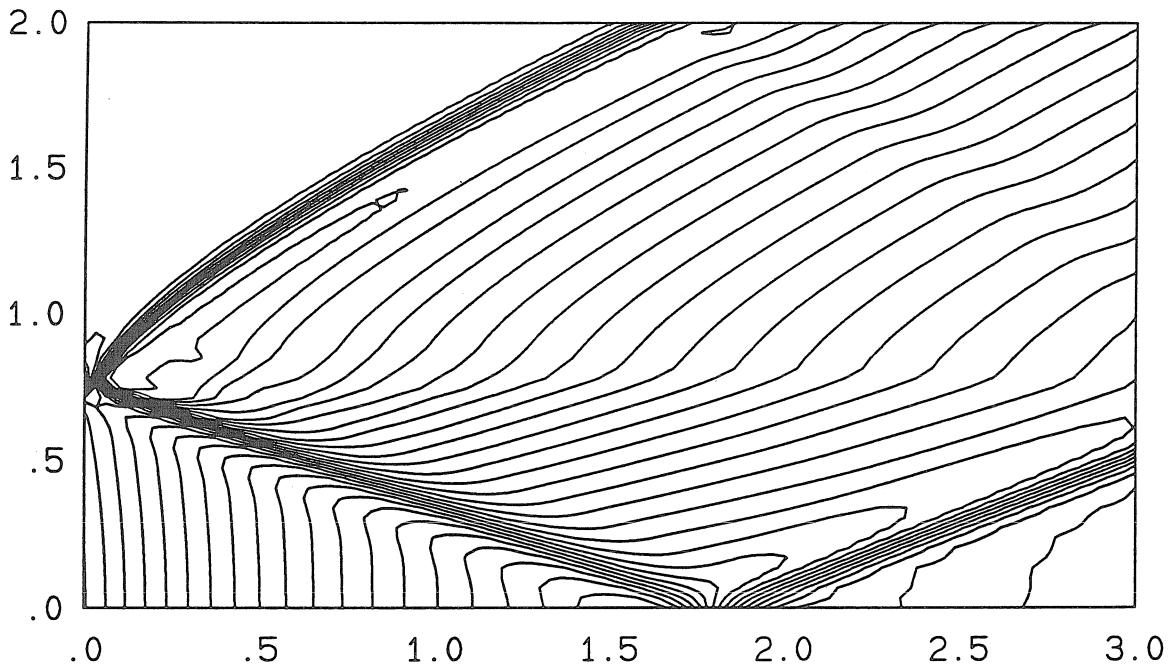

Figure 3.14: Pressure contours for the Mach 2.2 injection, in the presence of boundary layer, maximum $p/p_\infty = 1.24$ is at (0.15,0.83) and minimum $p/p_\infty = 0.60$ is at (1.56,0.0)

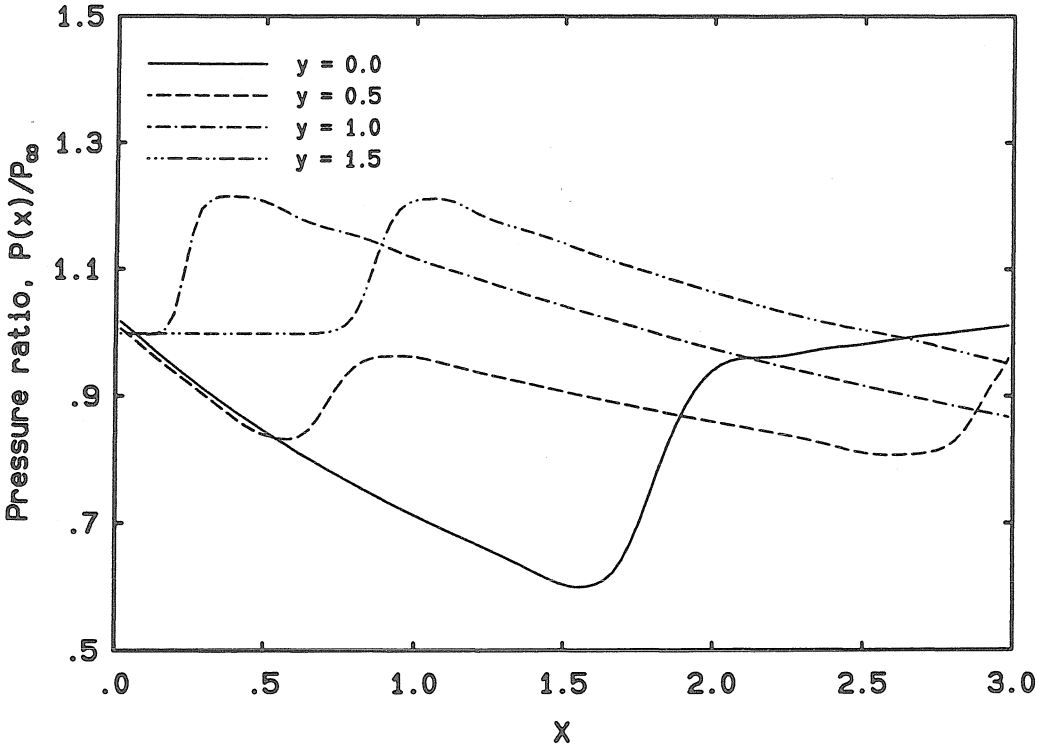

Figure 3.15: Pressure distribution for the Mach 2.2 injection, in the presence of boundary layer.

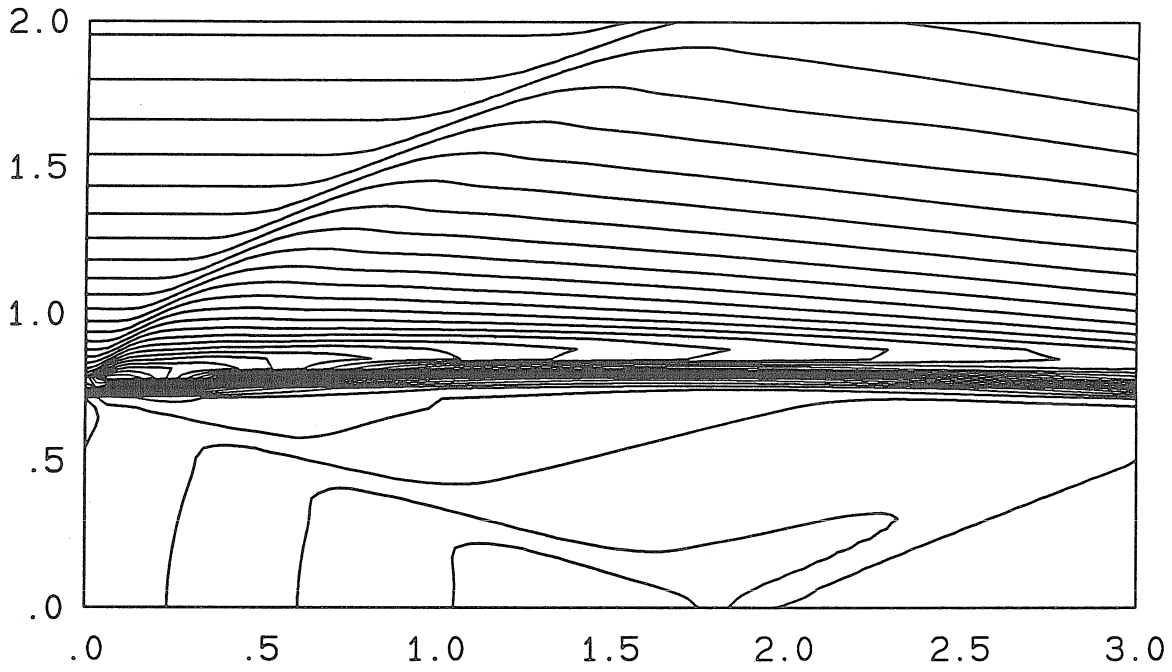

Figure 3.16: Axial velocity contours for the Mach 2.2 injection, in the presence of boundary layer, maximum $u/u_\infty = 1.02$ is at (1.56,0.0) and minimum $u/u_\infty = 0.49$ is at (0.12,0.80)

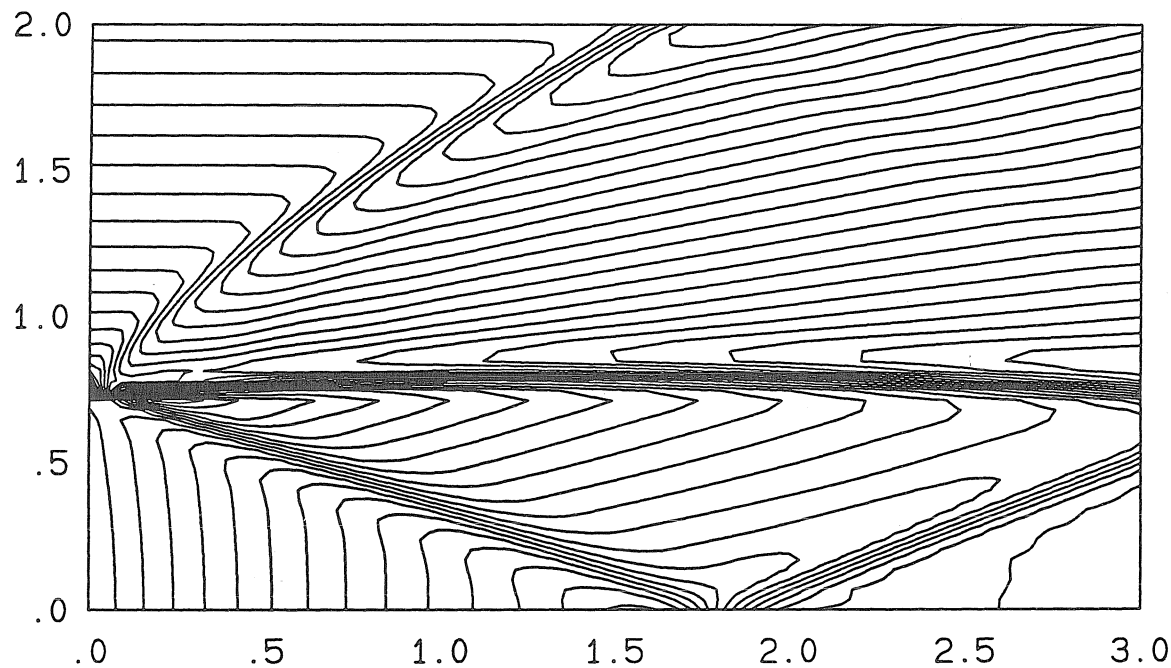

Figure 3.17: Density contours for the Mach 2.2 injection, in the presence of boundary layer, maximum $\rho/\rho_\infty = 1.05$ is at (1.86,2.0) and minimum $\rho/\rho_\infty = 0.46$ is at (0.0,0.77)

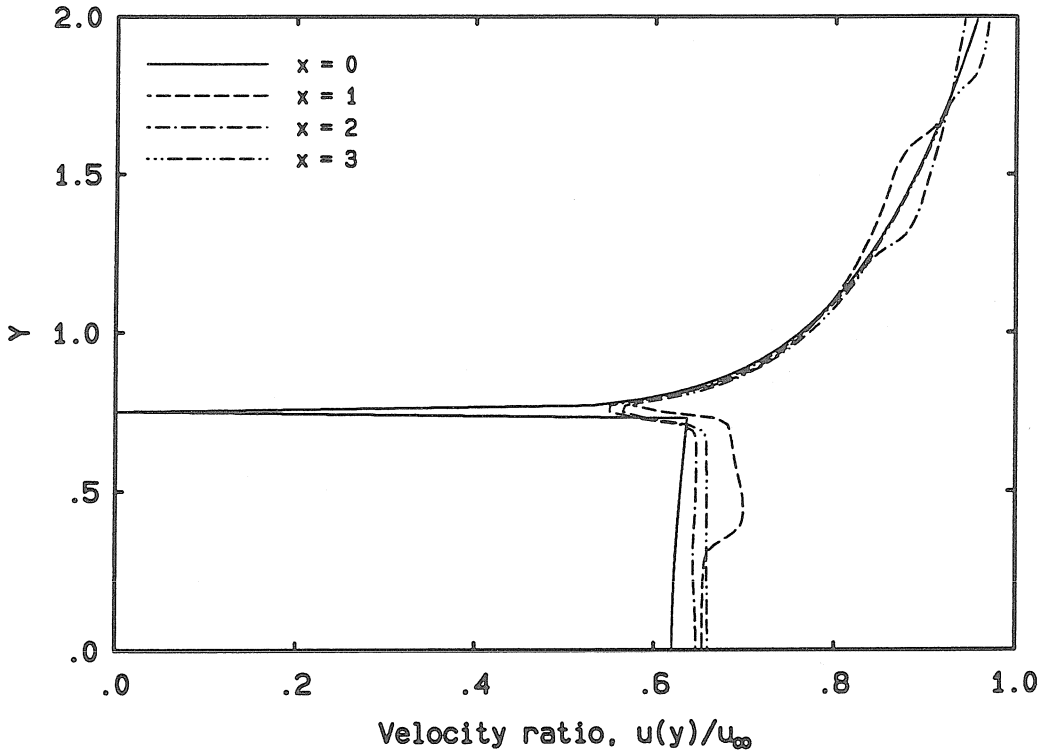

Figure 3.18: Axial velocity profiles at different axial locations for Mach 1.2 injection.

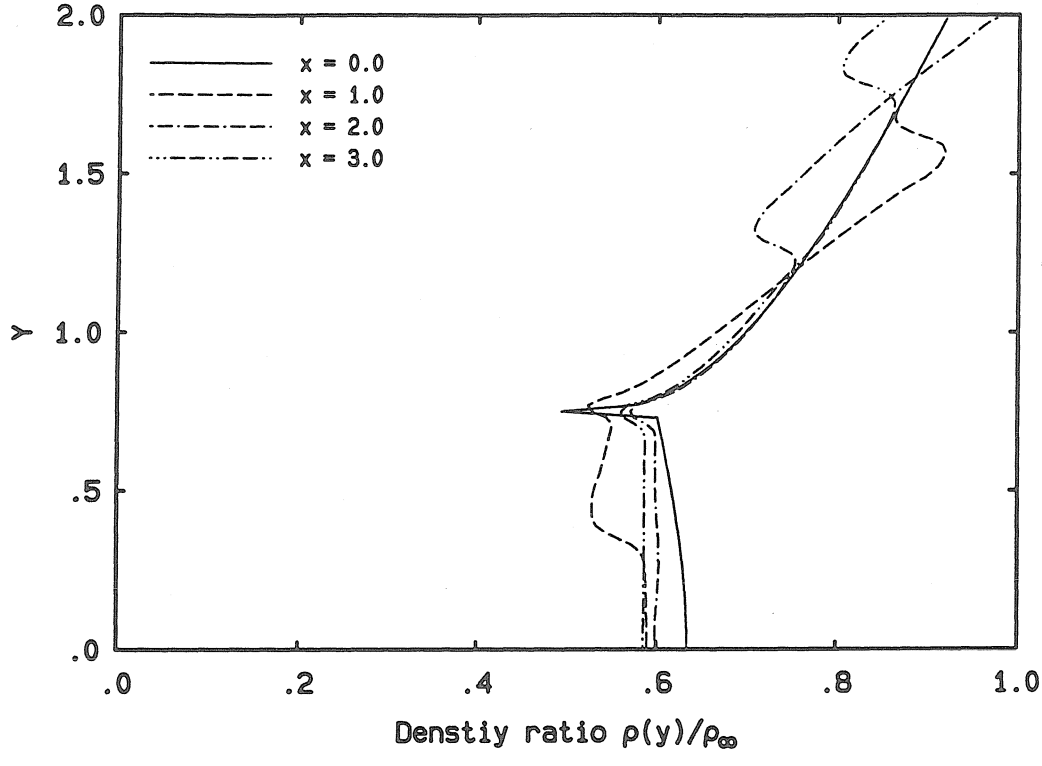

Figure 3.19: Density profiles at different axial locations for Mach 1.2 injection.

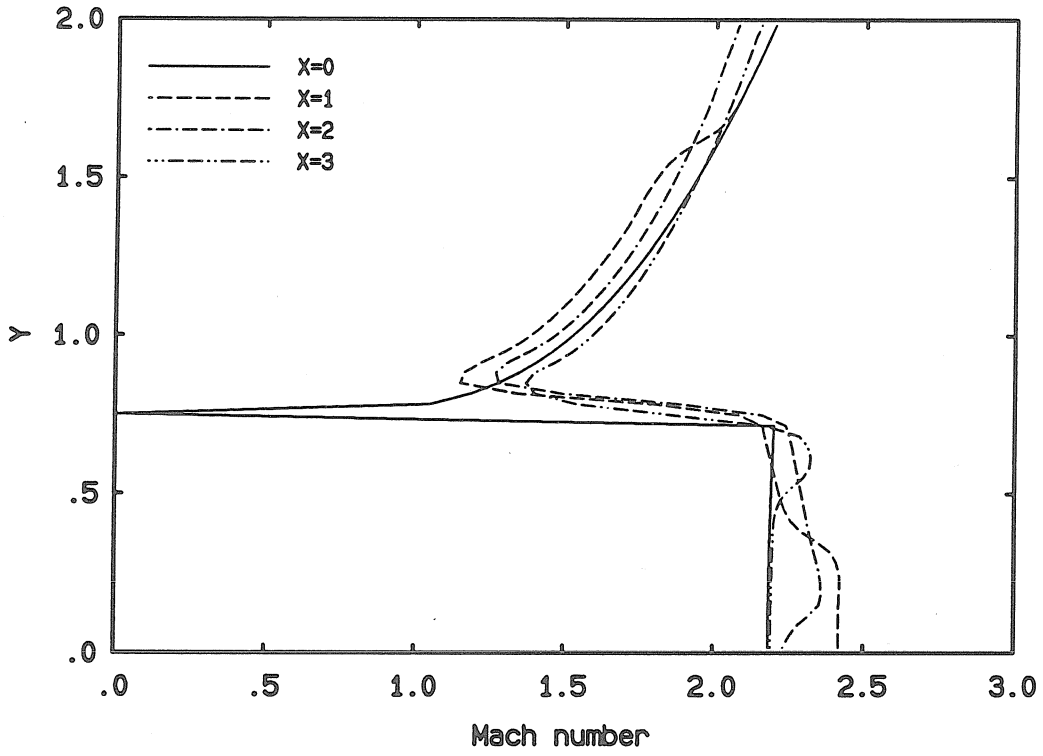

Figure 3.20: Mach number profiles at different axial locations for Mach 2.2 injection.

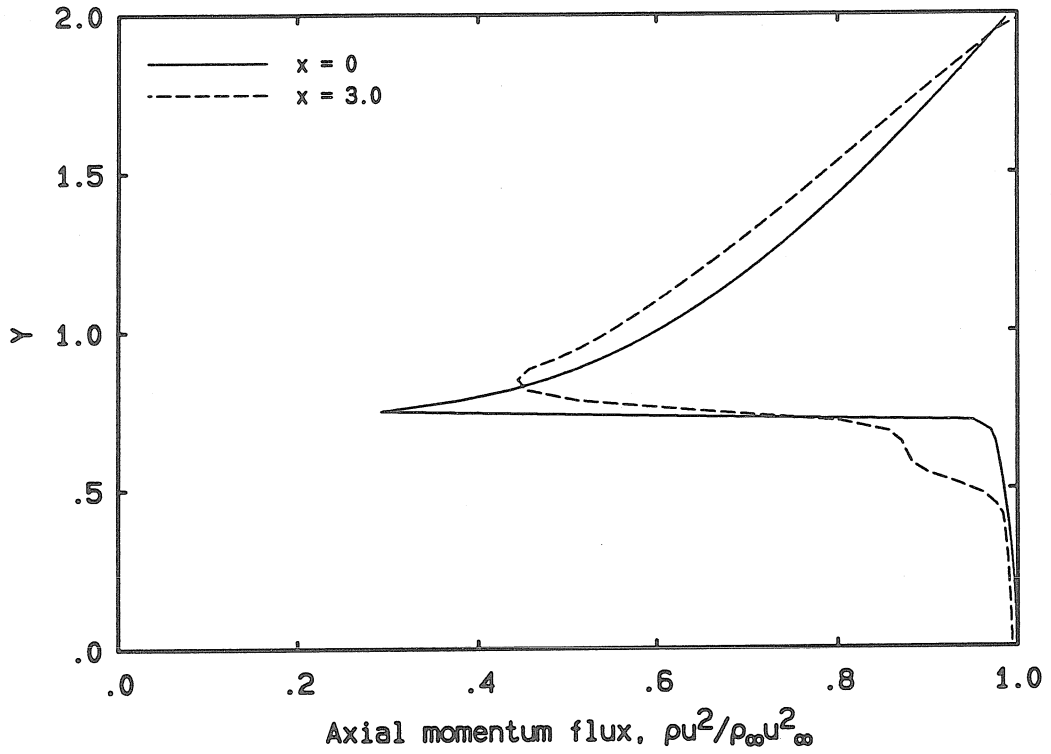

Figure 3.21: Momentum flux profiles at the initial and final computational domain for Mach 2.2 injection.

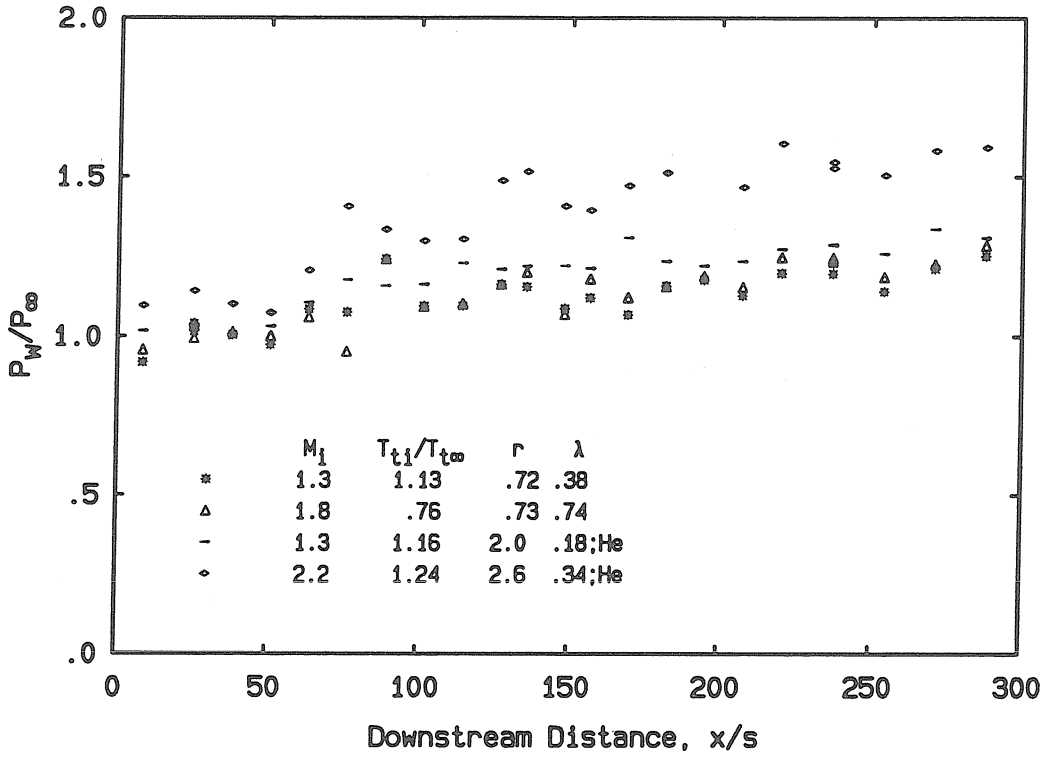

Figure 3.22: Wall static pressure distribution for air and helium injection

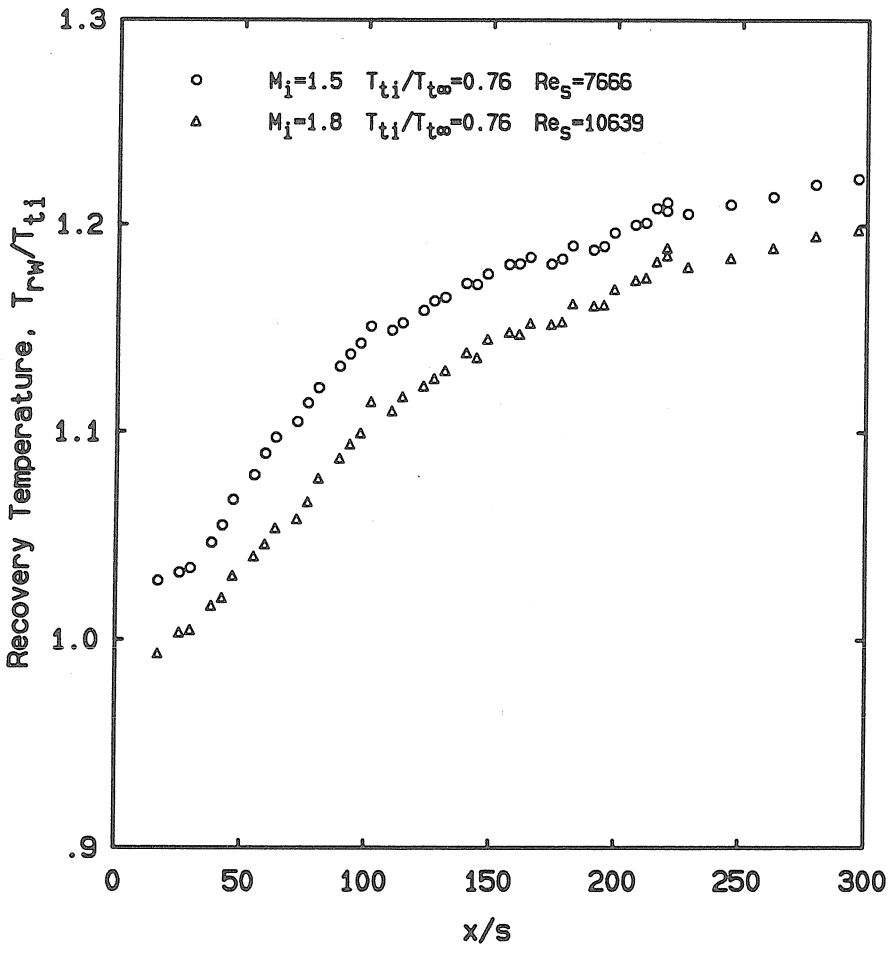

Figure 3.23: Cold air injection temperature distribution

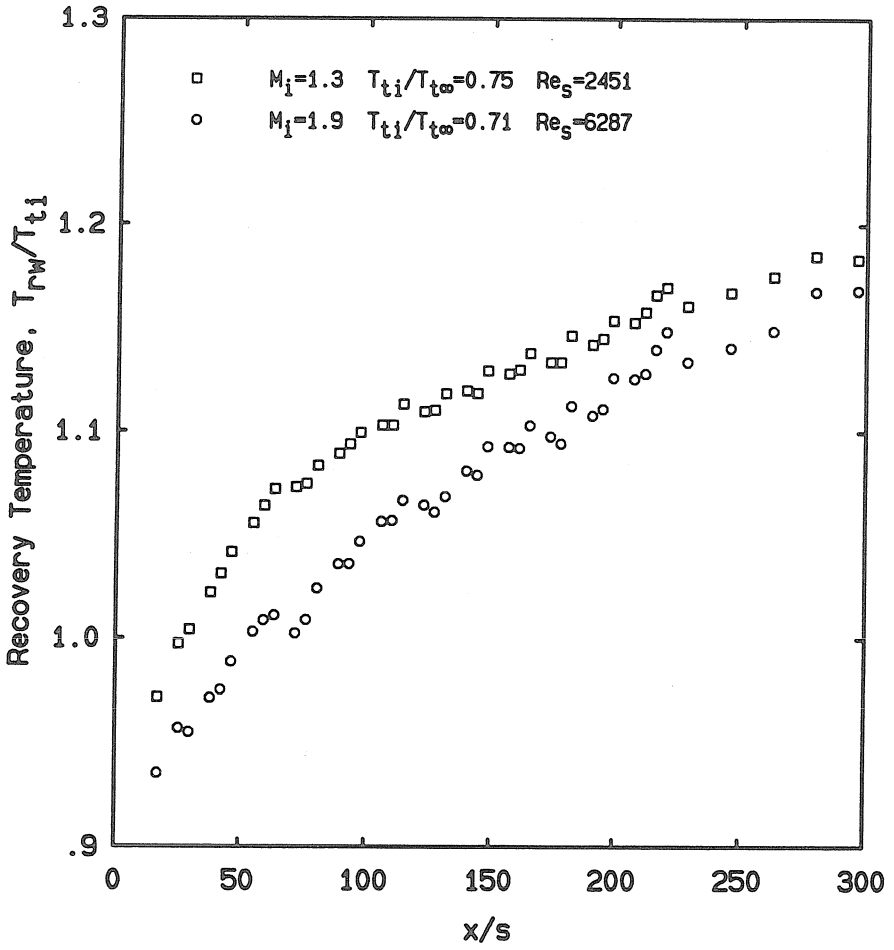

Figure 3.24: Cold helium injection temperature distribution

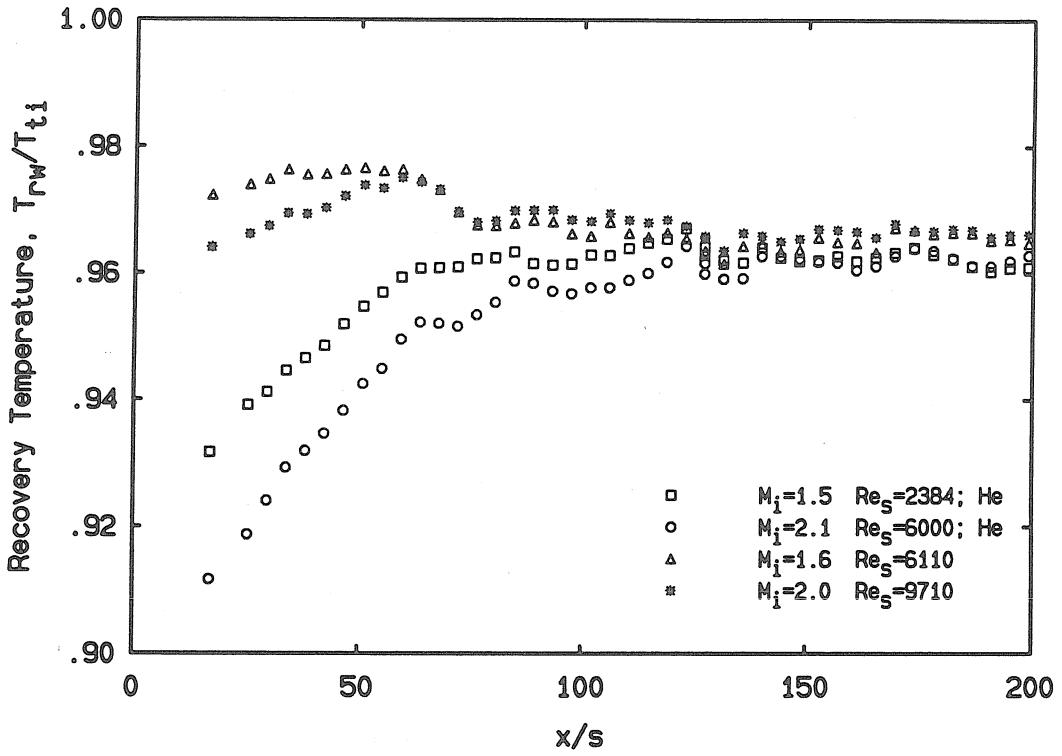

Figure 3.25: Isoenergetic injection temperature distribution

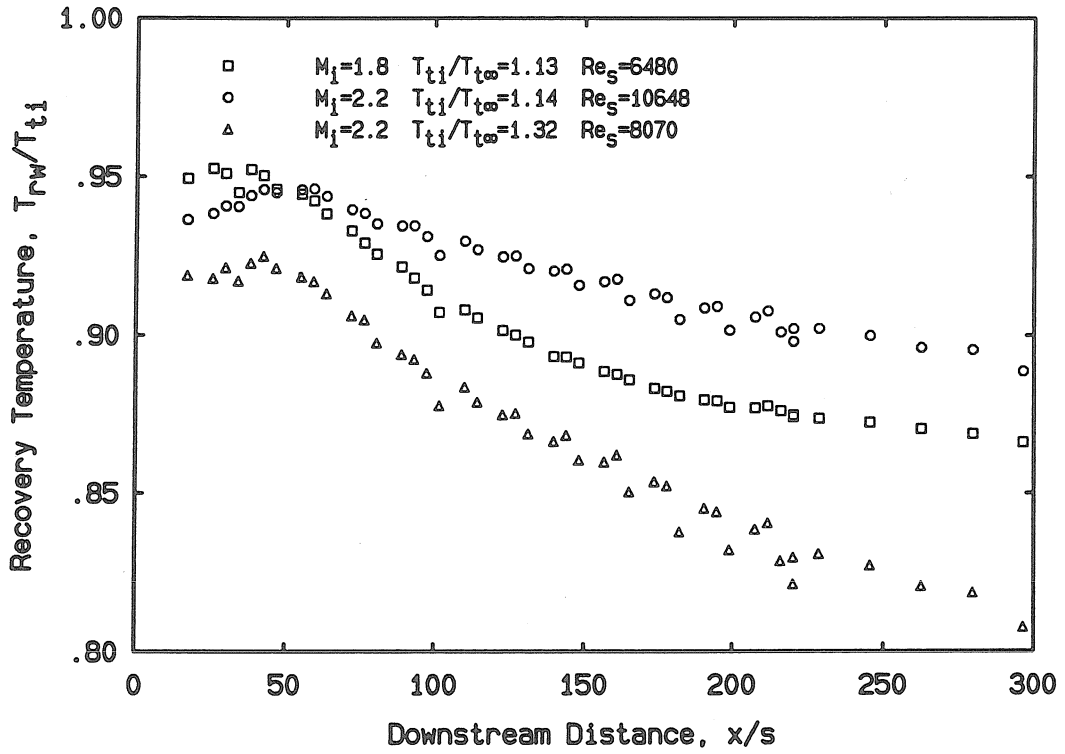

Figure 3.26: Hot air injection temperature distribution

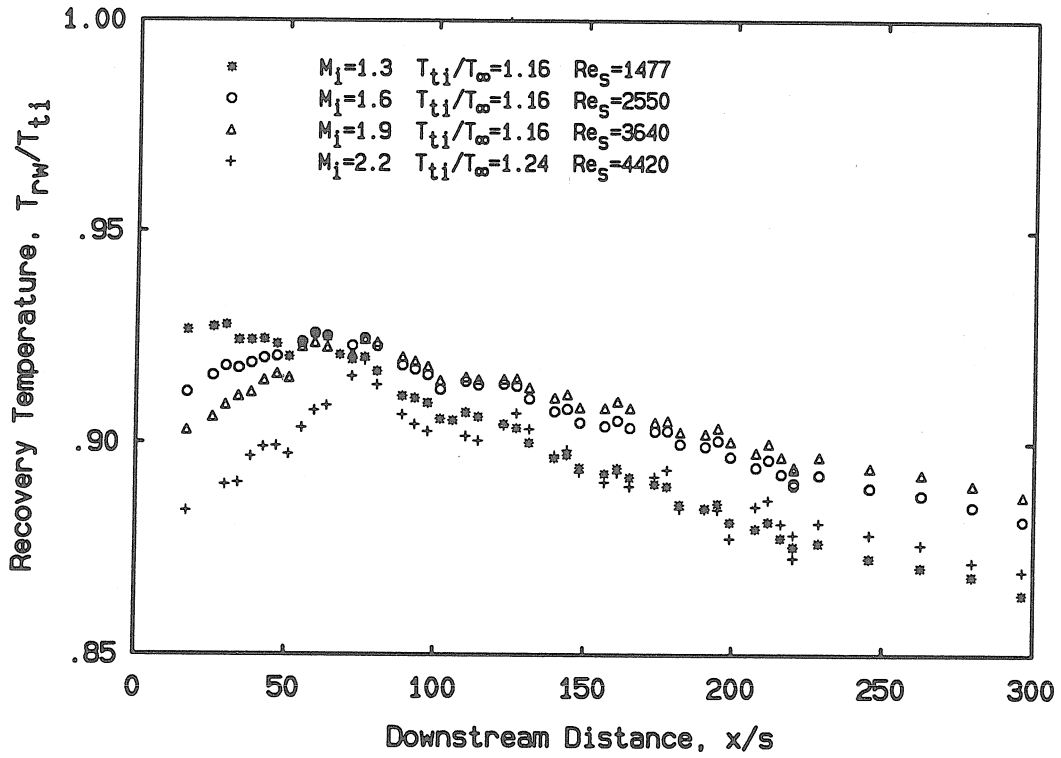

Figure 3.27: Hot helium injection temperature distribution

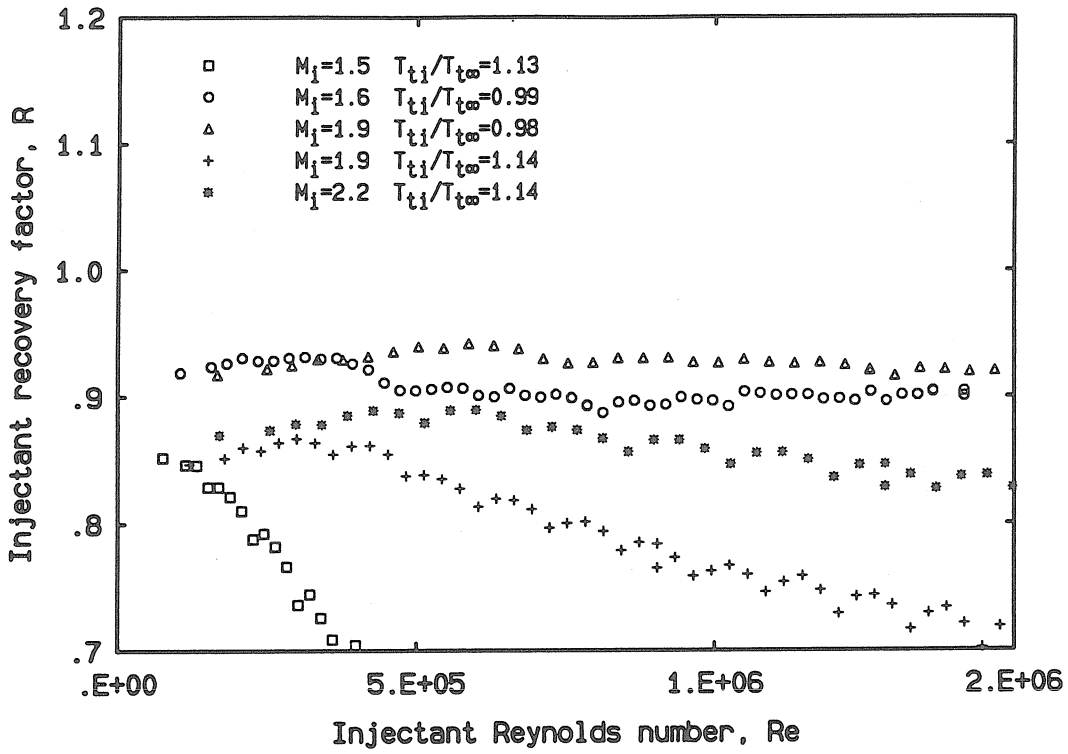

Figure 3.28: The recovery factor as a function of the Reynolds number based on the distance from the slot, for air injection

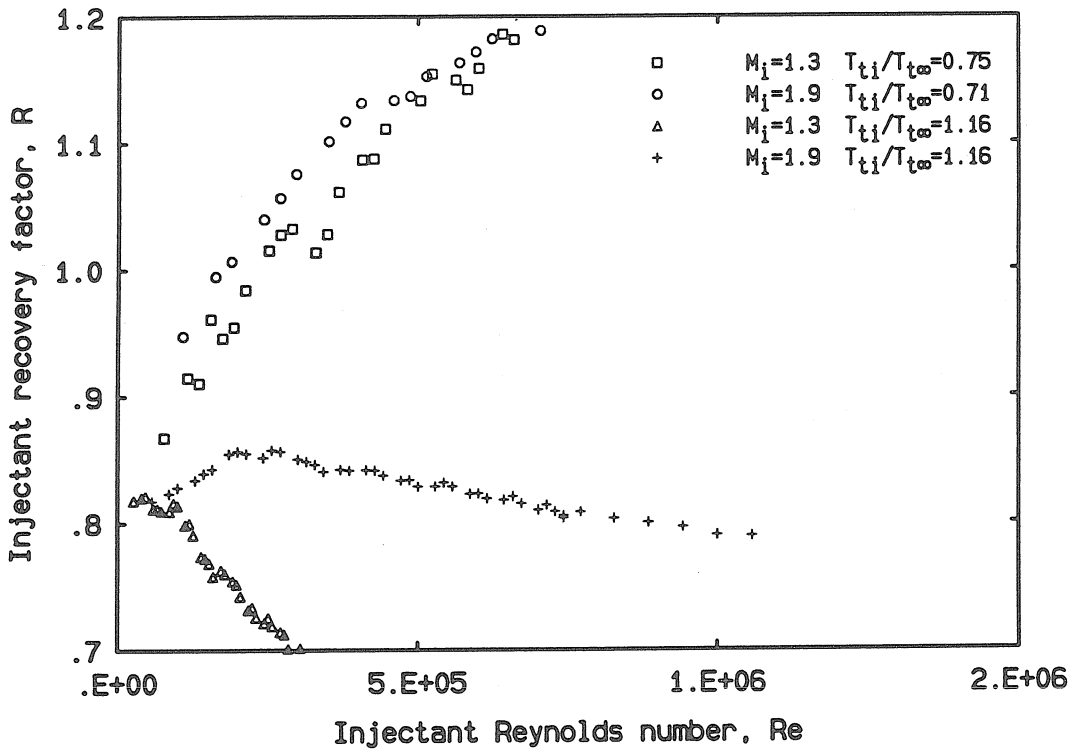

Figure 3.29: The recovery factor as a function of the Reynolds number based on the distance from the slot, for helium injection

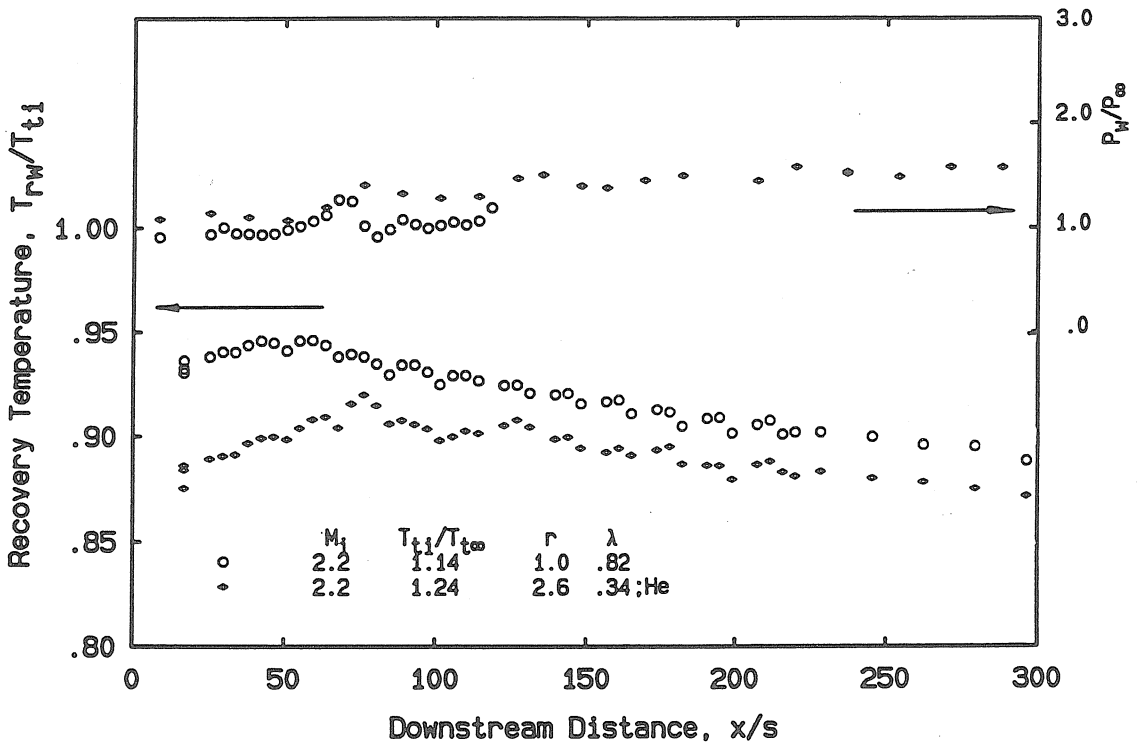

Figure 3.30: Temperature and pressure ratios of heated helium and air injections displaying an increase in temperature downstream of the slot

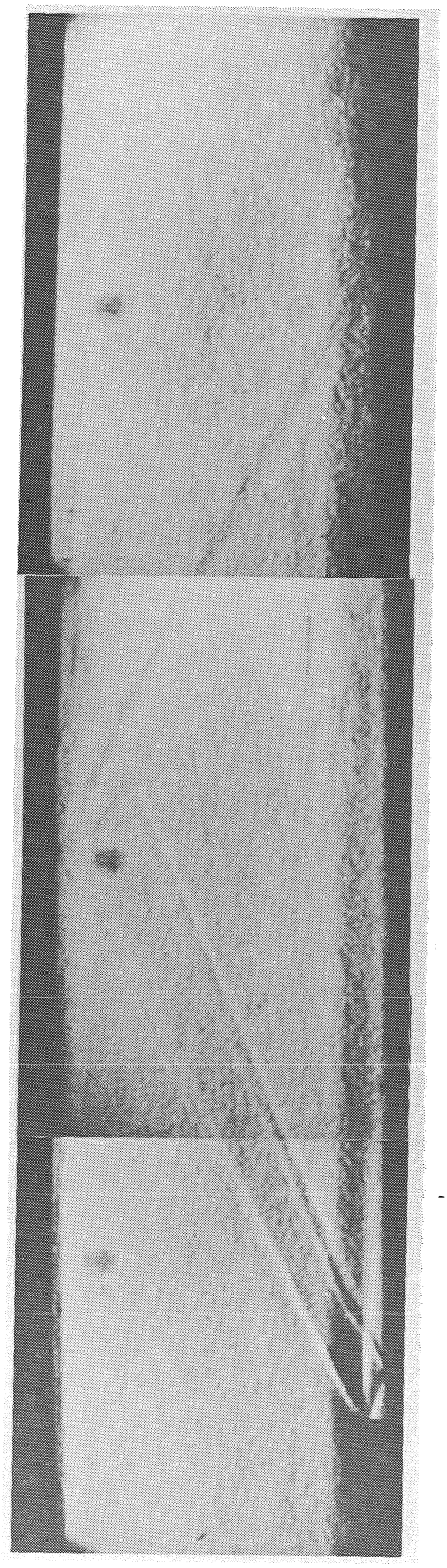

Figure 3.31: Schlieren photograph of Mach 2.2 heated air injection

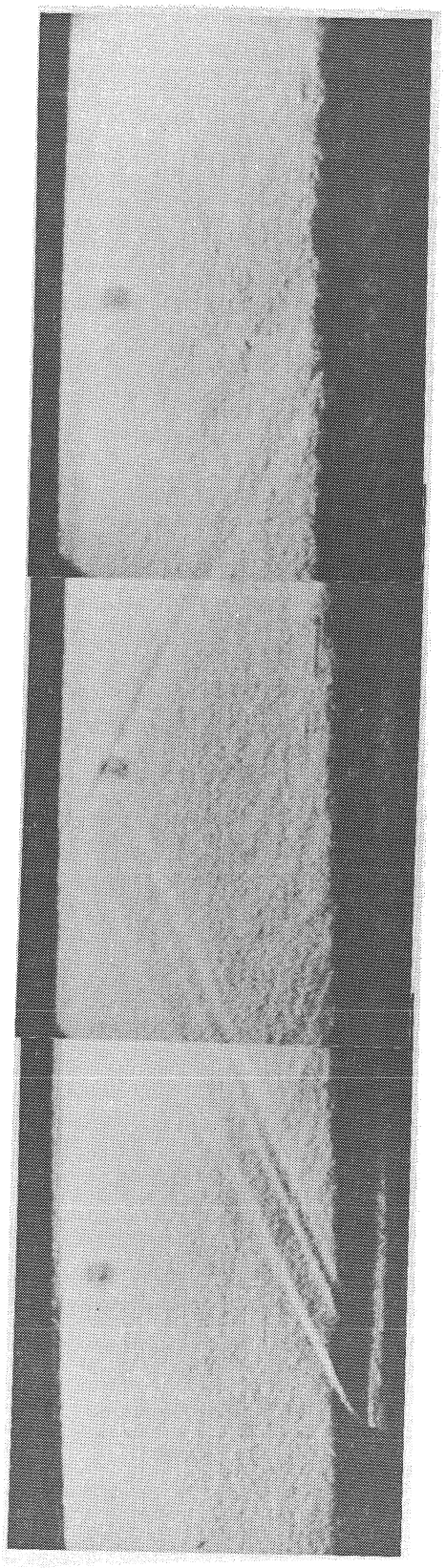

Figure 3.32: Schlieren photograph of Mach 2.2 heated helium injection

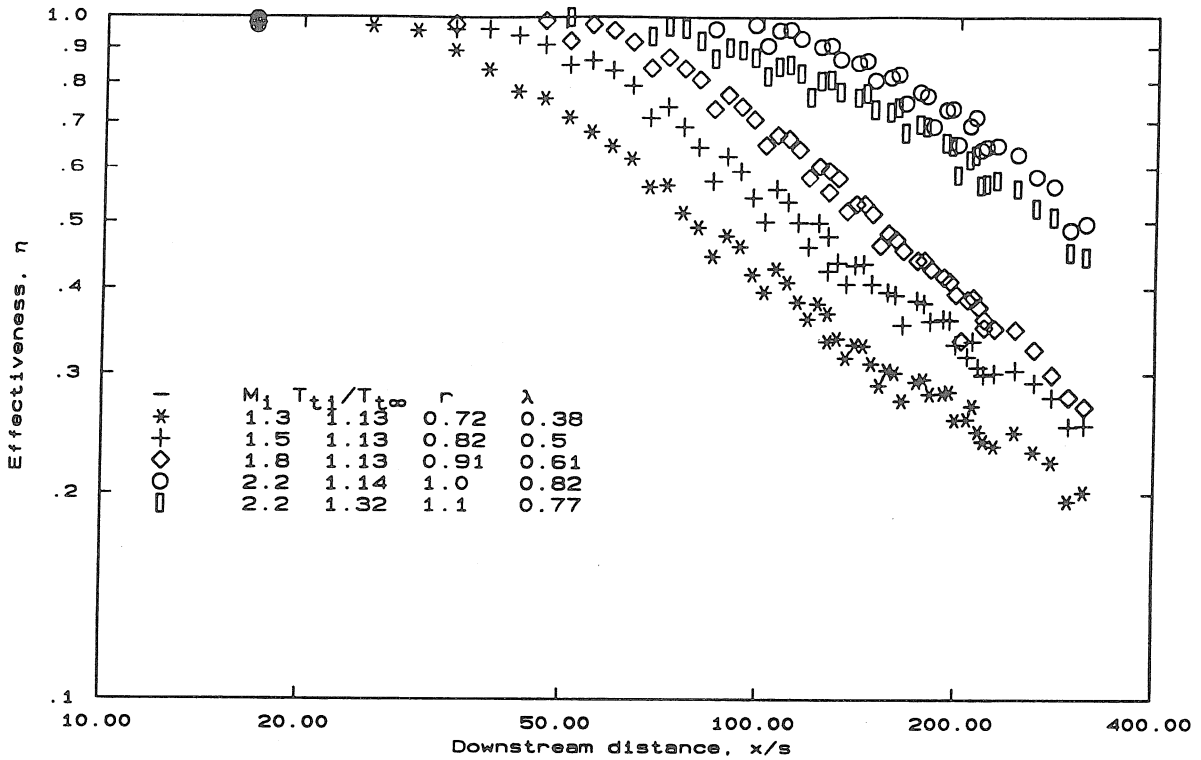

Figure 3.33: Film-cooling effectiveness, η, as a function of x/s for heated air injection

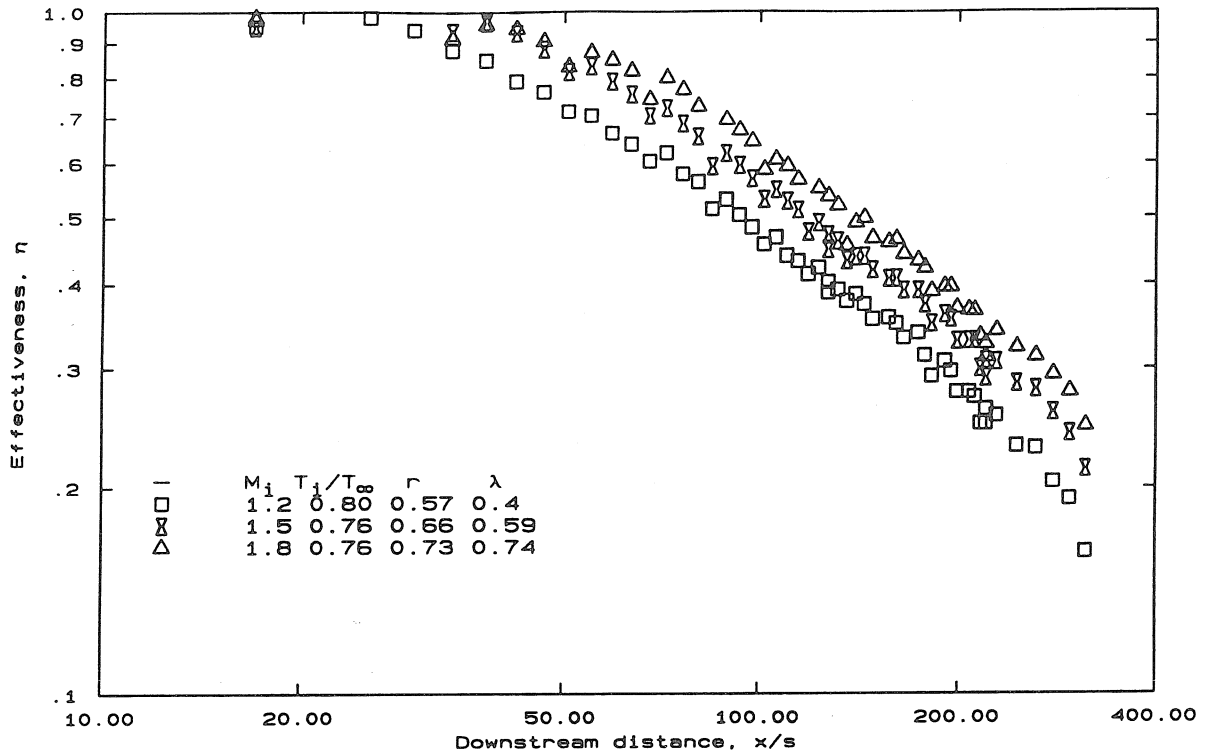

Figure 3.34: Film-cooling effectiveness, η, as a function of x/s for cooled air injection

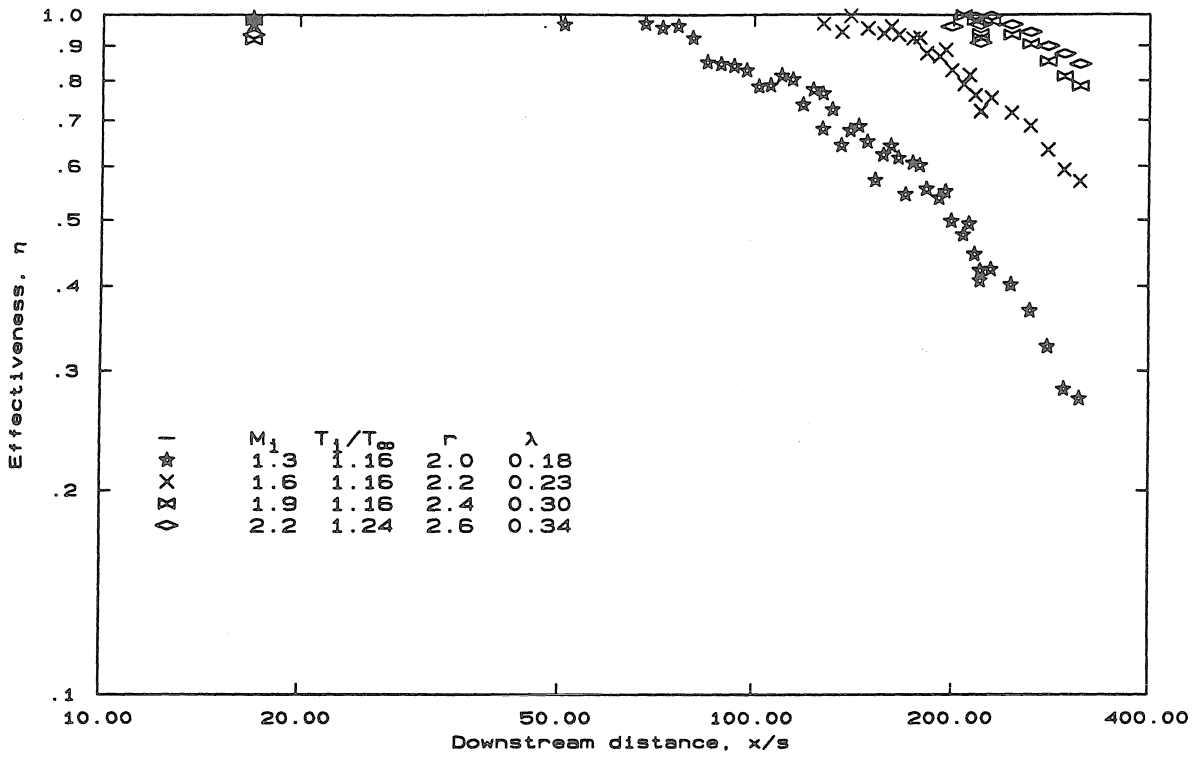

Figure 3.35: Film-cooling effectiveness, η, as a function of x/s for heated helium injection

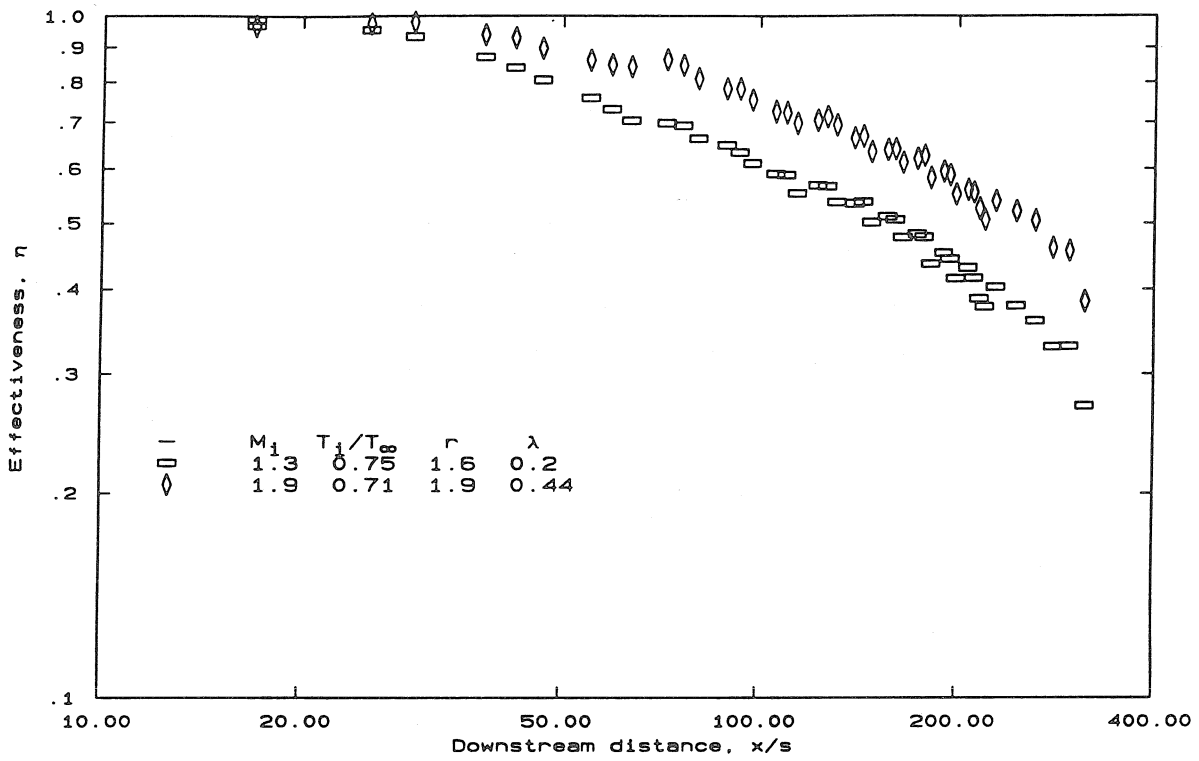

Figure 3.36: Film-cooling effectiveness, η, as a function of x/s for cooled helium injection

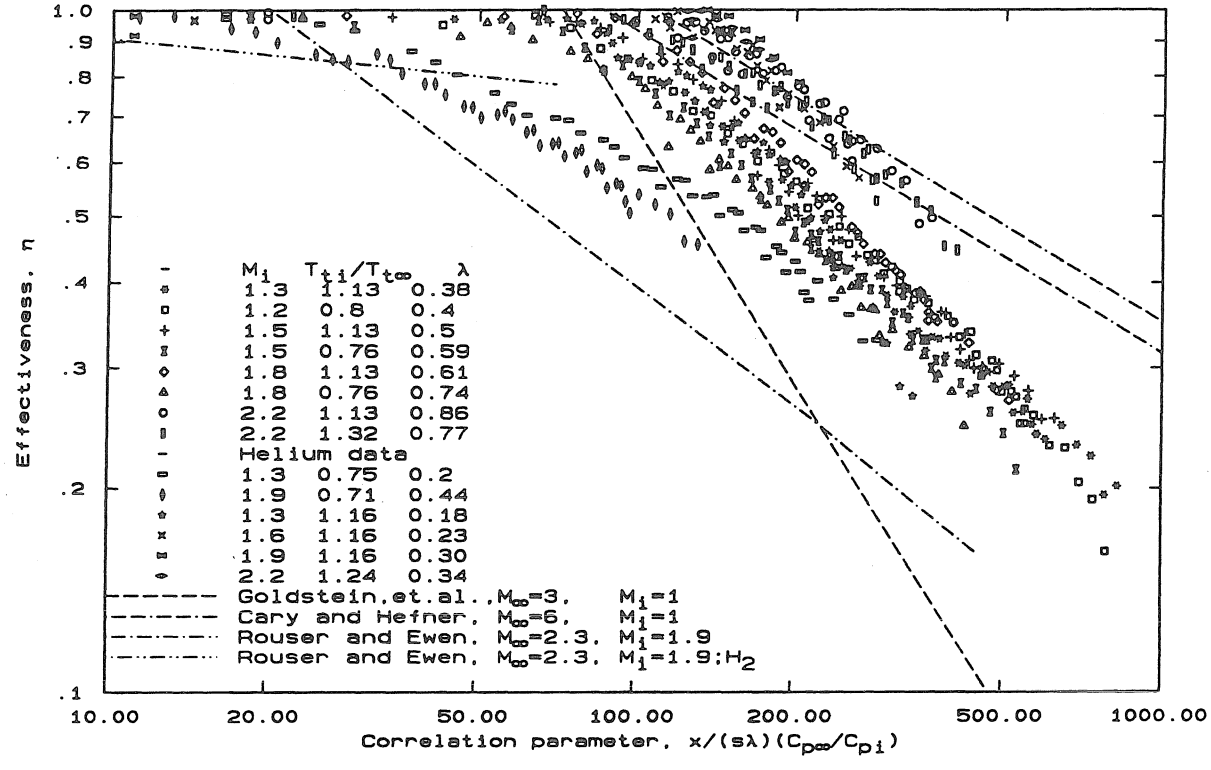

Figure 3.37: Comparison of experimental results with previous data using the correlation parameter

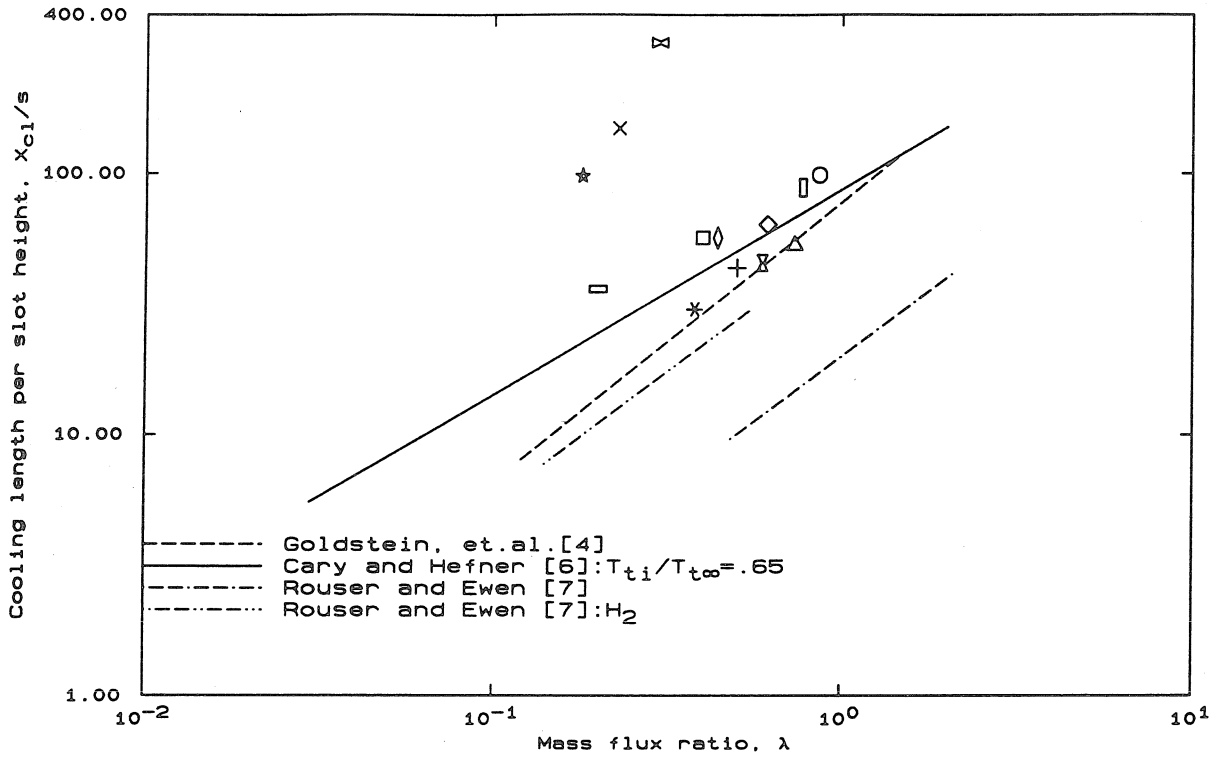

Figure 3.38: Cooling length X_{cl} as a function of the mass flux ratios. Symbols correspond to the ones in Fig. 3.37

Case	Fluid	$T_{ti}/T_{t\infty}$	M_i	λ	u_i/u_∞	$(\rho u^2)_i/(\rho u^2)_\infty$	Re_s
1	air	1	1.2	0.39	0.6	0.23	3660
2	air	1	2.2	0.87	1.0	0.87	12000
3	helium	1	1.3	0.19	1.9	0.36	1870
4	helium	1	2.2	0.41	2.4	0.98	6340
5	air	1.14	1.2	0.36	0.7	0.25	3070
6	air	1.14	2.2	0.82	1.0	0.82	10000
7	air	1.33	2.2	0.75	1.1	0.82	8040
8	helium	1.14	1.3	0.17	2.0	0.34	1560
9	helium	1.36	1.3	0.16	2.2	0.35	1270
10	helium	1.22	2.2	0.37	2.7	1.00	4700

Table 4.1: Experimental Parameters

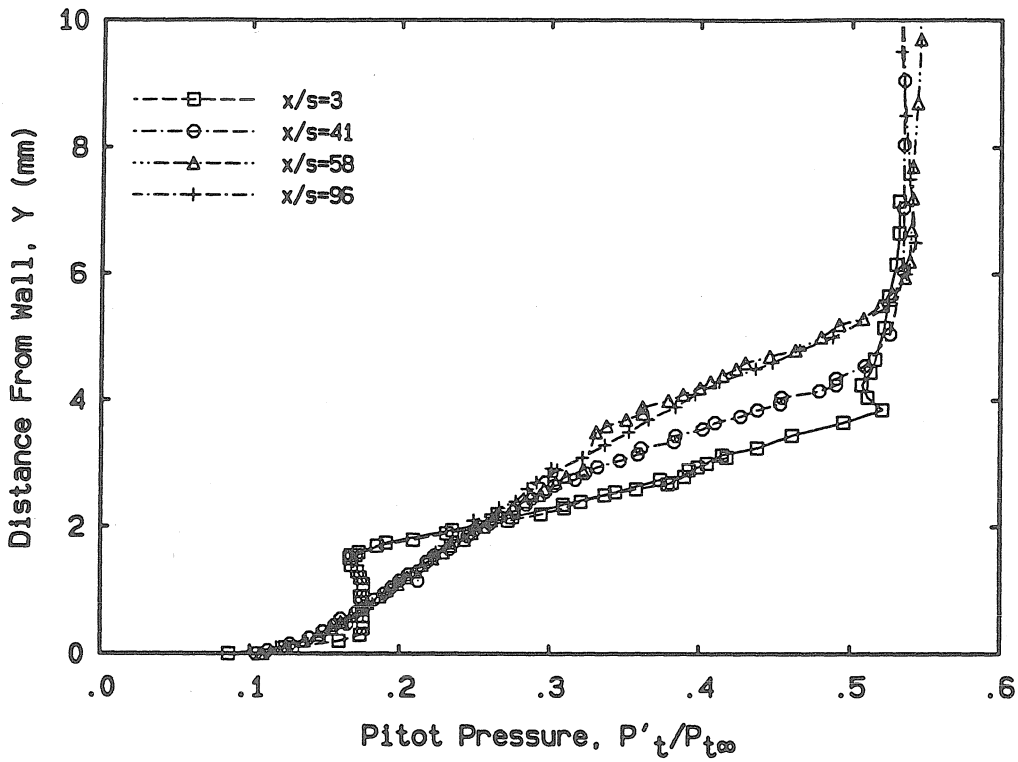

Figure 4.1: Pitot probe profile for air injection at $M_i = 1.2$

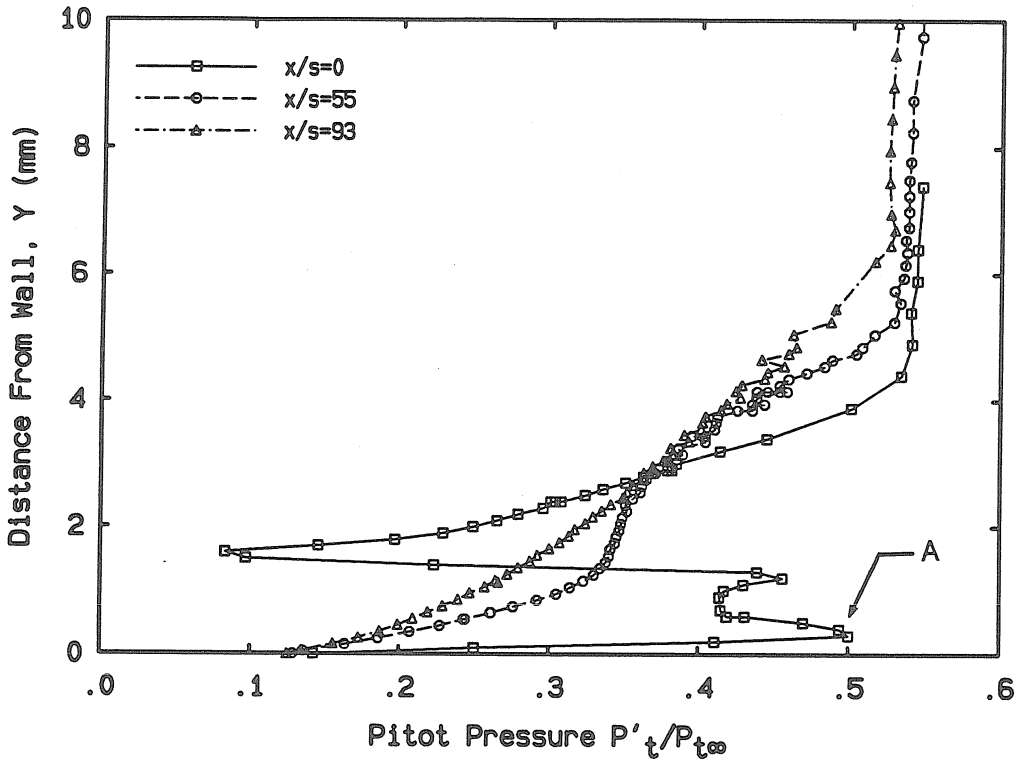

A: Indentation due to probe interference

Figure 4.2: Pitot probe profile for air injection at $M_i = 2.2$

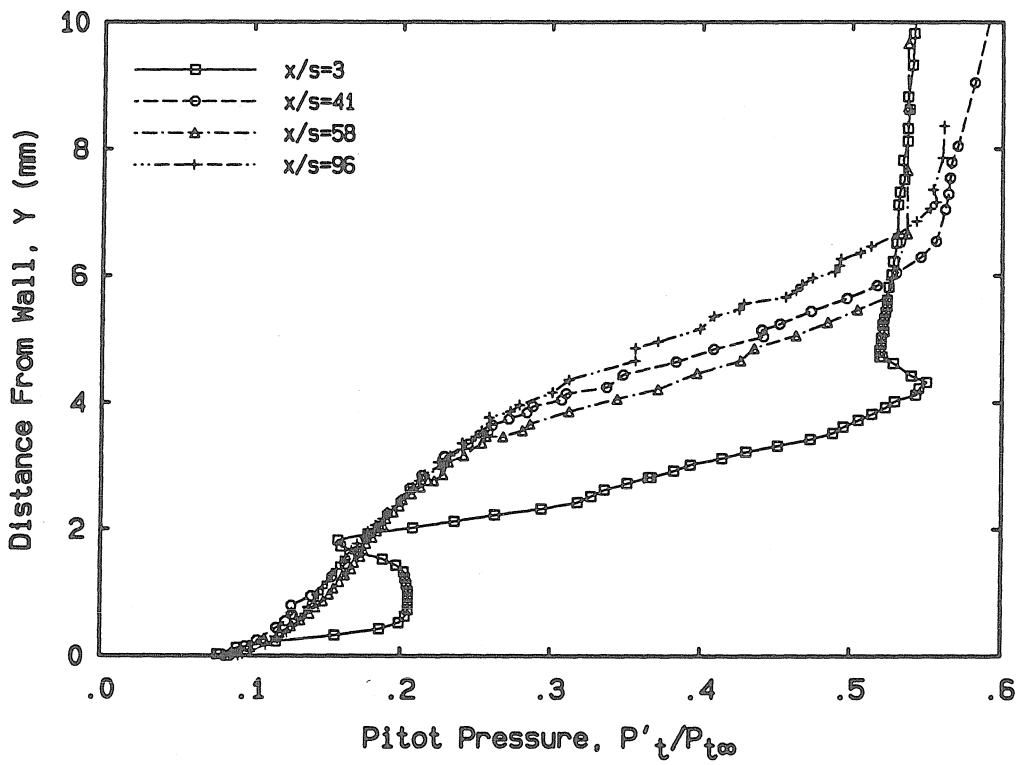

Figure 4.3: Pitot probe profile for helium injection at $M_i = 1.3$

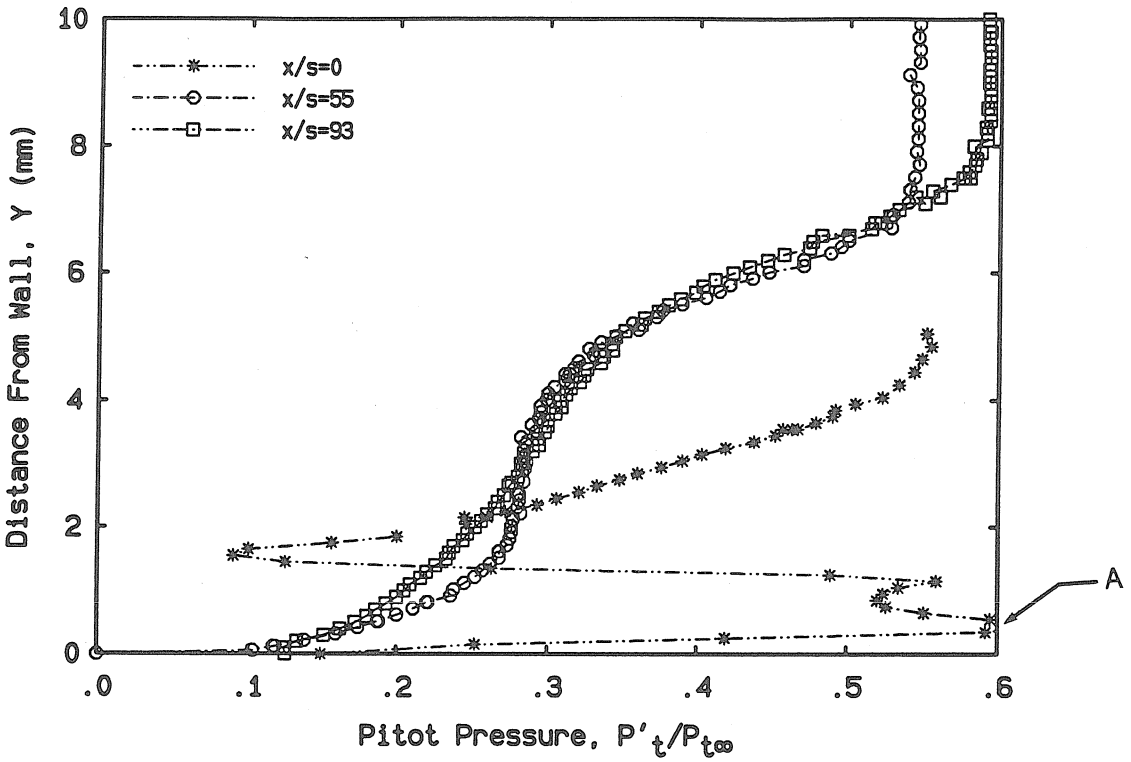

Figure 4.4: Pitot probe profile for helium injection at $M_i = 2.2$

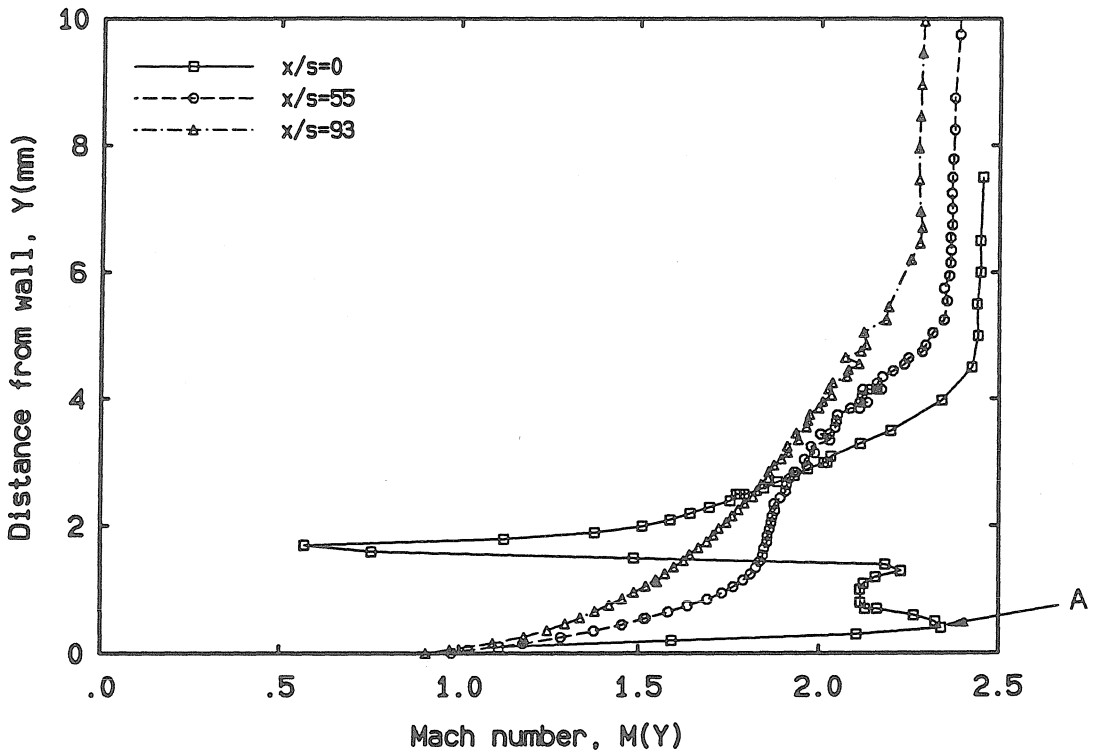

Figure 4.5: Mach number profile for air injection at $M_i = 2.2$

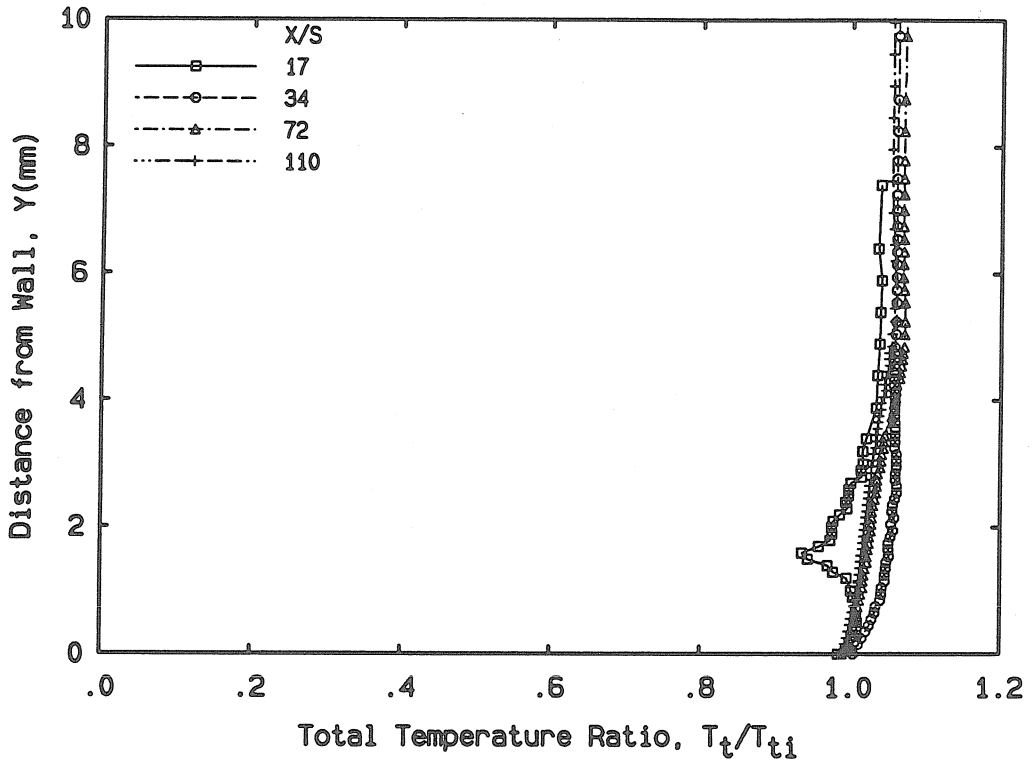

Figure 4.6: Temperature profile for isoenergetic air injection at $M_i = 2.2$

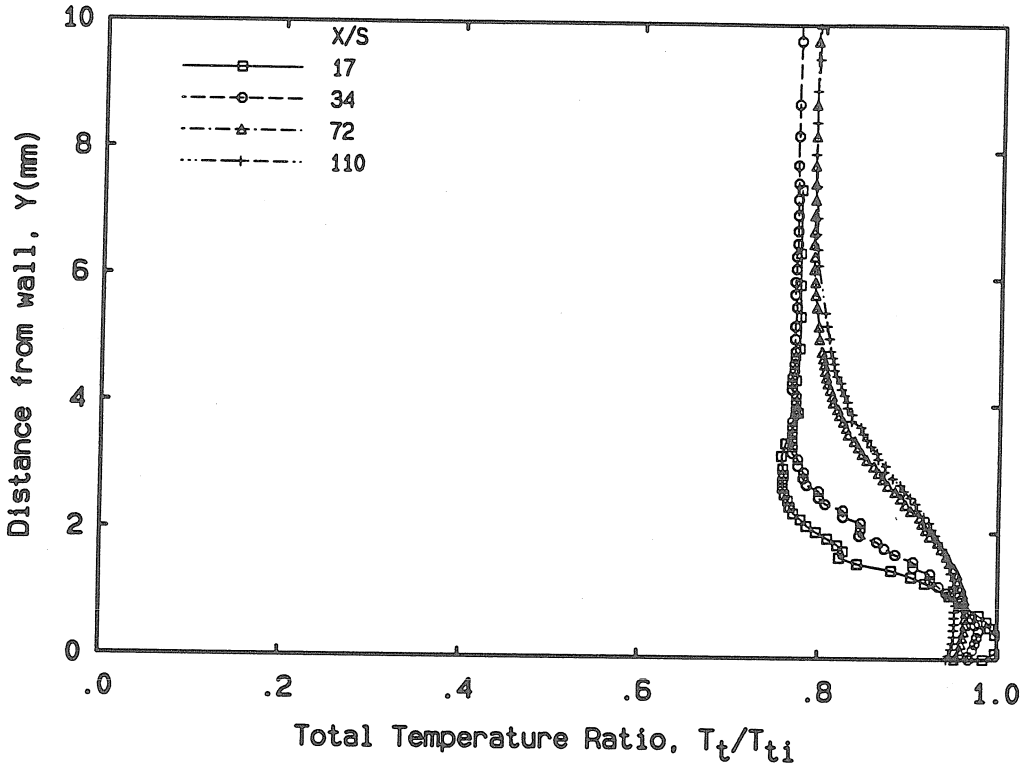

Figure 4.7: Temperature profile for heated air injection at $M_i = 2.2$

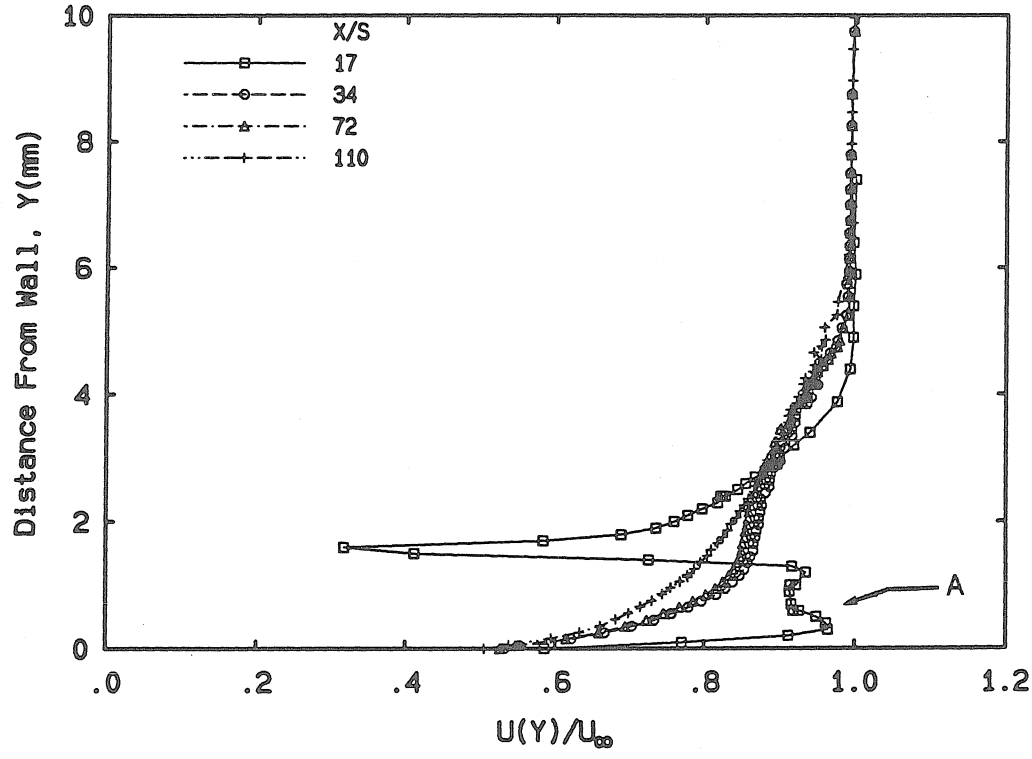

A: Indentation due to probe interference

Figure 4.8: Velocity profile for isoenergetic air injection at $M_i = 2.2$

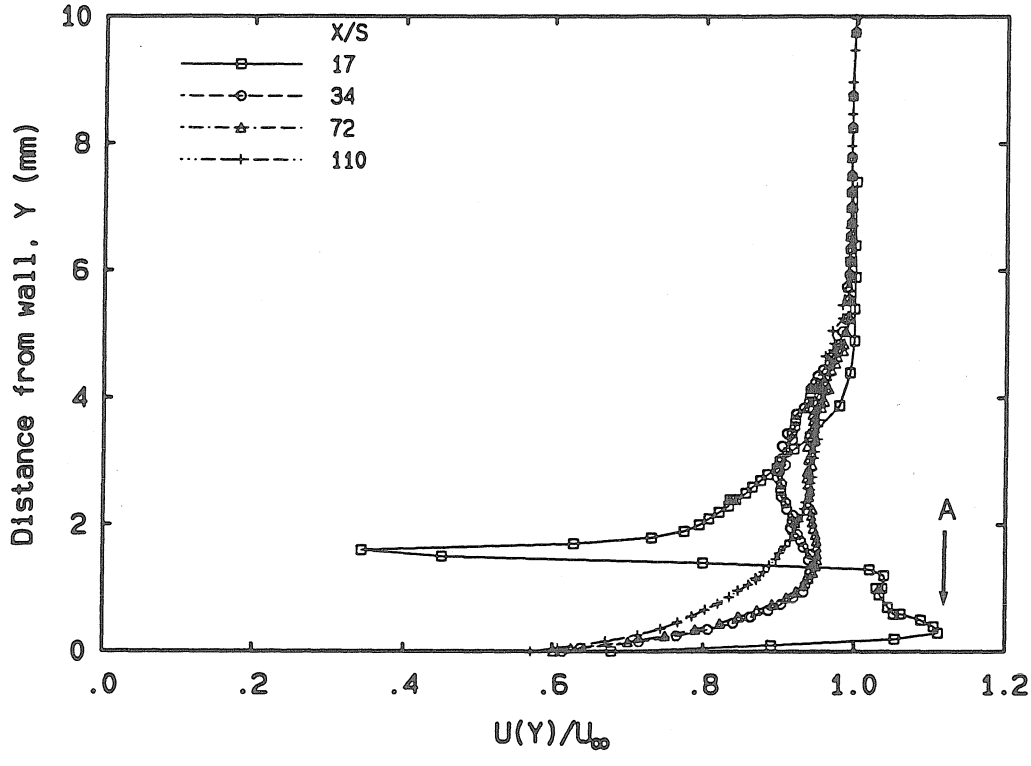

A: Indentation due to probe interference

Figure 4.9: Velocity profile for heated air injection at $M_i = 2.2$

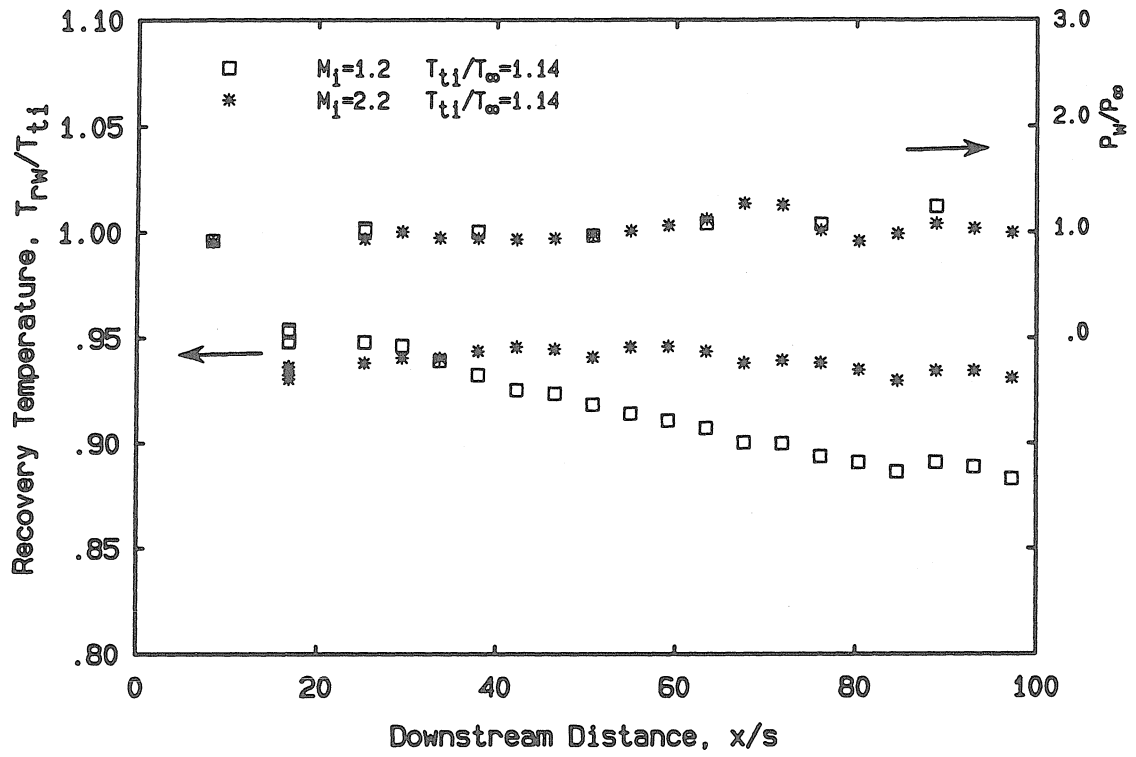

Figure 4.10: Heated air injections pressure and temperature ratios

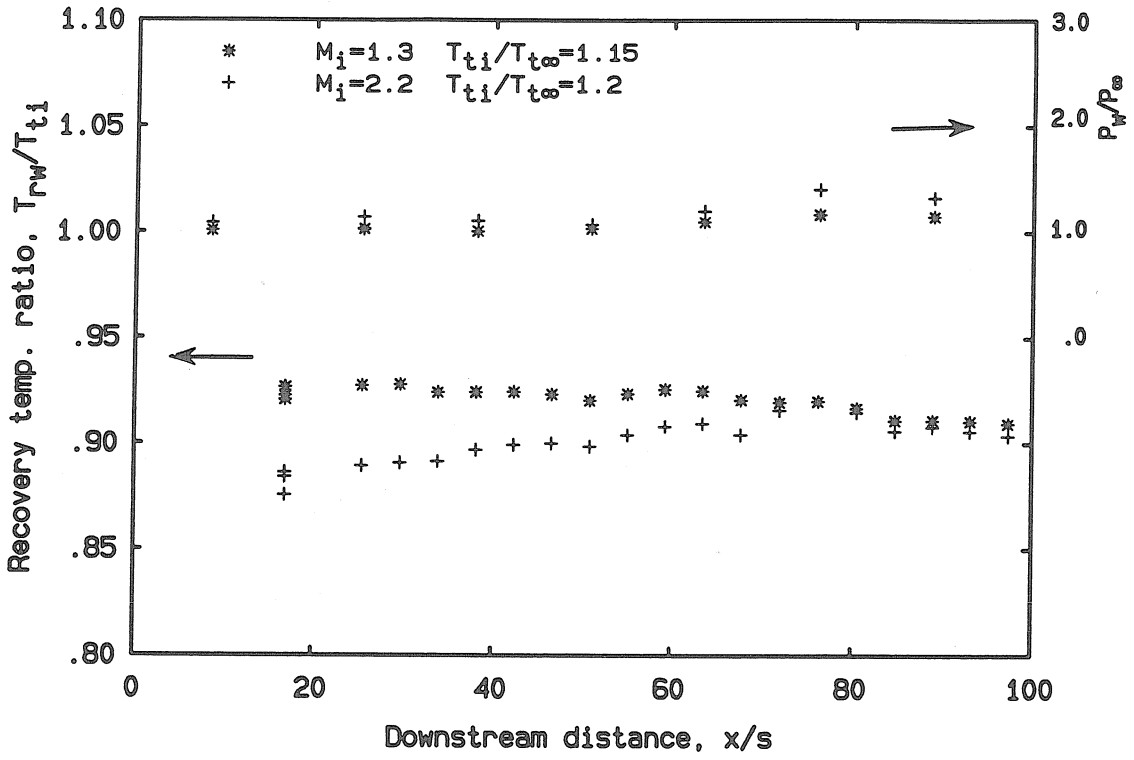

Figure 4.11: Heated helium injections pressure and temperature ratios

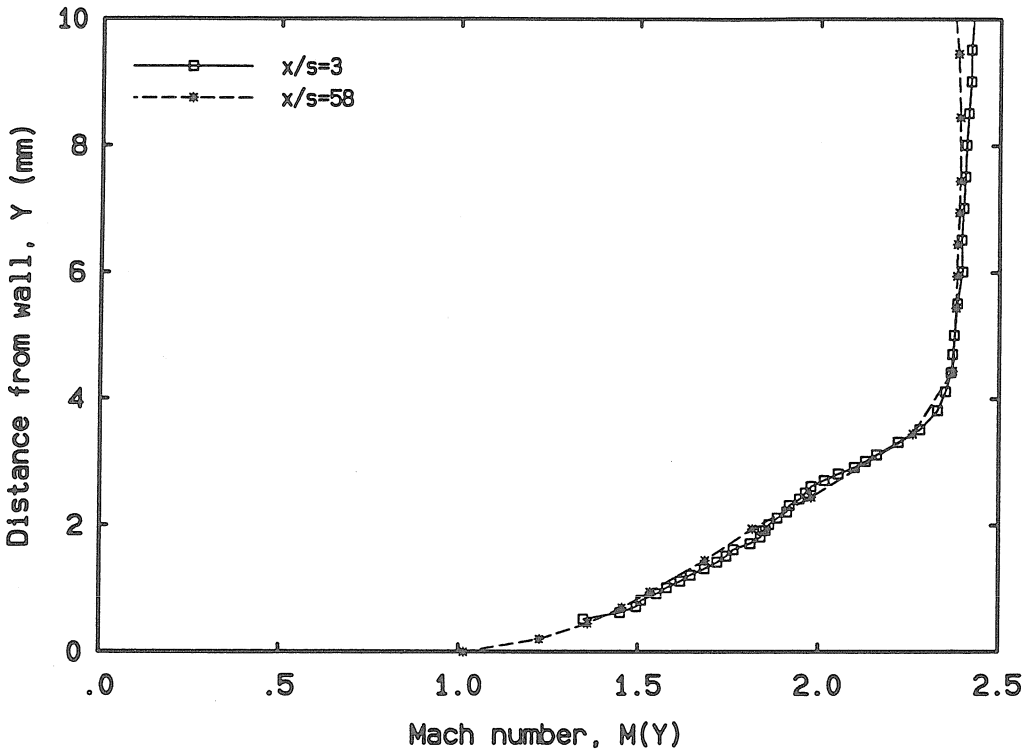

Figure 4.12: Comparison between the initial freestream boundary layer and the one at the shock impingement location, without injection

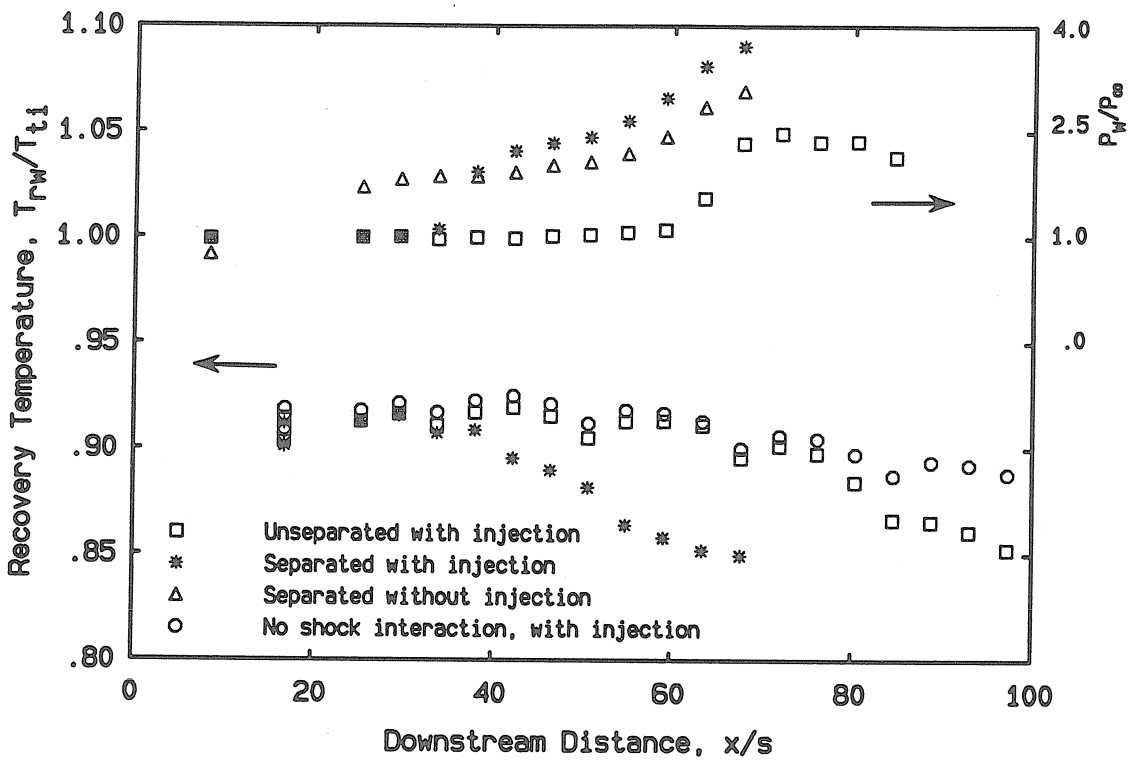

Figure 4.13: Shock interaction with heated air injection at $M_i = 2.2$, $T_{ti}/T_{t\infty} = 1.33$

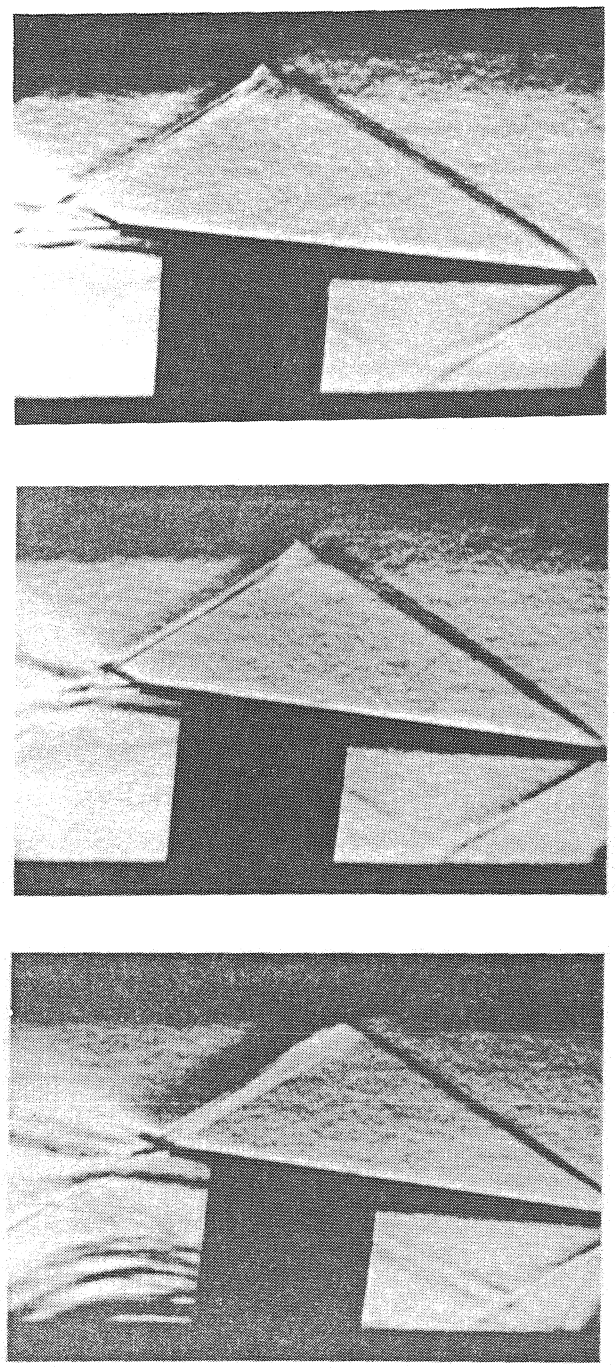

Figure 4.14: Series of schlieren photographs showing the interaction between a shock wave of different strength with heated air injection of Mach 2.2. The top photo is for the weakest shock, while the bottom one is the strongest

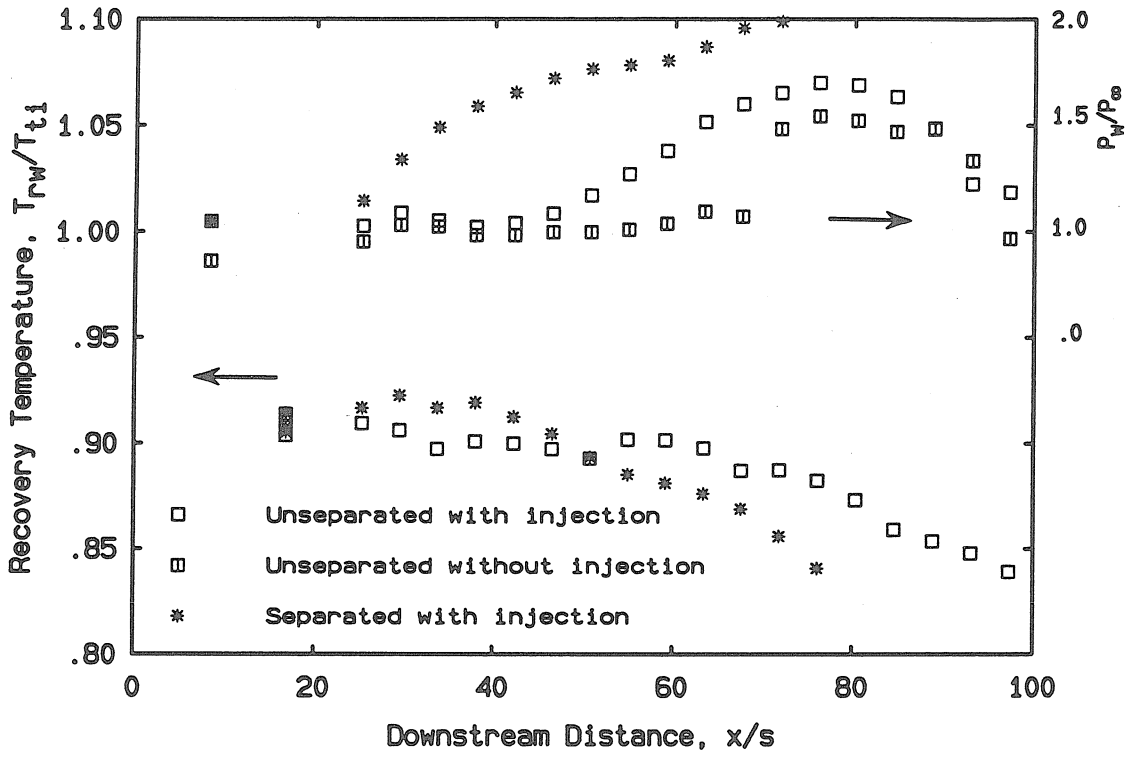

Figure 4.15: Shock interaction with heated helium injection at $M_i = 1.3$, $T_{ti}/T_{t\infty} = 1.36$

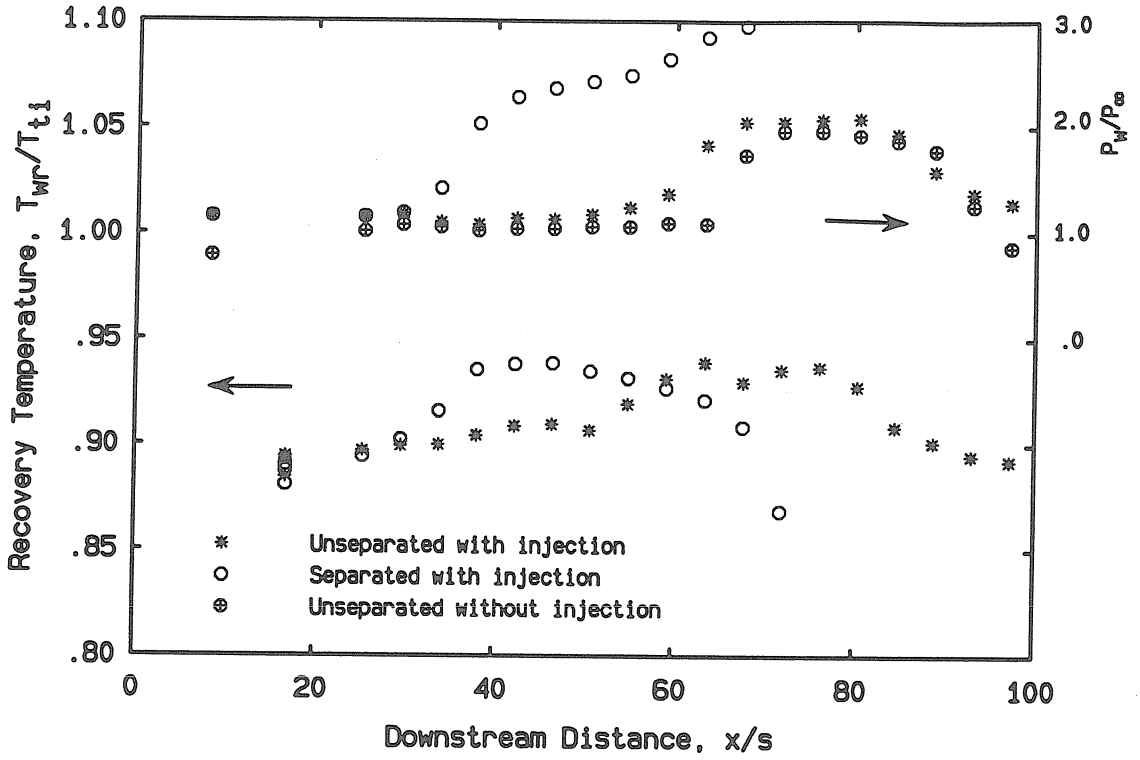

Figure 4.16: Shock interaction with heated helium injection at $M_i = 2.2$, $T_{ti}/T_{t\infty} = 1.22$

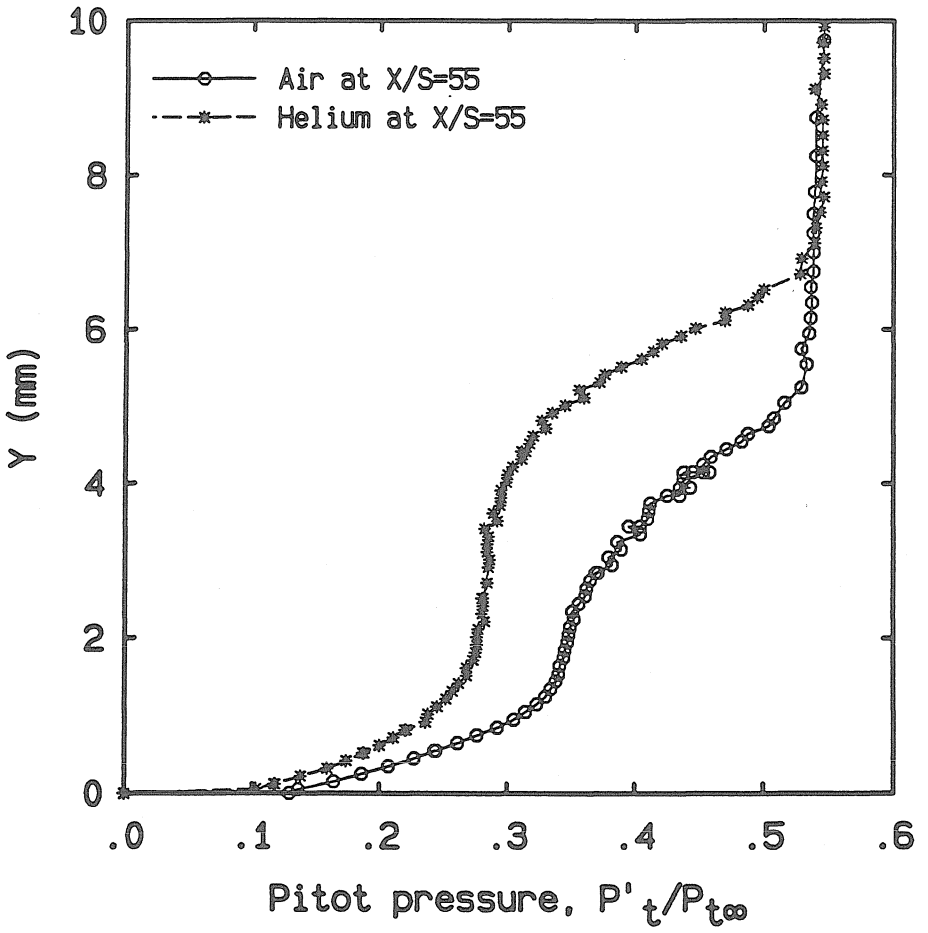

Figure 4.17: Comparison between pitot pressure profiles of both helium and air $M_i = 2.2$ injections upstream of the shock impingement location

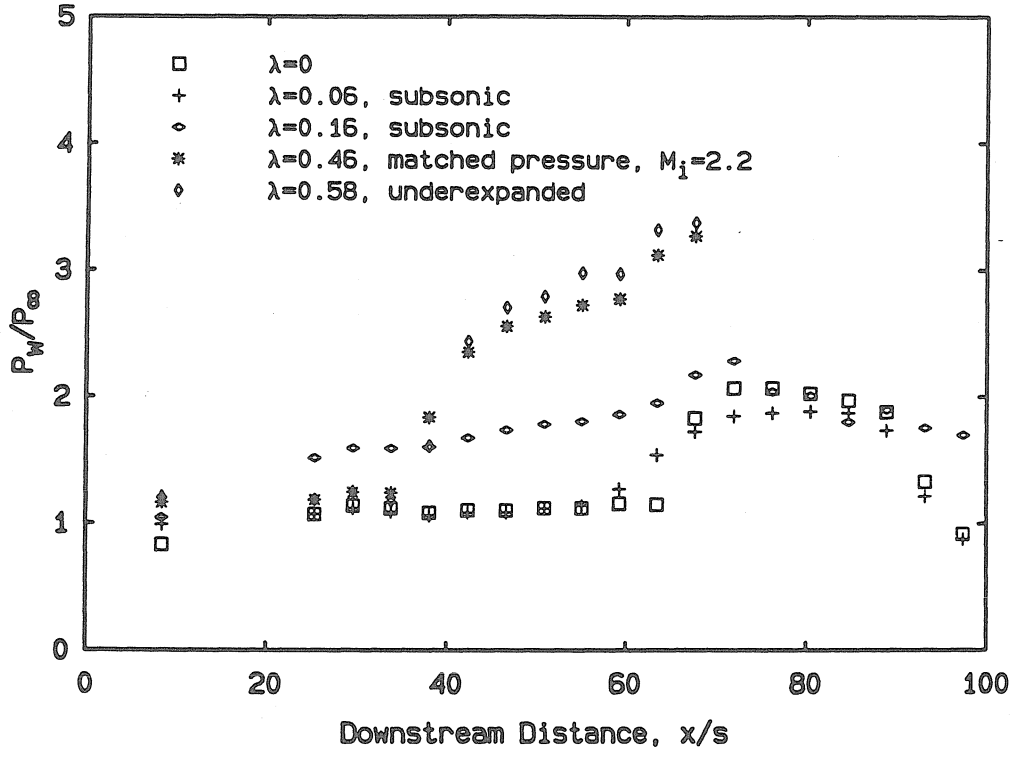

Figure 4.18: Effect of helium injection on strong shock interaction

Appendix A

Control Volume Analysis

To develop a correlation for the effectiveness, a simplified model is assumed to identify the parameters that effectiveness depends on. The model used in this analysis is shown in Fig. A1. The analysis here is more general than the analyses given by Goldstein (1971) and by previous incompressible studies that are summarized in his study, but it is similar. The equation of mass and energy are applied as follows:

Mass Balance

$$\dot{m}_{bl} = \dot{m}_i + \dot{m}_c + \dot{m}_e \ . \tag{1}$$

$\dot{m}$ is the total mass flow rate and the subscripts bl, i, c, and e denote that of the boundary layer downstream, the initial boundary layer, the coolant, and the entrained ambient flow.

Energy Balance

$$\dot{m}_{bl}\bar{C}_{pbl}\bar{T}_{0bl} = \dot{m}_i\bar{C}_{pi}\bar{T}_{0i} + \dot{m}_c\bar{C}_{pc}\bar{T}_{0c} + \dot{m}_e\bar{C}_{pe}\bar{T}_{0e} \ . \tag{2}$$

$\bar{T}_0$ is the mass averaged total temperature. The average specific heat is defined as

$$\dot{m}_{bl}\bar{C}_{pbl} = \dot{m}_i\bar{C}_{pi} + \dot{m}_c\bar{C}_{pc} + \dot{m}_e\bar{C}_{pe} \ . \tag{3}$$

Since the lip is adiabatic, $\bar{T}_{0i} = \bar{T}_{0e}$. Using this fact and combining Eqs. 1, 2, and 3, and after some rearranging, yields:

$$\frac{\bar{T}_{0bl} - \bar{T}_{0e}}{\bar{T}_{0c} - \bar{T}_{0e}} = \frac{1}{1 + \frac{\dot{m}_e\bar{C}_{pe}}{\dot{m}_c\bar{C}_{pc}} + \frac{\dot{m}_i\bar{C}_{pi}}{\dot{m}_c\bar{C}_{pc}}} \ . \tag{4}$$

The nondimensional temperature ratio is called effectiveness η. This equation is similar to Goldstein (1971) with the exception of the additional term resulting from the inclusion of the initial boundary layer. The right-hand side contains an unknown parameter $\dot{m}_e$, the amount of flow entrained from the freestream:

$$\dot{m}_e = \dot{m}_{bl} - \dot{m}_i - \dot{m}_c \ . \tag{5}$$

There are two common approaches to determine the value of $\dot{m}_e$. One is to assume that the initial boundary layer continues to grow as a boundary layer flow and its entrainment is not effected by the injection. The second is to assume that the ambient flow is entrained in the shear layer similar to a jet, so that the entrainment mass flux is proportional to that of the free stream, i.e., $\rho_e u_e = K\rho_\infty u_\infty$.

Let δ_0 be a fictitious boundary layer height at the injection location x_0, $\delta_0 \neq \delta_i + t + s$. The boundary layer mass flow rate at x_0, $\dot{m}_0$ is assumed to be equal to the combined mass flow rate of the injectant and the incoming free stream boundary layer:

$$\dot{m}_0 = \dot{m}_i + \dot{m}_c \tag{6}$$

$$\dot{m}_{bl} = \int_0^\delta \rho u dy \ . \tag{7}$$

If a boundary layer growth is assumed then, then the flow downstream of the slot grows as:

$$\delta/x = c_\delta Re_x^{-\frac{1}{m}} \tag{8}$$

where c_δ and m are constants. Also if a power law velocity profile is used then

$$\frac{\rho u}{\rho_\infty u_\infty} = (\frac{y}{\delta})^{1/n} \ . \tag{9}$$

Therefore,

$$\dot{m}_{bl} = \rho_\infty u_\infty \delta \int_0^\delta (\frac{y}{\delta})^{1/n} dy = (\frac{n}{n+1})\rho_\infty u_\infty \delta \tag{10a}$$

similarly

$$\dot{m}_i = (\frac{n}{n+1})\rho_\infty u_\infty \delta_i \tag{10b}$$

and

$$\dot{m}_c = \bar{\rho}_c \bar{u}_c s \ . \tag{11}$$

Using Eqn. (8), Eqn. (6) becomes:

$$(\frac{n}{n+1})\rho_\infty u_\infty c_\delta x_0 Re_{x_0}^{-\frac{1}{m}} = (\frac{n}{n+1})\rho_\infty u_\infty \delta_i + \bar{\rho}_c \bar{u}_c s \ . \tag{12}$$

Recall that $Re_{x_0} = \frac{\rho_\infty u_\infty x_0}{\mu_\infty}$ and that $\lambda = \frac{\bar{\rho}_c \bar{u}_c}{\bar{\rho}_\infty \bar{u}_\infty}$. The coolant Reynolds number Re_c and the Reynolds number based on the initial freestream boundary layer thickness Re_{δ_i} are:

$$Re_{\delta_i} = \frac{\rho_\infty u_\infty \delta_i}{\mu_\infty}$$

$$Re_c = \frac{\bar{\rho}_c \bar{u}_c s}{\mu_\infty} .$$

After some manipulation Equation (12) becomes

$$(\frac{x_0}{\lambda s})(\frac{1}{Re_c}\frac{\mu_\infty}{\mu_c})^{\frac{1}{m-1}} = (\frac{1}{c_\delta}\frac{Re_{\delta_i}}{Re_c}\frac{\mu_\infty}{\mu_c} + \frac{1}{c_\delta}\frac{n+1}{n})^{\frac{m}{m-1}} . \tag{13}$$

Equation (13) allows us to determine the value x_0 from initially known values. This equation will be used later to determine the effectiveness.

Combining (10 a), (10 b), and (11) in (6) results:

$$\dot{m}_e = (\frac{n}{n+1})\rho_\infty u_\infty \delta - (\frac{n}{n+1})\rho_\infty u_\infty \delta_i - \bar{\rho}_c \bar{u}_c s \tag{14}$$

$$\frac{\dot{m}_i}{\dot{m}_c} = \frac{1}{\lambda}\frac{\delta_i}{s}\frac{n}{n+1} \tag{15}$$

$$\frac{\dot{m}_e}{\dot{m}_c} = \frac{1}{\lambda}\frac{\delta}{s}\frac{n}{n+1} - \frac{1}{\lambda}\frac{\delta_i}{s}\frac{n}{n+1} - 1 . \tag{16}$$

The denominator of equation 4 is given by

$$1 + \frac{\dot{m}_e \bar{C}_{pe}}{\dot{m}_c \bar{C}_{pc}} + \frac{\dot{m}_i \bar{C}_{pi}}{\dot{m}_c \bar{C}_{pc}} \tag{17}$$

becomes

$$1 + \frac{1}{\lambda}\frac{n}{(n+1)}(\frac{\bar{C}_{pi}}{\bar{C}_{pc}}\frac{\delta_i}{s} + \frac{\bar{C}_{pe}}{\bar{C}_{pc}}(\frac{\delta}{s} - \frac{\delta_i}{s})) - \frac{n+1}{n}\lambda) . \tag{18}$$

If C_p is assumed to be independent of temperature then $\bar{C}_{pi} = C_{p\infty}$ and the denominator becomes

$$1 + \frac{n}{n+1}\frac{C_{p\infty}}{C_{pc}}(\frac{\delta}{s\lambda} - \frac{n+1}{n}) . \tag{19}$$

To solve for δ/s, Re_x is introduced and using Eqn. (8) results in the following:

$$\frac{\delta}{s\lambda} = \frac{x}{\lambda s} c_\delta Re_x^{-\frac{1}{m}} \tag{20}$$

$$Re_x = \frac{x}{\lambda s} Re_c \frac{\mu_c}{\mu_\infty} . \tag{21}$$

Solving for $\frac{\delta}{s\lambda}$ and substituting in the denominator expression results in:

$$1 + \frac{n}{n+1} \frac{C_{p\infty}}{C_{pc}} (c_\delta (\frac{x_s + x_0}{\lambda s} (Re_c \frac{\mu_c}{\mu_\infty})^{\frac{1}{m-1}})^{\frac{m-1}{m}} - \frac{n+1}{n}) \tag{22}$$

where $x_s + x_0$ has been substituted for x.

Introducing $\xi_s$and ξ_0

$$\xi_s = \frac{x_s}{\lambda s} (Re_c \frac{\mu_c}{\mu_\infty})^{\frac{1}{m-1}} \tag{23}$$

$$\xi_0 = \frac{x_0}{\lambda s} (Re_c \frac{\mu_c}{\mu_\infty})^{\frac{1}{m-1}} = (\frac{1}{c_\delta} \frac{Re_{\delta_i}}{Re_c} \frac{\mu_\infty}{\mu_c} + \frac{1}{c_\delta} \frac{n+1}{n})^{\frac{m}{m-1}} \tag{24}$$

ξ_0 is the same expression in Eqn. (13) and was substituted above

Therefore the effectiveness η becomes

$$\eta = \frac{\bar{T}_{0bl} - \bar{T}_{0e}}{\bar{T}_{0c} - \bar{T}_{0e}} = \frac{1}{1 + (\frac{C_{p\infty}}{C_{pc}} (\frac{n}{n+1} c_\delta (\xi_s + \xi_0)^{\frac{m-1}{m}} - 1))} . \tag{25}$$

Equation (25) represents the generalized effectiveness equation using a boundary layer growth rate. All existing boundary layer correlations in low-speed flow are a simplification of the above equation. If the flow behaves like a turbulent boundary layer then $c_\delta = 0.376$, $m = 5$ and if a $1/7^{th}$ power law is used then Eqn. 2 becomes:

$$\eta = \frac{1}{1 + (\frac{C_{p\infty}}{C_{pc}}(0.329(\xi_s + \xi_0)^{0.8} - 1))} . \tag{26}$$

As indicated earlier, Goldstein (1971) ignores the initial boundary layer. If δ_i is neglected ξ_0 becomes 4.01, and the effectiveness is reduced to

$$\eta = \frac{1}{1 + (\frac{C_{p\infty}}{C_{pc}}(0.329(\xi_s + 4.01)^{0.8} - 1))} \tag{27}$$

which is identical to Kutateladze and Leontév equation given by Goldstein (1971). Stollery and El-Ehwany equation given by Goldstein (1971) neglects ξ_0 and assume that $C_{p\infty} = C_{pc}$ and η is reduced to

$$\eta = \frac{1}{(0.329(\xi_s)^{0.8})} \tag{28}$$

or

$$\eta = 3.04(\xi_s + \xi_0)^{-0.8} . \tag{29}$$

The jet entrainment model assumes that the entrainment of ambient flow in the shear layer is similar to a free jet, so that the entrainment mass flux is proportional to that of the freestream, i.e., $d\dot{m}_e/dx = \rho_\infty u_\infty / K$. In addition, the initial boundary layer is commonly ignored, i.e., $m_i = 0$. Equation 4 becomes

$$\eta = \frac{1}{1 + \frac{\dot{m}_e \bar{C}_{pe}}{\dot{m}_c \bar{C}_{pc}}} \tag{30}$$

$$\frac{\dot{m}_e \bar{C}_{pe}}{\dot{m}_c \bar{C}_{pc}} = \frac{\dot{m}_e}{\dot{m}_c} = K \frac{\bar{\rho}_\infty \bar{u}_\infty}{\bar{\rho}_c \bar{u}_c} \frac{x}{s} \frac{\bar{C}_{pe}}{\bar{C}_{pc}} = K \frac{x}{\lambda s} \frac{\bar{C}_{pe}}{\bar{C}_{pc}} . \tag{31}$$

Therefore, η becomes

$$\eta = \frac{1}{1 + K\frac{x}{\lambda s}\frac{C_{pe}}{C_{pc}}} \tag{32}$$

which is identical to Juhasz and Marek equations given by Goldstein (1971).

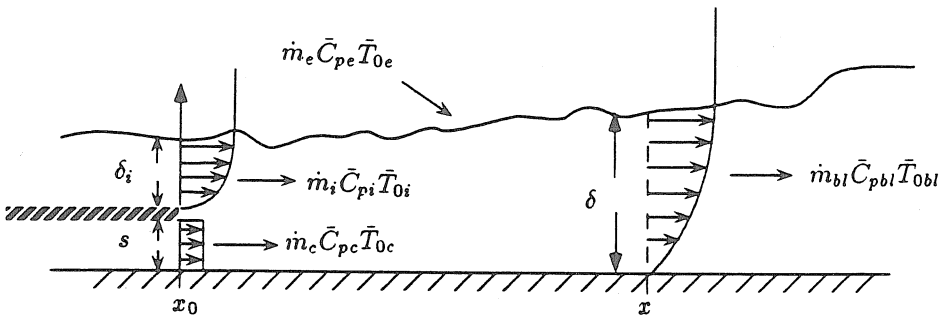

Figure A.1: Control volume used for analysis

Appendix B

Energy Equation Analysis

When applying film cooling to cool turbine blades or combustor walls, the coolant fluid is passed through internal passages and then is directed through a slot where it is injected to serve as a film coolant. A combination of convective cooling, radiation cooling and film cooling takes place. To attempt to solve this conjugated problem is a formidable task. In order to solve for the temperature field the problem is simplified by assuming that the flow has a constant property. The two-dimensional, incompressible boundary layer energy equation with constant property:

$$u\frac{\partial\theta}{\partial x} + v\frac{\partial\theta}{\partial y} = (\alpha + \epsilon)\frac{\partial^2\theta}{\partial y^2} \tag{1}$$

where $\theta = T - T_\infty$, α and ϵ are the thermal diffusion and the turbulent thermal diffusion, repectively. The boundary conditions are

$$x = 0, y < s \qquad \theta = \theta_c = T_c - T_\infty \tag{2a}$$

$$x = 0, y > s \qquad \theta = 0 \tag{2c}$$

$$x > 0, y = 0 \qquad q = q_w \; . \tag{2b}$$

For constant fluid properties the velocity field (u, v) is independent of the temperature field. Therefore, Equation (1) is linear, and superposition is allowed. The temperature field for the complete problem can be obtained by superposing the solutions of the two problems, one with an adiabatic wall of $q_w = 0$ and injecting at a temperature T_c; $\theta = \theta_c$, and the other with an a finite heat flux q_w and injecting at a temperatue equal to the freestream temperature T_∞;$\theta = 0$.

$$\theta = \theta_a + \theta_q \; . \tag{3}$$

To obtain θ_a, the boundary conditions for the adiabatic wall $q_w = 0$

$$x = 0, y = 0 \qquad \theta = \theta_c = T_c - T_\infty \tag{4a}$$

$$y = 0 \qquad (\frac{\partial \theta}{\partial y})_w = 0 \tag{4b}$$

$$y = \infty \qquad \theta_a = 0 \; . \tag{4c}$$

Note that the effectiveness is obtained under these conditions by evaluating θ_a at the wall θ_{aw} and noting that

$$\eta = \frac{\theta_{aw}}{\theta_c} \; . \tag{5}$$

To obtain θ_q, the boundary conditions for the wall with heat transfer $q_w \neq 0$

$$x = 0, y = 0 \qquad \theta_q = 0 \tag{6a}$$

$$y = 0 \qquad -k(\frac{\partial \theta}{\partial y})_w = q_w \tag{6b}$$

$$y = \infty \qquad \theta_q = 0 \, . \tag{6c}$$

The heat transfer coefficient h is obtained from the equation

$$q_w = h\theta_{qw} \tag{7}$$

and the temperature field solution is obtained using Eqn. 3. Evaluating Eqn. 3 at the wall

$$\theta_w = \theta_{aw} + \theta_{qw} \tag{8}$$

and the heat flux using Eqn. (7) is then

$$q_w = h\theta_{qw} = h(\theta_w - \theta_{aw}) \, . \tag{9}$$

This demonstrates that in order to obtain the overall heat transfer, two separate experiments have to be undertaken, one is to obtain the adiabatic wall temperatures as represented by conditions $4a - c$ and another is a heat transfer experiment in which conditions $6a - c$ are applied.

Fortunately, in low speed flow, it has been shown that the heat transfer coeffecient with injection h quickly approaches the no injection value (the no injection heat transfer coefficient is that of the boundary layer h_{bl}) as the downstream distance is increased. Therefore, the adiabatic solution θ_{aw} can be obtained using boundary layer heat transfer coefficient h_{bl} and the heat transfer value obtain by the conditions in $6a - c$. In other words, only one experiment is required to obtain θ_{aw}. Using Eqns. 8 and 9

$$\theta_{aw} = \theta_w - \theta_{qw} = \frac{q_w}{h_{bl}} - \theta_{q_w} = q_w(\frac{1}{h_{bl}} - 1) \, . \tag{9}$$

Therefore, effectiveness can be obtained using equation

$$\eta = \frac{\theta_{aw}}{\theta_c} = \frac{q_w(\frac{1}{h_{bl}} - 1)}{\theta_c} .$$

Bibliography

E. Alzner and V. Zakkay. Turbulent boundary layer shock interaction with and without injection. *A.I.A.A. Journal*, 9:1769–1776, 1971.

E. Alzner and V. Zakkay. *Turbulent Boundary Layer Shock Interaction with and without Injection.* ARL 70-0092, Aerospace Research Laboratories, USAF, 1970.

G. J. Banken, D. W. Roberts, J. E. Holcomb, and S. F. Birch. An investigation of film cooling on a hypersonic vehicle using a p.n.s. flow analysis code. 1985. AIAA Paper 85-1591.

Y. V. Baryshev, A. I. Leont'yev, and V. I. Rozhdestvenskiy. Heat transfer in the zone of interaction between a shock and the boundary layer. *Heat Transfer-Soviet Research*, 7:19–23, 1975.

I. E. Beckwith and D. M. Bushnell. *Calculation by a Finite-Difference Method of Supersonic Turbulent Boundary Layers with Tangential Slot Injection.* NASA TN D-6221, 1971.

W. Behrens. Total temperature thermocouple probe based on recovery temperature of circular cylinder. *Int. J. Heat Mass Transfer*, 14:1621–1630, 1971.

A. M. Cary and J. N. Hefner. Film cooling effectiveness in hypersonic turbulent flow. *A.I.A.A.*, 8:2090–2091, 1970.

A. M. Cary and J. N. Hefner. Film-cooling effectiveness and skin friction in hypersonic turbulent flow turbulent flow. *A.I.A.A.*, 10:1188–1193, 1972.

J. M. Delery. Shock-wave turbulent boundary layer interaction and its control. *Progress in Aerospace Sciences*, 22:209–280, 1985.

J. M. Delery and J. G. Marvin. *Shock-Wave Boundary Layer Interactions.* AGARD AG-280 , February 1986. edited by Reshotko, E.

R. DeMeis. Multimodes to Mach 5. *Aero-Space America*, 25:50–53, 1987.

E. R. G. Eckert and M. R. Drake jr. *Analysis of Heat and Mass Transfer.* McGraw Hill, New York, 2 edition, 1972.

H. J. Gladden and R. J. Simoneau. Review and assessment of the database and numerical modeling turbine heat transfer. In *Symposium Toward Improved Durability in Advanced Aircraft Engine Hot Sections* , pages 39–56, ASME International Gas Turbine Conference, D.E. Sokolowski (ed.), Amsterdam, The Netherlands, 1988.

R. J. Goldstein. Film cooling. *Advances in Heat Transfer*, 7:321–380, 1971.

R. J. Goldstein, E. R. G. Eckert, F. K. Tsou, and A. Haji-Sheikh. Film cooling with air and helium injection through a rearward-facing slot into a supersonic air flow. *A.I.A.A. Journal*, 4:981–985, 1966.

V. T. Grin and N. N. Zakharov. Experimental investigation of effect of tangential blowing and wall cooling on flow with separation. *Fluid Dynamics (English)*, 6:1035–1038, 1974.

J. N. Hefner. Effect of geometry modification on effectiveness of slot injection in hypersonic flow. *A.I.A.A. Journal*, 14:817–818, 1976.

M. S. Holden, R. J. Nowak, G. C. Olsen, and K. M. Rodriguez. Experimental studies of shock wave/wall jet interaction in hypersonic flow. January 1990. AIAA Paper 90-0607.

G. A. Howell and R. E. Tatro. Tangential fluid injection for control of shock-boundary layer interaction. June 1966. AIAA Paper 66-656.

C. R. Hyde, B. R. Smith, J. A. Schetz, and D. A. Walker. Turbulence measurements for heated gas slot injection in supersonic flow. *A.I.A.A. Journal*, 28:1605–1614, 1990.

P. S. Kamath, M. S. Holden, and C. R. McClinton. Experimental and computational study of the effect of shocks on film cooling effectiveness in scramjet combustor. 1990. AIAA Paper 90-1713.

D. L. Kors and R. D. Kissinger. The challenge of demonstrating the x-30. *Aerospace America*, 28:22–24, 1990.

F. T. Kwok, P. L. Andrew, W. F. Ng, and J. A. Schetz. Experimental investigation of a supersonic shear layer with slot injection of helium. 1990. AIAA Paper 90-0093.

A. Lappas. *An Adaptive Lagrangian Method for Computing 1-D Reacting Slows and the Theory of Riemann Invariant Manifolds For the Compressible Euler Equations.* PhD thesis, California Institute of Technology, Pasadena, 1993.

R. E. Launder and W. Rodi. The turbulent wall jet, measurements and modeling. *Annual Review of Fluid Mechanics*, 15:429–459, 1983.

O. C. Ledford and J. L. Stollery. *Film Cooling of Hypersonic Inserts.* Aero Report 72-15, Imperial College, 1972.

J. G. Lucas and R. L. Golladay. *Gaseous-Film Cooling of A Rocket Motor With Injection Near the Throat.* NASA TN D-3836, 1967.

J. A. Majeski and H. Morris. An experimental and computational investigation of film cooling effects on an interceptor forebody at Mach 10. 1990. AIAA Paper 90-0622.

J. A. Majeski and R. H. Weatherford. Development of an empirical correlation for film-cooling effectiveness. 1988. AIAA Paper 88-2624.

NASA. *Langley Aerospace Test Highlights.* NASA TM 90-104090, Langley Research Center, 1991.

S. M. Nosek and D. M. Straight. *Heat-Transfer Characteristics of Partially Film Cooled Plug Nozzle on A J-85 Afterburning Turbojet Engine.* NASA TM X-3362, 1976.

G. C. Olsen, R. J. Nowak, M. S. Holden, and N. R. Baker. Experimental results for film cooling in 2-d supersonic flow including coolant delivery pressure, geometry and incident shock effects. 1990. AIAA Paper 90-0605.

K. Parthasarathy and V. Zakkay. An experimental investigation of turbulent slot injection at Mach 6. *A.I.A.A. Journal*, 8:1302–1307, 1970.

D. J. Peak. *The Use of Air Injection to Prevent Separation of the Turbulent Boundary Layer in Supersonic Flow.* A.R.C. CP No. 890, Aeronautical Research Council, 1966.

B. E. Richards. *Film Cooling In Hypersonic Flow.* PhD thesis, University of London, London, 1967.

D. C. Rousar and R. L. Ewen. *Hydrogen Film Cooling Investigation.* NASA CR-121235, 1973.

R. A. Seban and L. H. Back. Velocity and temperature profiles in turbulent boundary layers with tangential injection. *Journal of Heat Transfer*, 84:45–54, 1962.

R. J. Simoneau, R. C. Hendricks, and H. J. Gladden. Heat transfer in aerospace propulsion. In *Proceedings of A.S.M.E. National Heat Transfer Conf.*, pages 1–22, Houston, 1988. Vol. 3.

D. B. Spalding. Velocity and temperature profiles in a wall jet. *Journal of Heat Transfer*, 3:255–265, 1961.

D. A. Walker, R. L. Campbell, and J. A. Schetz. Turbulence measurements for slot injection in supersonic flow. 1988. AIAA Paper 88-0123.

W. J. Yanta. *A fine-wire stagnation temperature probe.* NOLTR 70-81, U.S. Naval Ordnance Laboratory, 1970.

C. L. Yates. *Two-Dimensional, Supersonic Mixing of Hydrogen and Air Near a Wall.* NASA CR-1793, 1971.

V. Zakkay, L. Sakell, and K. Parthasarathy. An experimental investigation of supersonic slot cooling. In *Proceedings of the 1970 Heat Transfer and Fluid Mechanics Institute*, pages 88–103, Stanford U. Press, Stanford, CA, 1970. edited by T. Sarpkaya.

V. Zakkay, C. R. Wang, and M. Miyazawa. Effect of adverse pressure gradient on film cooling effectiveness. *A.I.A.A. Journal*, 8:1302–1307, 1970.